UNIVERSIDADE DE LISBOA
FACULDADE DE CIÊNCIAS

Environmental magnetism and paleomagnetism of speleothems: a new tool for documenting high-frequency instabilities of the Earth's magnetic field and climate

" Documento Definitivo"

Doutoramento em Ciências Geofísicas e da Geoinformação

Especialidade de Geofísica

Jorge Miguel Nogueira da Silva Ponte

Tese orientada por:
Eric Font, Cristina Veiga-Pires, Claude Hillaire-Marcel

Documento especialmente elaborado para a obtenção do grau de doutor

2019

UNIVERSIDADE DE LISBOA
FACULDADE DE CIÊNCIAS

Environmental magnetism and paleomagnetism of speleothems: a new tool for documenting high-frequency instabilities of the Earth's magnetic field and climate

Doutoramento em Ciências Geofísicas e da Geoinformação
Especialidade de Geofísica

Jorge Miguel Nogueira da Silva Ponte

Tese orientada por:
Eric Font, Cristina Veiga-Pires, Claude Hillaire-Marcel

Júri:

Presidente:

- Doutor João Manuel de Almeida Serra, Professor Catedrático e Presidente do Departamento de Engenharia Geográfica, Geofísica e Energia da Faculdade de Ciências da Universidade de Lisboa

Vogais:

- Doutor Francisco Jávier Pavón Carrasco, Associate Professor, Facultad de Ciencias Físicas da Universidad Complutense de Madrid (Espanha)
- Doutora Maria Alexandra Faria Pais, Professora Auxiliar, Faculdade de Ciências e Tecnologias de Coimbra
- Doutor Eric Font, Professor Auxiliar, Faculdade de Ciências e Tecnologias de Coimbra (orientador)
- Doutora Helena Maria Sant' Ovaia Mendes da Silva, Professora Associada, Faculdade de Ciências da Universidade do Porto

Documento especialmente elaborado para a obtenção do grau de doutor

Fundação para a Ciência e Tecnologia (FCT): SFRH/BD/96241/2013

2019

Index

Abstract

Speleothems are secondary mineral deposits formed in caves and are considered as very good archives of the Earth's magnetic field and climate. In this thesis, I provide new high-resolution magnetic data of a speleothem (SPA) collected in Algarve, in order to evaluate the effect of speleothem surface slope on the remanent magnetic directions, a still poorly studied and undemonstrated aspect of speleothem magnetism, and to provide new paleomagnetic data for the calibration of paleosecular variation (PSV) models. Paleomagnetic directions obtained from samples collected along subhorizontal to gradually subvertical calcite layers of a transversal cross-section of the SPA speleothem show very stable and high intensity magnetic directions, but with magnetic inclinations varying according to the slope of the calcite layers. Increased misalignment of the ferromagnetic particles due to their rolling along the surface, determined by Anisotropy of Anhysteretic Remanent Magnetization (AARM) techniques, results in a net distribution of shallower inclinations compared to PSV models. A correction factor is calculated based on the extrapolation of the magnetic inclinations to hypothetical horizontal layers, allowing a better comparison with PSV models, particularly consistent with the SHA.DIF.14K model. In addition, relative paleointensity data estimated using two different methods display consistent and comparable results. Finally, I provide detailed concentration- and coercivity-dependent magnetic proxy obtained through the analysis of isothermal remanent magnetization (IRM) curves and compared them with carbon and oxygen isotope composition measured in selected samples of the SPA stalagmite. Results show a low statistical correlation between magnetic and isotopic composition. However, higher content of pedogenic magnetite, often correlated with lower $^{13}\delta C$ and $^{18}\delta O$ compositions, suggests a casual-to-effect link between climate and magnetic mineralogy. These findings open new perspectives for reconstructing high-resolution PSV and climate records from speleothems and provide new insights into their NRM acquisition mechanisms.

Key-words: Speleothems, paleomagnetism, environmental magnetism, paleosecular variation

Resumo

Os espeleotemas são formações rochosas secundárias que ocorrem tipicamente em grutas e resultam da precipitação de carbonato de cálcio previamente dissolvido na água. Na ciência, são reconhecidos pela sua capacidade de registar o clima e o campo magnético da terra no momento da sua formação. Neste trabalho, vários dados de magnetismo e paleomagnetismo são obtidos através de um espeleotema recolhido numa gruta do Algarve, datado entre aproximadamente 3000 e 4500 AC. O principal objectivo é reconstruir o campo magnético terrestre gravado pelo espeleotema, assim como discutir a sua fiabilidade. Em particular, uma das perspectivas será avaliar a influência da inclinação da superfície do espeleotema na direcção do vector magnético gravado, um aspecto que nunca foi resolvido até hoje e é importantíssimo para avaliar e melhorar a fiabilidade dos registos magnéticos em espeleotemas.

O campo magnético terrestre é alvo de intensa investigação há várias décadas, sendo que alguns aspectos ainda são mal compreendidos. Um dos debates actuais prende-se com a origem do mesmo, que sabe-se ser no núcleo externo e é geralmente aceite que resulta de correntes eléctricas geradas por movimentos convectivos, mas muitas dúvidas se mantêm. É de conhecimento geral a existência de reversões do campo magnético terrestre no passado, que ocorrem na escala dos milhões de anos, mas o campo magnético varia igualmente a escalas bem mais curtas. Diariamente o campo magnético terrestre num dado local está em permanente mudança, em magnitudes porém extremamente mais baixas, reflectindo mudanças na ionosfera e magnetosfera. No entanto, é a variação secular do campo magnético terrestre que atrai grande parte dos investigadores actualmente. Esta acontece à escala de apenas alguns anos, e reflecte mudanças no interior do planeta, nomeadamente no núcleo externo. A compreensão da variação secular do campo, no presente e no passado, é muito importante para o estudo da origem do campo magnético da Terra, pelo que vários modelos de variação secular foram desenvolvidos com base em vários dados paleomagnéticos recolhidos em todo o globo. As direcções magnéticas incorporadas nesses modelos são obtidas através de objectos arqueomagnéticos, lavas e sedimentos marinhos ou lacustres. Cada tipo de dados tem as suas vantagens e desvantagens: os objectos arqueomagnéticos e as lavas têm normalmente magnetizações mais estáveis e bem determinadas por terem uma origem térmica, mas são dados discretos no tempo, correspondendo a uma data específica,

sendo necessário recolher muitas amostras de idades distintas para ter uma boa representação; por outro lado, os sedimentos fornecem dados contínuos durante um intervalo de tempo, mas as magnetizações, sendo detríticas, são mais complicadas de determinar, e estão sujeitas a efeitos secundários que podem alterar a magnetização original. Os espeleotemas, por seu lado, podem fornecer direcções magnéticas continuamente num dado intervalo de tempo, e a magnetização, sendo detrítica, é estável e não está sujeita aos efeitos posteriores como outros sedimentos. O seu maior problema está relacionado com a pequena quantidade de minerais ferromagnéticos, o que dificulta a detecção de direcções magnéticas estáveis pelos magnetómetros. Porém, devido à melhoria da sensibilidade dos equipamentos, nos últimos anos têm sido possível estudar e obter registos de variação secular do campo magnético em vários espeleotemas de todo o mundo.

Este trabalho começou com a aquisição de dados paleomagnéticos, através de desmagnetização em campo alternado, de amostras cúbicas com 2 cm de lado retiradas de uma fatia do espeleotema, chamada de SPAIII. Os primeiros dados mostraram uma magnetização estável, com vectores bem determinados e com baixa incerteza na determinação das direcções. A magnetização é primária, adquirida em grande parte por minerais magnéticos de baixa coercividade (magnetite), o que foi confirmado com a posterior aquisição e análise de curvas de magnetização remanescente isotérmica (IRM). Detecta-se uma magnetização viscosa nos primeiros passos (até 6 mT), que é facilmente removível no cálculo do vector magnético por análise de componentes principais. Analisando os dados, percebe-se que existe uma tendência para a inclinação magnética ser mais baixa quanto mais perto da base do espeleotema. Este espeleotema apresenta características muito particulares, mantendo um espaçamento quase constante entre as linhas de crescimento desde o topo à base, quando normalmente se dá um estreitamento das linhas nas zonas laterais de uma estalagmite. Isso permite amostrar várias amostras ao longo das mesmas linhas de crescimento, sendo possível comparar direcções com a mesma idade, que na teoria deveriam ser iguais. Desse modo, os primeiros resultados sugerem uma influência do ângulo das camadas de calcite na inclinação magnética gravada. Por outro lado, a declinação magnética é independente desse factor.

Numa segunda fase, amostras cilíndricas com um diâmetro de 1.1 cm foram retiradas de outra fatia do espeleotema (nomeada SPAIV). O objectivo era não só obter uma resolução maior, como permitir furar exactamente ao longo das mesmas linhas de crescimento do espeleotema, o que não foi perfeitamente alcançável com as amostras cúbicas. Os dados

paleomagnéticos são extremamente semelhantes aos obtidos com as amostras cúbicas, e voltou a verificar-se o efeito da inclinação das camadas na inclinação magnética. Esse efeito acontece de forma sistemática em todas as linhas de crescimento amostrada, com declives semelhantes, em média de 1º de variação na inclinação magnética por cada 10º no ângulo das camadas. Por ter um comportamento linear, aplica-se uma simples correcção por extrapolação linear para um ângulo zero, simulando camadas horizontais que se observariam no centro do espeleotema e onde teoricamente a inclinação magnética não teria sofrido qualquer efeito do declive das camadas. As direcções magnéticas foram comparadas com vários modelos de variação secular e dados paleomagnéticos contemporâneos obtidos com espeleotemas dos Alpes, lavas das Ilhas Canárias e objectos arqueomagnéticos do norte de Espanha. Em termos gerais, os valores de declinação e inclinação magnética encontram-se dentro dos previstos pelos modelos e dados utilizados para comparação. No entanto, os valores da inclinação magnética encontram-se subestimados, aproximando-se significativamente dos modelos quando corrigidos para uma teórica camada horizontal, reforçando o efeito de "achatamento" do vector magnético nas camadas mais verticais. Outro aspecto relevante é o facto de a inclinação magnética registada pelo espeleotema SPAIV mostrar um aumento gradual, seguido de uma brusca diminuição, o que é retratado de forma muito semelhante pelo modelo *SHA.DIF.14K*. A anisotropia da susceptibilidade magnética (ASM) foi igualmente analisada, como tentativa de explicar a influência da inclinação das camadas na magnetização remanescente. Porém, o diamagnetismo da calcite esconde o sinal da ASM, pelo que se teve de recorrer à anisotropia da magnetização remanescente anisterética (AMRA), uma técnica que detecta apenas o sinal dos minerais ferromagnéticos presentes na amostra. Os resultados demonstram um baixo grau de anisotropia, sugerindo partículas aproximadamente esféricas, e uma tendência para a inclinação do eixo de maior susceptibilidade ser perpendicular à superfície do espeleotema, mas com maior dispersão de valores na base (camadas verticais). Com o suporte de estudos acerca da magnetização remanescente detrítica e do efeito de "achatamento" do vector magnético, chegamos à conclusão que as partículas quase esféricas de magnetite tendem a rolar ao longo da superfície do espeleotema. Quanto maior a inclinação mais as partículas rolam, tornando as direcções dos momentos magnéticos mais dispersas. Tendo em conta todos os dados disponíveis, permite-se concluir que no espeleotema em estudo, os factores que controlam a magnetização remanescente são principalmente o campo magnético terrestre, e em menor escala, o declive das camadas.

Além da direcção do vector magnético, também se testou o cálculo da paleointensidade relativa do campo magnético. Para tal, utilizou-se dois métodos: normalização por medidas da concentração em minerais ferromagnéticos, e método de pseudo-Thellier. Ambos os métodos mostram resultados semelhantes e com repetibilidade entre diferentes sequências de amostras (representando o mesmo intervalo temporal). De salientar a identificação de um mínimo relativo destacado em todos os métodos utilizados. Deste modo, este trabalho demonstra que os espeleotemas são fontes válidas de dados paleomagnéticos e podem vir a ser incluídos nos modelos de variação secular. O efeito do declive das camadas não deve ser ignorado, mas pode ser resolvido. Os resultados aqui apresentados são relevantes para a investigação nesta área, como comprovam as duas publicações em revistas conceituadas como são o Journal of Geophysical Research e o G-cubed, ambos da American Geophysical Union (AGU).

Para finalizar, houve ainda uma tentativa de relacionar o magnetismo e clima neste espeleotema, como foi feito recentemente em dois estudos. Para tal foram recolhidos dados de isótopos de oxigénio e carbono, que foram comparados com a concentração em minerais ferromagnéticos, mais concretamente, em magnetite. Nos picos de máxima magnetização, há de facto uma tendência para ocorrem os valores mais baixos dos isótopos de oxigénio e carbono. Porém, a correlação entre os parâmetros é muito baixa, o que dificulta qualquer conclusão. A relação entre o magnetismo e o clima nos espeleotemas tem no entanto bastante potencial para ser explorado, até porque se encontra no princípio da sua investigação.

Palavras chave: Espeleotemas, paleomagnetismo, magnetismo ambiental, variação secular do campo magnético

Acknowlegments/ Agradecimentos

Por mais difícil que seja colocar em texto a importância das pessoas que fizeram parte da minha vida nestes últimos anos durante o doutoramento, não posso deixar de a registar neste espaço. Foram imensas as pessoas que me ajudaram, que provalmente me esquecerei de algumas, mas naturalmente que tenho de começar pelos meus orientadores. Eric Font, que foi fundamental não só na parte científica e pelos conhecimentos que me transmitiu, mas também pela parte motivacional. Muito obrigado pela enorme paciência! Cristina Veiga-Pires, sempre que foi preciso me ajudou e me recebeu, tal como o Claude Hillaire-Marcel, com todos os dados, medições e conselhos, principalmente na área da geologia e geoquímica. A todos os investigadores que de alguma forma contribuiram, o meu enorme agradecimento: Mark Dekkers, Mark Bourne, Ron Shaar e cientistas anónimos pelas revisões dos manuscritos; Joshua Feinberg pela revisão e edição de um dos artigos publicados, assim como pelas conversas e conselhos via e-mail; Ioan Lascu também pela sua crítica e opinião; Elena Zanella pelos dados das estalagmites dos Alpes; Martin Chadima pela orientação e ajuda na medição da AARM no LDA-3A demagnetizer; Dario Bilardello pela ajuda na interpretação dos dados de paleomagnetismo; Paulo Santana da Universidade do Algarve, por ter fornecido a máquina para moer as amostras e pela ajuda; Pedro Silva e Mário Moreira, do laboratório de magnetismo do IDL, por vários conselhos e orientações; Marta Neres, sempre disponível para me ajudar e aconselhar. Aos meus colegas e amigos Francisco Almeida, Diogo Lourenço, Sérgio den Boer, Ana Lopes, Vírgilio Bento, Daniela Lima e Maria João, pelo companheirismo e amizade também fundamentais ao longo de um curso. Também deixo o meu agradecimento à FCT pela bolsa atribuida (SFRH/BD/96241/2013), sem a qual este trabalho não teria sido realizado. Para o fim deixo o que mais importante tenho na minha vida: a minha família. Desde a minha companheira e esposa Inês, que está sempre comigo nos bons e maus momentos; à minha mãe e ao seu companheiro João, ambos com valor inestimável para mim; à minha avó Madalena; aos meus sogros Alexandre e Maria José e aos meus "avós" Alice, Companheiro Tó e Vitória, todos fazem parte do pilar que me sustenta. Sem esquecer os primos, tios e tias que estão no meu coração. Uma palavra muito especial para os que já partiram: o meu pai, que ainda faz parte de mim e recordo com muita saudade, o meu avô e a minha querida Avó Deolinda, que sempre me acarinhou de uma forma muito especial, e que faz praticamente um mês que partiu no dia que escrevi este texto. Por fim, e porque tudo o que tenho e todas as pessoas que fazem parte da minha vida foram colocadas

por Ele, agradeço a Deus, por nunca desistir de mim e me amar incondicionalmente com todos os meus defeitos e virtudes.

1.Introduction

1.1 Objectives

The main objectives of this PhD thesis are the following:

1. Collect magnetic and paleomagnetic data from the speleothem under study.

2. Characterize and discuss the magnetism of speleothems: advantages and disadvantages.

3. Obtain an age model for the speleothem.

4. Reconstruct the paleosecular variation curve (direction and intensity) recorded by the speleothem.

5. Discuss the reliability of the paleomagnetic record.

6. Link magnetic properties of the speleothem to climate proxies.

1.2 State of the art

Speleothems are considered as very good archives of the Earth's magnetic field and climate, but very few speleothem magnetism studies were published hitherto, probably because earlier researchers were limited by the sensitivity of their magnetometers. The magnetism of speleothems was first studied in the late 70's by *Latham et al.* (1979), who presented paleomagnetic data from speleothems (calcite stalagmites and flowstones), and concluded that their original magnetic directions are preserved. Since the recent review by Lascu and Feinberg (2011), and thanks to the development of precise magnetometers, speleothem magnetism has experienced a revival in the last decade, contributing to a better understanding about the earth's magnetic field behavior.

The Earth's magnetic field has been the subject of intense research for a long time. Particularly, its origin is still in under debate, although it is generally accepted that movements in the liquid outer core due to convection create electric currents which generate a magnetic field. The variation of the Earth's magnetic field in timescales of few years to decades (referred as paleosecular variation) is thought to reflect the changes of non-dipolar component, so that scientists started developing high-resolution magnetic field models describing the geomagnetic field direction and intensity during the last thousand years, known as Paleosecular variation (PSV) models. The reconstruction of the geomagnetic field is based on the magnetic directions preserved and calculated in archaeological objects, volcanic rocks and sediments (lacustrine or marine). Archaeological material and volcanic rocks record the Earth's magnetic field during the original cooling, in a process called thermoremanent magnetization (TRM). The original magnetic vector may be well identified, preserved and accurately dated, but these materials provide only episodic snapshots of the Earth's magnetic field. The sediments, both lacustrine and marine, can also be used to reconstruct the geomagnetic field at the time of their deposition [e.g. *Sagnotti et al*., 2011*; Gómez-Paccard et al.,* 2012], providing continuous time-serie records. However, age uncertainties from sediments are typically on the order of hundreds to thousand years, and such data is affected by several problems [*Lascu and Feinberg*, 2011]. There is a large uncertainty about the time when the sediments lock the magnetic vector. Fresh sediments are unconsolidated and water-rich, allowing the magnetic minerals to rotate freely until these sediments are compacted by overlying sediments, and resulting in a delay between the age of sedimentation and the age of the magnetization. Compaction, turbidity currents, slumping, bioturbation, dewatering, diagenesis, disturbances during collection, transport and sampling,

are examples of the large number of issues that after the magnetization recorded in sediments, generally producing shallower magnetic vectors.

In counterpart, speleothems have hold good advantages over sediments and represent robust candidates for paleomagnetic studies [*Lascu and Feinberg,* 2011]. Both are continuous records in time, but speleothems are solid and compact mineral deposits, avoiding the complications in measuring remanence in unconsolidated sediments. The time between the deposition of magnetic minerals and their immobilization by calcite precipitation is short, but sufficient to allow them to align with the magnetic field. As in sediment deposits, there are also post-depositional processes in speleothems, such as calcite recrystallization or dissolution that may change the original magnetic vector. However, in speleothems this effects is easily recognizable, and researchers can avoid measurements in that altered areas. Additionally, they can be dated with a very high precision using ^{230}Th dating. On the other hand, one limitation about using speleothems for paleomagnetic studies is the typical low magnetic mineral concentration. In order to avoid this problem, the studies have been using speleothems that grew in regions with a high supply of detrital particles such as clays, rich in iron oxides. However, this solution offers another complication, as the detrital material also contains high levels of detrital thorium. As referred before, the dating technique is based on the ^{230}Th, product of decay from the Uranium initially present in the calcite matrix. In consequence, the contamination with detrital thorium will decrease the age calculation accuracy, although certain corrections may be applied in limited cases [*Latham et al*., 1982]. Besides the correction techniques, it's advised to avoid dating darker layers, supposedly with high detrital content.

1.2.1 Magnetic mineralogy and acquisition of magnetic remanence in speleothems

There is a large consensus that the main natural remanent magnetization (NRM) in speleothems is a depositional remanent magnetization (DRM), as the drip water that regularly hit the surface contains detrital sediments transported into the cave by floods or flow along rock fissures [*Latham and Ford,* 1993]. This detrital material contains iron oxides, which align with the Earth's magnetic field before the precipitation of calcite imprison the magnetic minerals and conserve the original magnetization. Despite its minor contribution for the total NRM, a chemical remanent magnetization is also possible [*Latham et al.,* 1989]. This mechanism is explained by the chemical precipitation of magnetic minerals from the drip water containing dissolved iron oxides. Since the redox conditions in the speleothem's

surface are not favourable to magnetite precipitation, CRM is usually associated to minerals with weaker magnetic signal, such as goethite [*Lascu and Feinberg*, 2011*; Strauss et al.,* 2013]. The whole process of the acquisition of magnetic remanence in speleothems is resumed in Figure 1.1, published by *Lascu and Feinberg* (2011).

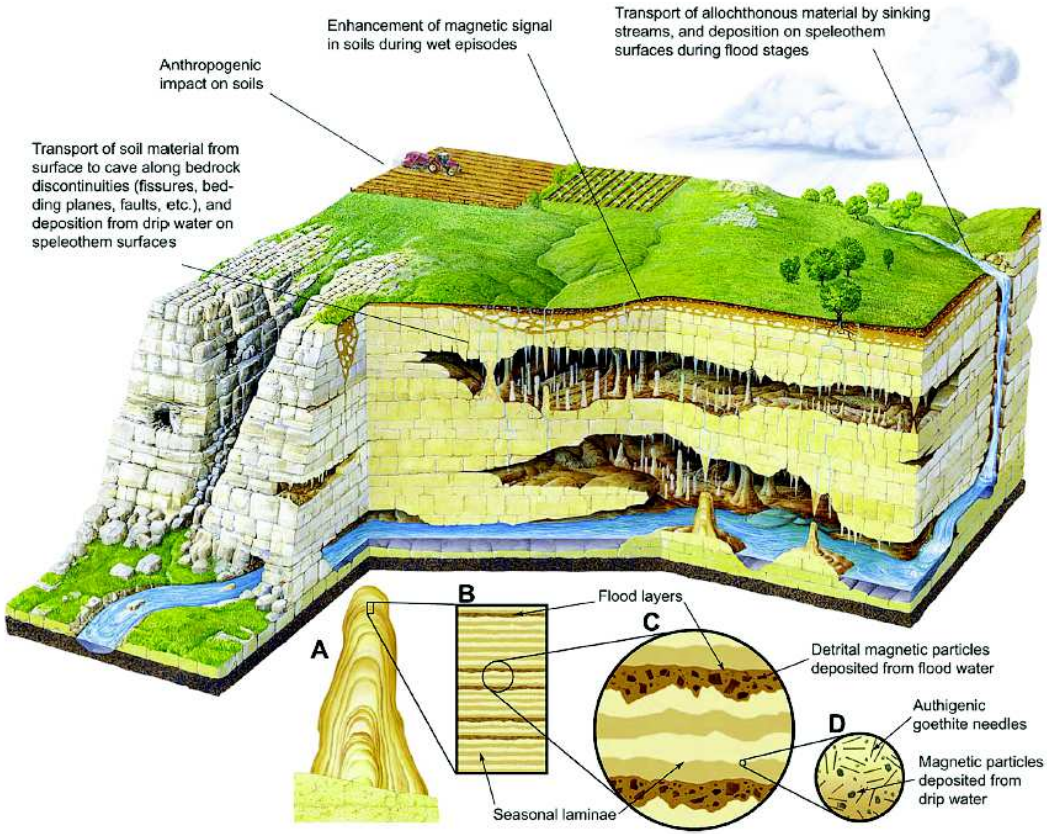

Figure 1.1 Conceptual model of the processes affecting magnetism of speleothems. Magnetic enhancement in the topsoil occurs during wet periods, when magnetite is formed by inorganic precipitation, or possibly mediated by dissimilatory iron reducing bacteria. Addition of eolian dust to soils occurs during dry periods. Magnetic material is transported from the surface to the spelean environment by water percolating from the soil via cracks and fissures to the point sources for drip water from which speleothems form. Rivers transport larger detrital magnetic particles, which are deposited on speleothem surfaces during the quiescent stages of water retreat after a flooding episode. Insets show detailed structure of a periodically flooded stalagmite (A) at mm (B), sub-mm (C) and sub-mm (D) scales. Magnetic particles in flood layers are on the order of a few microns to tens of microns, with an upper grain size limit of w100 mm controlled by the thickness of the water film coating the speleothem. The seasonal laminae are on the order of several tens of microns to a few hundred microns and can contain dissolved or particulate organic matter, which gives the calcite luminescent properties when exposed to ultraviolet light. Finegrained magnetic particles transported by drip water or precipitated in situ are on the order of a few nanometers to a couple of hundred nanometers (from *Lascu and Feinberg* (2011)).

Font et al. (2014) applied paleo and rock magnetic methods in the SPA speleothem from Algarve (Portugal) studied here. The results show that the main magnetic carrier is detrital titanomagnetite, identified by microscopic observation (Scanning Electron Microscopy (SEM) coupled to Energy Dispersive Spectra (EDS) composition) and magnetic properties (Cumulative Log-Gaussian (CLG) decomposition of IRM acquisition curves) (Figure 1.2). Comparison with the magnetic properties of the characteristic terra rossa soils capping the cave suggested that the detrital titanomagnetite is inherited from these terra soils and deposited in the speleothem's surface by drip waters. This is comforted by the occurrence of magnetite grains observed in glass plates positioned below a drip water during 3 months (Figure 1.2A). The observation that magnetite is the main carrier of the NRM recorded in speleothems was also reported by: *Osete et al.,* (2012), *Strauss et al.,* (2013), *Bourne et al.,* (2015), *Jaqueto et al.,* (2016), *Lascu et al.,* (2016), *Zhu et al.,* (2017), *Zanella et al.,* (2018) and *Trindade et al.,* (2018), who identified magnetite by using several rock magnetic techniques (e.g. IRM, ARM, AF demagnetization, thermomagnetic curves) and scanning electroscopy. The main NRM mechanism is then a DRM, what together with stable magnetic directions (Figure 1.2), points the Algarve stalagmites as good candidates for paleo and environmental magnetic studies.

Despite the promising preliminary magnetic results in speleothems for paleomagnetic studies, some important aspects about the acquisition of magnetic remanence has not yet been well investigated. One of the possible problems pointed by some authors is related to the influence of the calcite growth dip angle in the recorded magnetic directions. They made a very simple test by comparing the obtained directions in central (horizontal layers) and lateral (vertical layers) samples, but the influence could not be confirmed. According to them, the differences observed in the magnetic directions between central and lateral samples are within the typical range of paleomagnetic measurement errors. However, the speleothems used in this study do not have a favourable shape for evaluating calcite dip effects since they are very thin and only 2/3 specimens could be sampled along the same growth lines. A different approach was conducted by *Zhu et al.* (2012), who studied the magnetic fabric of two speleothems. Similar directions of maximum principal axis of Anistropy of Isothermal Remanent Magnetization (AIRM) and NRM suggests that orientation of ferromagnetic minerals have been likely controlled by the geomagnetic field, and not by the orientation of calcite laminae growth.

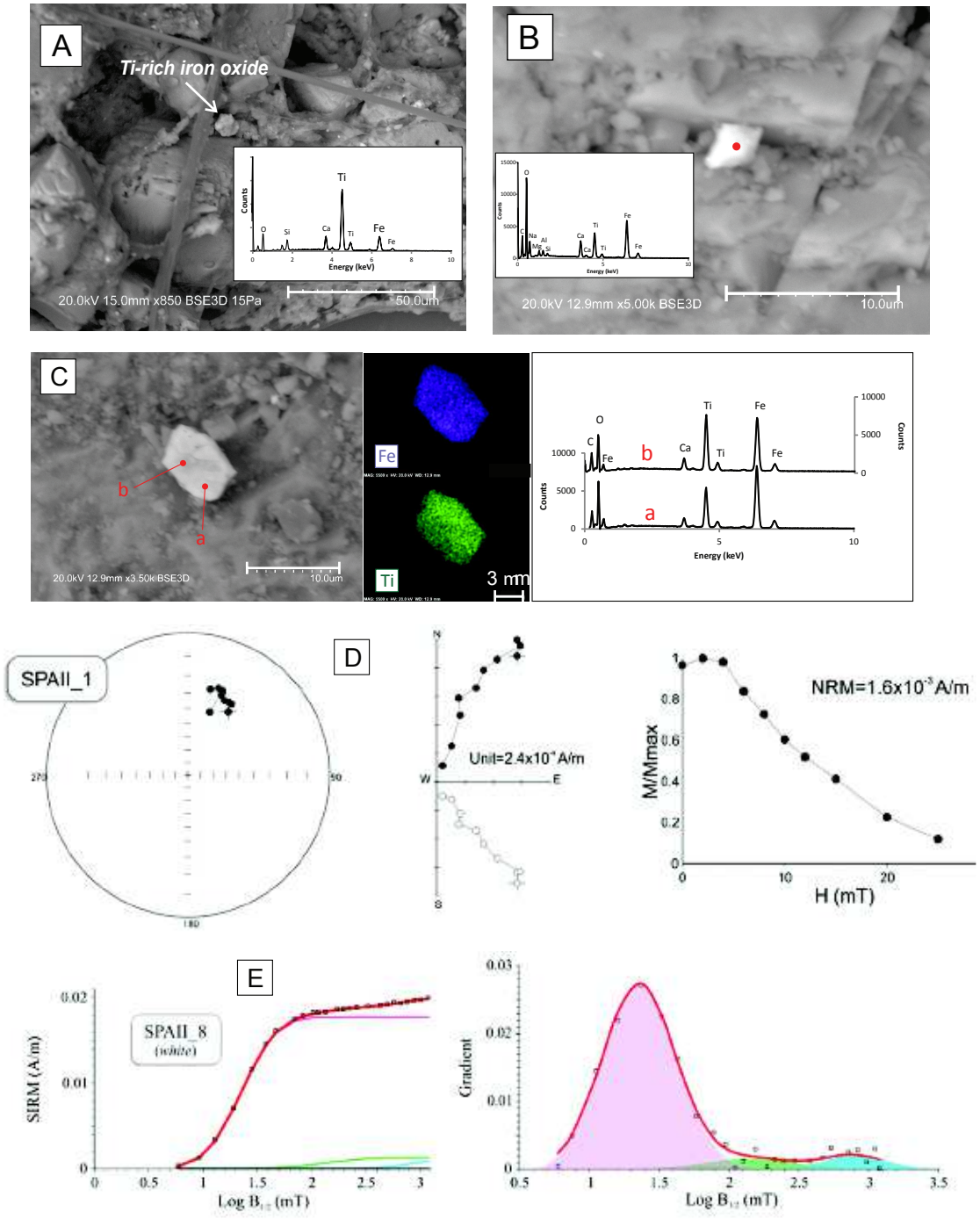

Figure 1.2 Scanning electron microscope (SEM) back-scattered images and EDS (Energy Dispersive Spectra) of a glass plate positioned bellow a drip water during three months (A) and SPA stalagmite studied here (B-C), showing the presence of detrital Fe-Ti iron oxides, probably titanomagnetite. D) Stereographic and orthogonal projections of the magnetic direction obtained after Alternating Field demagnetization, as well as normalized magnetic intensity versus applied field H (mT), showing a stable and high intensity primary remanent magnetization. E) The decomposition of IRM acquisition curves using a Cumulative Log-Gaussian function shows the presence of a mixture of a low-coercivity (i.e. magnetite) and high coercivity (hematite) magnetic phases. (Modified from *Font et al.* (2014).

1.2.2 Contribution of speleothem magnetic archives in the calibration of Paleosecular variation records of the Earth's magnetic field

Reconstruction of the ancient Earth's magnetic field reconstructions is one of the most important challenge in geomagnetism to better understand the dynamics in the Earth's core and the origin of the Earth's magnetic field. More specifically, several models were developed during the last decade in order to reconstruct the high-frequency and short-term variations of the Earth's magnetic field, called paleosecular variation (PSV), in the last 10-15 kyr. For example, *Korte et al.* (2011) and *Nilsson et al.* (2014) proposed the CALS10k.1b and pfmk models, respectively, for which reconstruction is based on archaeomagnetic, lava and sediment data of the last 10,000 years. Recently, *Pavón-Carrasco et al.* (2014) discarded sediment data, but used new data sets from volcanic and archaeological materials to propose the SHA.DIF.14k model for the last 14.000 years.

One of the greatest speleothem's advantages is the possibility to obtain high-resolution paleomagnetic records, which allow documenting high-frequency instabilities of the geomagnetic field (in timescales of few years). For example, *Osete et al.* (2012) not only identified for the first time the Blake geomagnetic excursion in a speleothem from northern Spain, but also managed to date the different phases of the excursion (Figure 1.3). Accurate timing of geomagnetic excursion is crucial for understanding the geodynamo processes and for magnetostratigraphic correlation. More recently, *Lascu et al.* (2016) reported a paleosecular variation record from a North American speleothem, showing a geomagnetic excursion within the age interval 42.25-39.7 kyrs BP, peaking at 41.1 kyrs BP, which has been identified as the Laschamp excursion (Figure 1.4). This is the first age bracketing of the Laschamp excursion using radioisotopic dating, which had already been reported before using volcanic paleomagnetic data ($^{40}Ar/^{39}Ar$ dating), with similar ages (between 40.7 and 41.3 kyrs BP), and other sedimentary and ice core records. This geomagnetic excursion corresponds to the most studied example of a geomagnetic excursion, since it coincides with the demise of *Homo Neanderthalensis* and to the Last Glacial Maximum and massive Mediteranean eruptions. Thus, precise determination of the timing and duration of the Laschamp excursion helps elucidating major scientific questions in diverse areas such as geology, paleoclimatology and anthropology. *Zanella et al.* (2017) presented a 10.000 yrs high-resolution paleosecular variation record from two cores of an Alpine flowstone, covering almost the entire Holocene (0.5 - 9 kyrs). Comparison with PSV models and data obtained from lavas and archaeomagnetic objects shows that the flowstone is an excellent

record of the Earth's magnetic field during the last 9.000 years (Figure 1.5), providing promising data both for the detection of short term variations of the geomagnetic field and for calibration of regional PSV curves, in time intervals where paleomagnetic data is scarce. *Trindade et al.* (2018) report a unique geomagnetic record for the last ~1500 years combining data of two well-dated speleothems from Brazil, located near the present day minimum of the geomagnetic South Atlantic Anomally (SAA). The SAA marks the position of the weakest geomagnetic field on Earth, and historical geomagnetic data from ship logs, observatories and satellites indicate that the area of the anomaly has been growing and migrating continuously westward. However, the origin and longevity of the SAA are still poorly understood given the scarcity of paleomagnetic data in the southern hemisphere. This work successfully describes the evolution of the SAA through the last 1500 years, confirming that fast geomagnetic field variations derived from SAA are a recurrent feature in the region. Magnetic directions are consistent with historical observations of the Earth's magnetic field in the last 500 years and with model ARCH3K.1 for older periods (Figure 1.6), what validates the paleomagnetic data provided by the speleothems.

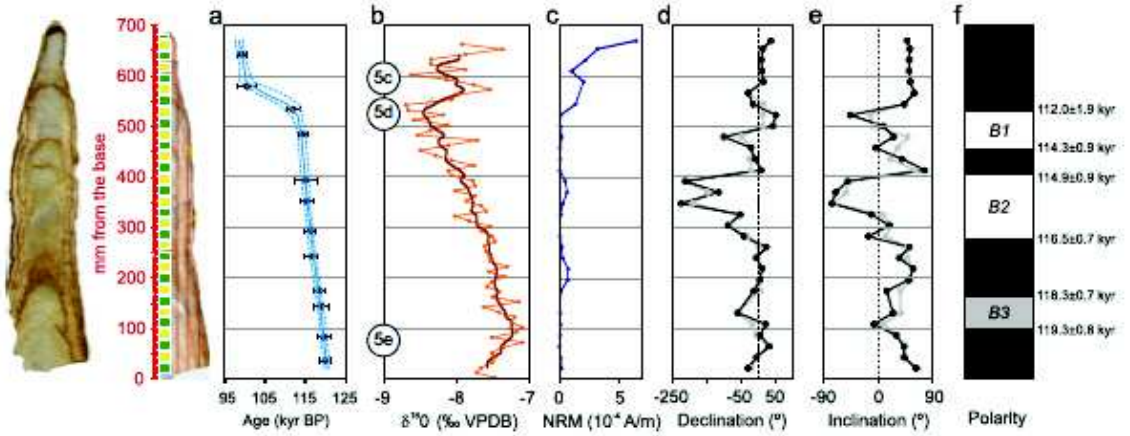

Figure 1.3 The Blake Geomagnetic excursion (with three phases B1, B2 and B3) recorded by a speleothem, here identified by quick shifts in the magnetic declination and inclination values (Figure from *Osete et al.,* 2012).

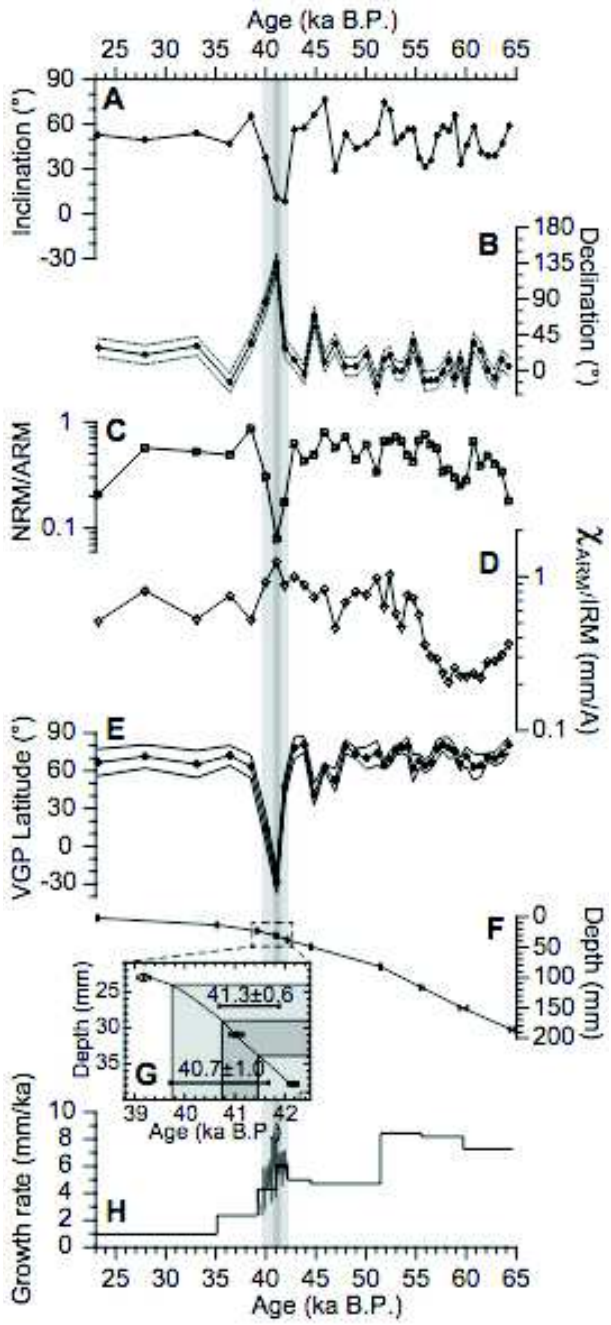

Figure 1.4 Magnetic properties and chronology of the Laschamp excursion in the speleothem specimen studied from Crevice Cave, Missouri (USA). A: Inclination. B: Declination. C: Relative paleointensity (NRM/ARM). D: Magnetic grain size. E: Virtual geomagnetic pole (VGP) latitude. F: Age-depth model based on ^{230}Th dates. G: Incremental chronology (from confocal microscopy layer counting) across the Laschamp, anchored to radioisotopic dates. H: Speleothem growth rates from the radioisotopic (black) and incremental (gray) age models (*Lascu et al.*, 2016).

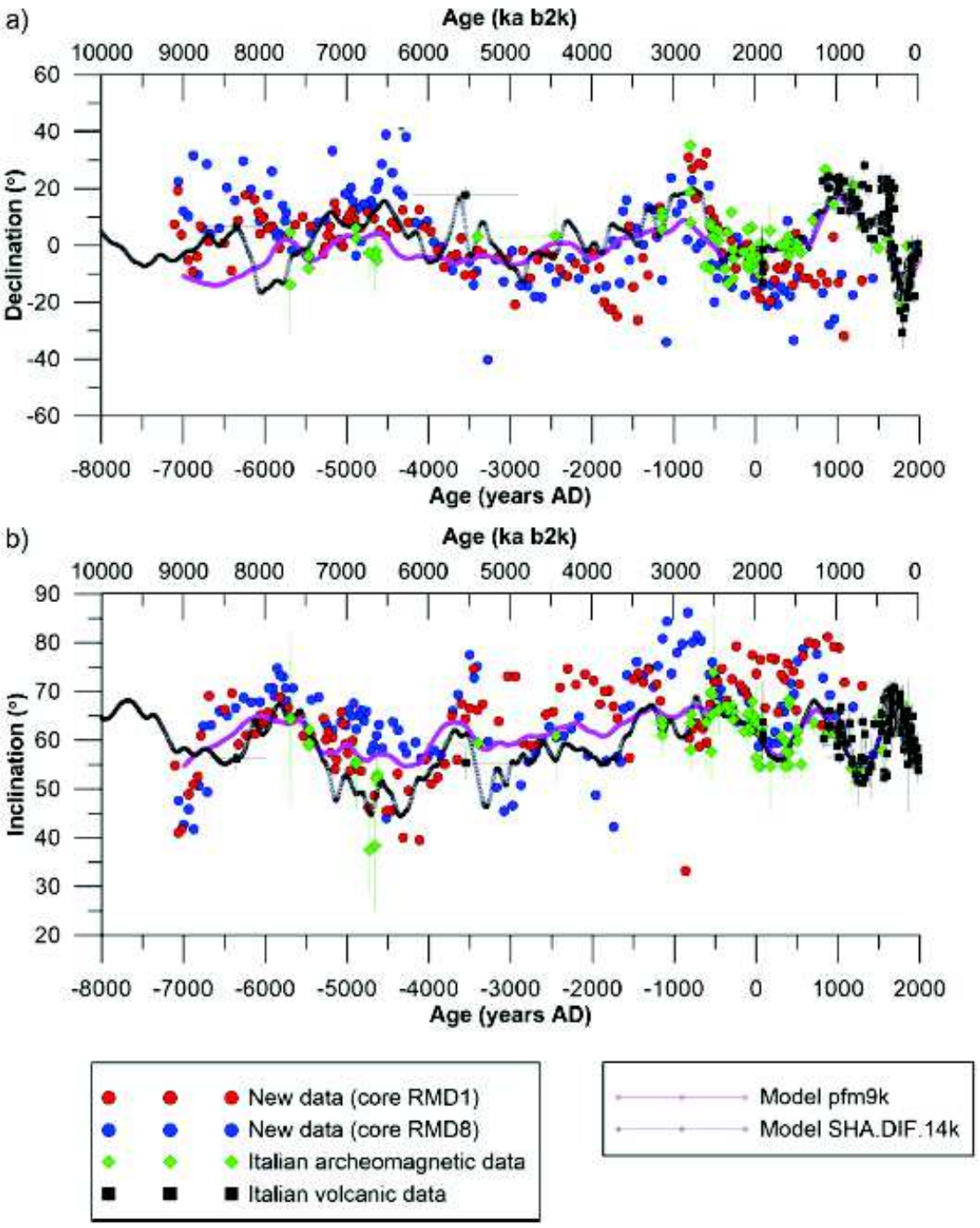

Figure 1.5 Speleothem data collected from Alpine speleothems, compared to paleomagnetic data from archaeomagnetic and volcanic sources and to PSV models (*Zanella et al.,* 2017).

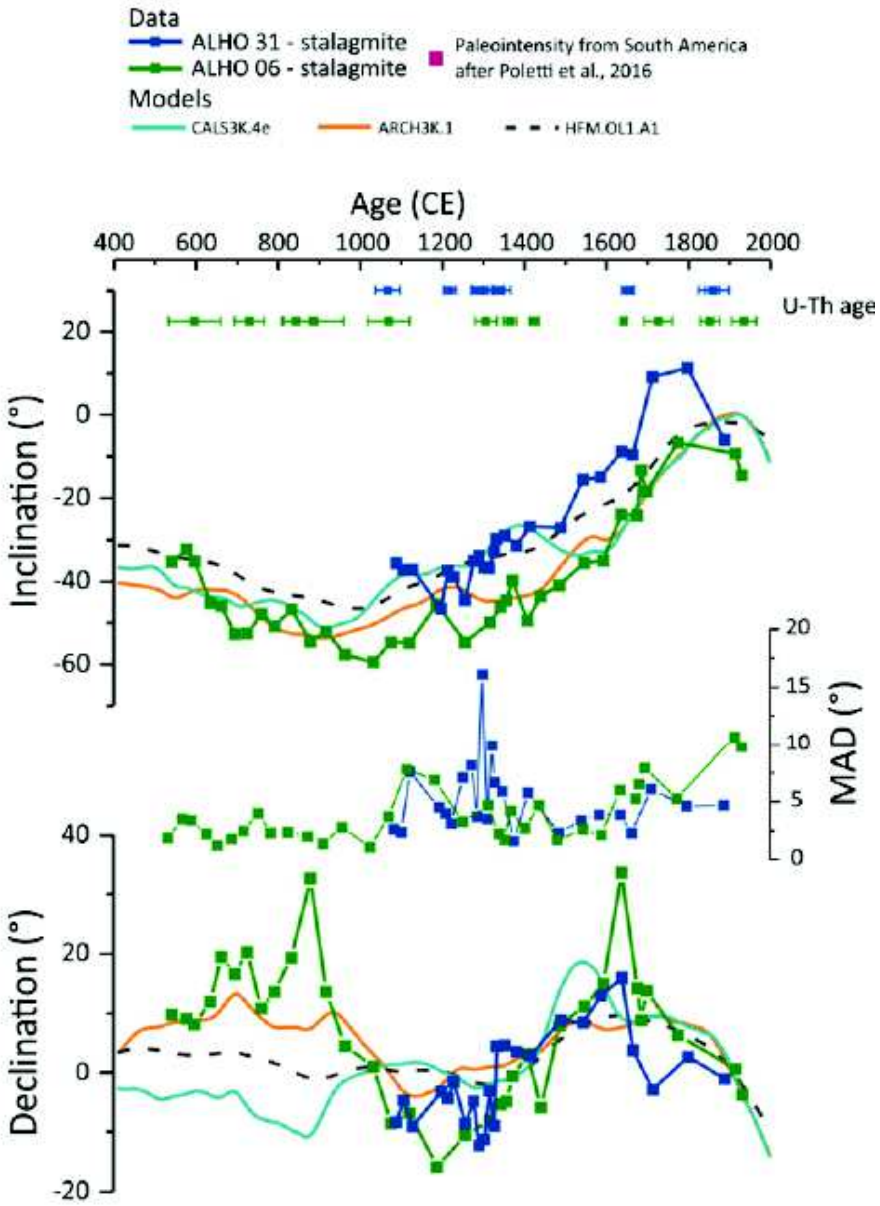

Figure 1.6 Paleomagnetic record from two speleothems from Brazil, compared with PSV models (*Trindade et al.,* 2018).

1.2.3 Speleothem's magnetism as a climate proxy

Speleothems have been used for past climate reconstructions using several proxies. Particularly, oxygen and carbon isotopes are widely used, and even a database (SISAL) has been created resuming all speleothem $\delta^{18}O$ and $\delta^{13}C$ data collected worldwide [*Atsawawaranunt et al.,* 2018; *Lechleitner et al.,* 2018]. On the other side, magnetic proxies in speleothems have been poorly used. Past climate reconstructions using magnetic susceptibility of cave sediments have been successfully correlated with records obtained from other proxies [*Elwood et al.*, 2001; *Elwood et al.*, 2004; *Elwood and Gose*, 2006], but

magnetic parameters obtained from a speleothem has only been used for climate reconstruction recently [*Bourne et al.,* 2015; *Jaqueto et al.,* 2016; *Zhu et al.,* 2017]. A significant positive correlation between ferromagnetic mineral concentration (quantified by IRM of the soft component, magnetite) and oxygen isotope values measured in a speleothem from Virginia, USA, has been detected by *Bourne et al.,* (2015). According to the authors, $\delta^{18}O$ values in the cave site are controlled by seasonal precipitation: enriched ^{18}O rain during Summer enhanced production of pedogenic magnetite and results in high concentrations of magnetic minerals. *Jaqueto et al.,* (2016) used a similar approach in stalagmites from Brazil, and suggested that more negative (positive) values of oxygen and carbon isotopes correspond to lower (higher) values of magnetic mineral content. In this region, higher isotopic values are interpreted as drier periods, suggesting that vegetation cover controls the magnetic input in the cave: drier periods (higher $\delta^{18}O$ and $\delta^{13}C$) drives less vegetation cover, more erosion and therefore more transport of Fe-rich sediments into the cave resulting in higher magnetizations (and vice versa). *Zhu et al.,* (2017) also used magnetic mineral concentration in Chinese speleothems to infer about rainfall amount: a high number of storms and consequent extreme rainfall events enhances the flux of pedogenic magnetite from soils to the cave, increasing magnetic mineral quantities. Since the frequency of storms in central China is correlated with El Niño Southern Oscillation (ENSO), the authors used the speleothem and its magnetic mineral content to study the variability of ENSO during the Holocene. As observed in Figure 1.7, high peaks in IRM of the soft component generally coincides with stronger ENSO periods (El Niño) and higher values of carbon isotopes, which is interpreted here as wetter periods.

Interpretation of climate proxies in speleothems is a very complex issue, and a multi-proxy approach has been suggested to improve the reliability and quality of the data [*Fairchild et al.,* 2012]. Speleothem magnetism brings new clue s to unravel past climate record, but still needs further investigation, notably in different regional and geological settings.

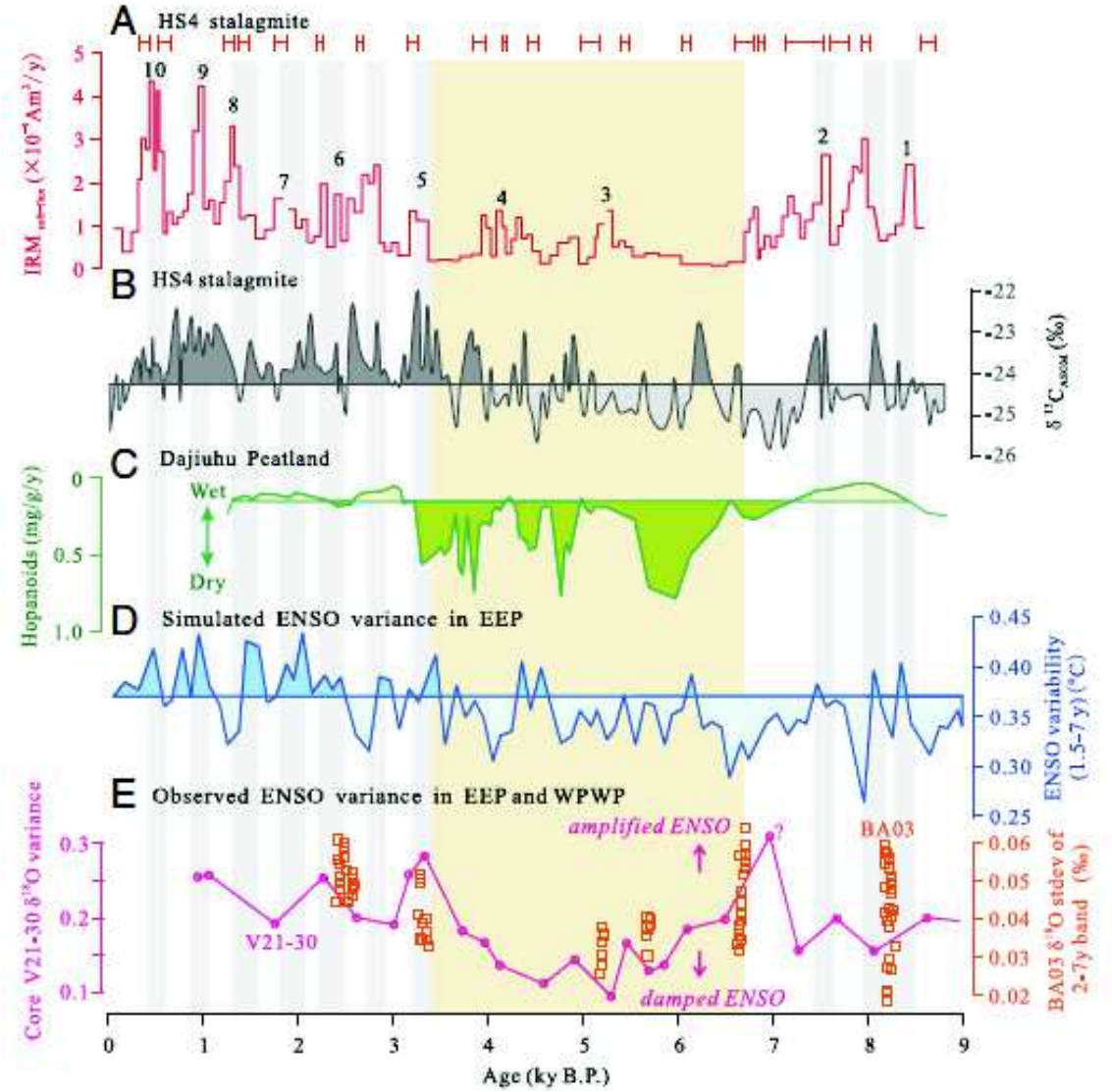

Figure 1.7 Relationship of low-coercive magnetic mineral concentration with climate in central China: high-peaks in IRM soft componentes (A) correlates with higher (less negative) carbon isotope values and stronger ENSO periods, characterized by higher number of storms and consequent incresse in the amount of rainfall and extreme paleoflood events (*Zhu et al.,* 2017).

2. Theoretical principles

2.1 Speleothems

The studied rock formations during this PhD are speleothems (Figure 2.1). For this reason, starting with a general definition and a simple description of how they are formed is required. Speleothems are secondary mineral deposits formed by chemical precipitation of calcium carbonate ($CaCO_3$). They are generally found in karstic environments, characterized by underground drainage systems, like sinkholes or caves, formed due to dissolution of soluble rocks such as limestones or dolomites, for example. Speleothem is the general term used to define all cave mineral deposits types. Stalactites, stalagmites, columns or flowstones are just a few examples of hundreds of variations of cave mineral deposits. The vast majority of speleothems are composed by $CaCO_3$, in form of calcite or aragonite crystals. The rainwater becomes more acid, with lower pH, after reacting with soil's CO_2, according to the following equation:

$$H_2O + CO_2 \rightarrow H_2CO_3$$

As the acid water travels trough the calcium carbonate bedrock, it dissolves the rocks via the equation:

$$CaCO_3 + H_2CO_3 \rightarrow Ca^{2+} + 2\,HCO_3^-$$

Once the water reaches the cave, it loses the CO_2 through degassing to equilibrate the partial pressure of CO_2 in the cave atmosphere, which drives precipitation of $CaCO_3$:

$$Ca^{2+} + 2\,HCO_3^- \rightarrow CaCO_3 + H_2O + CO_2$$

Speleothems may grow through thousands of years, although not necessarily at the same rate. Over time, changes in climate, in the environment and morphology of the caves, water courses and several other factors may lead to variatiations in the speleothem's growth rate. Some speleothems even present long hiatus in time and others have not grown to this day. If a speleothem section is cut, it is possible to observe the growth layers, similar to tree rings. Naturally, the growth layers age increase from the speleothem surface to the interior. Speleothems can be accurately dated at several growth layers, so that it is possible to estimate an age model for the whole speleothem. By collecting several data along a speleothem growth axis, it is possible to study its variation during a certain time interval with a very high resolution. For example, carbon or oxygen isotopic data profile provide important information about the past climate of the Earth since one of the most important factors controlling it is climate (temperature or amount of precipitation). In fact, speleothems are

considered by scientific community as important climate archives of the Earth, but their potential does not end there. A few studies indicate that speleothems may also provide information about the past geomagnetic field, which is one of the major discussions during this PhD.

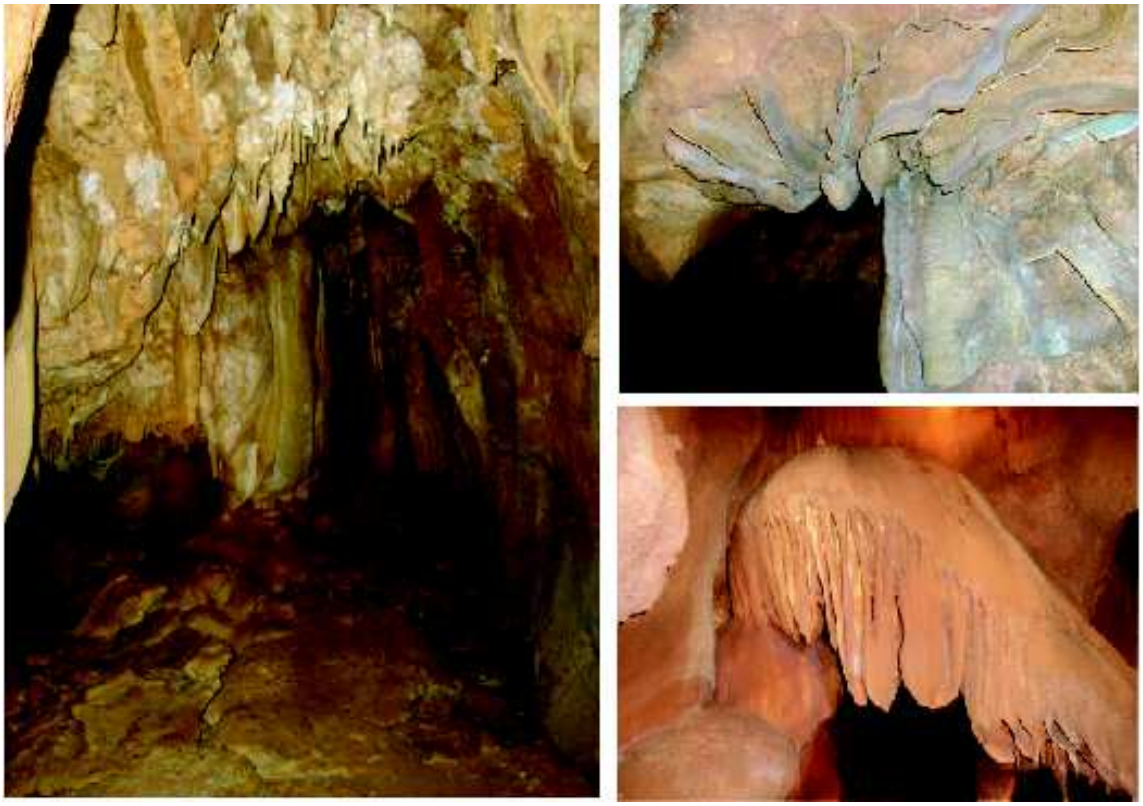

Figure 2.1 Photos of some mineral cave deposits (speleothems) from Excentricas Cave (Algarve, Portugal).

2.2 Geomagnetism

The main focus of my PhD is the magnetism in speleothems, particularly the reconstruction of the past Earth's Magnetic Field. Thus, understanding the most basic definitions and equations in geomagnetism and paleomagnetism is required.

2.2.1 The Earth's Magnetic Field

The first signs of the existence of a magnetic field on Earth were discovered by the Chinese about two thousand years ago when they realized that a magnet tended to align in the north-south direction. Since then, much about the Earth's magnetic field has been discovered and documented. The surface geomagnetic field, *H*, can be defined as a three-dimensional vector

at any location on the Earth, characterized by a vertical (H_v) and horizontal (H_h) components, and an intensity as follows:

$$H_v = H\,sin(I)$$

$$H_h = H\,cos(I)$$

Where I is the magnetic inclination, the angle of H with the horizontal plane. The horizontal component is divided in the East (H_E) and North (H_N) components:

$$H_N = H\,cos(I)\,cos\,(D)$$

$$H_E = H\,cos(I)\,sin\,(D)$$

Where D is the magnetic declination, defined as the angle of H_h with the geographic north. The total intensity is given by:

$$H = \sqrt{H_V^2 + H_N^2 + H_E^2}$$

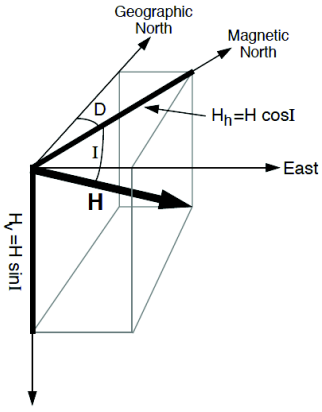

Figure 2.2 Description of the magnetic field H (from *Robert Butler*, 1992).

Magnetic declination values range between 0º and 360º, positive clockwise, while magnetic inclination range between -90º and 90º, and is positive downward. The magnetic field direction is commonly described by its declination and inclination values. Figure 2.2 resumes the standard definition of the geomagnetic field.

The Earth's magnetic field at the surface can be approximated by a magnetic field of a giant magnetic dipole located at the center of the Earth aligned with its rotational axis, which is called Geocentrical Axial Dipole (GAD) field. The present geomagnetic field is naturally more complex than the simple GAD model, attested by the fact that the real geomagnetic poles do not coincide with the geographic poles, as expected for the GAD model. For this reason, the model should be improved to an inclined geocentric dipole. The inclined GAD model that better describes the Earth's present magnetic field has an angle of about 11.5º with the rotation axis, and explains around 80 to 90% of the surface magnetic field. The remaining part of the magnetic field is called the non-dipolar field, which is determined by subtracting the best-fitting inclined GAD approximation to the observed magnetic field.

The geomagnetic field is continuously changing in several timescales, from milliseconds to millions of years. The shorter timescale variations are mainly due to currents in the ionosphere and magnetosphere. The solar wind, which carries charged particles, varies in density, temperature and speed, resulting in small diurnal fluctuations of the geomagnetic field at surface. Changes with timescales of one year or more are thought to reflect changes in the Earth's interior, particularly in the outer core, and are referred as Paleosecular variation (PSV). It is generally accepted that electric currents due to convection (heating transfers) in the liquid outer core generate the geomagnetic field, but the knowledge about the origin of the Earth's magnetic field is still in great development. The study of PSV is therefore object of intense research at present. Important geomagnetic field changes may also occurs in timescales of millions of years: geomagnetic reversals, when the north and south poles trade places, have been occurred several times in Earth's history. How is it possible to know the existence of such events? They have been recorded in rocks. The study of the past geomagnetic field recorded in rocks has been object of intense research for a long time and is called paleomagnetism.

2.2.2 Magnetization in rocks

In paleomagnetism, one of the fundaments is that some rocks possess the ability to record the Earth Magnetic Field at the time they were formed. The first question is how does that happen. To answer this question, we need to understand the concept of magnetic dipole moment, or simply magnetic moment, *M*. The magnetic moment can be defined referring to a pair of magnetic charges or to a loop of electric current. In magnetization of rocks, it is convenient to consider the magnetic moment resulting from a pair of magnetic charges. So, the magnetic moment is proportional to the magnitude of charge *m* and an infinitesimal distance vector *I* between the plus and minus charges.

$$M = m\,I$$

When exposed to a magnetic field *H*, a force experienced by a magnetic charge with certain intensity and direction, the magnetic moment *M* tends to align with the magnetic field. The potential energy of this alignment is defined as follow:

$$E = -MH\cos\theta$$

Where θ is the angle between the magnetic moment *M* and the magnetic field *H*. Note that the minimum energy configuration is achieved when $\theta = 0°$, or, in another words, when *M* and *H* are parallel.

Almost all rocks in the Earth contain some ferromagnetic minerals, so they contain atoms with magnetic moments, which will align with the Earth Magnetic Field at the moment of the rock formation, when they are free to rotate. The total magnetization of a rock, *J*, is defined by the net magnetic moment per unit volume. In a single rock, *J* is calculated by the sum of the magnetic moments contained in the rock divided by its volume *V*:

$$J = \frac{\sum_i M_i}{V}$$

There are basically two types of magnetization: induced magnetization J_i and remanent magnetization J_r. The induced magnetization is the magnetization acquired by a rock when exposed to a magnetic field *H*. J_i is proportional to the magnetic susceptibility χ, which may be interpreted as the "magnetizability" of the rock.

$$J_i = \chi H$$

It results from the summed contributions of diamagnetic, paramagnetic and ferromagnetic materials composing the rock. Paramagnetic (diamagnetic) material acquires a weak magnetization in the same (contrary) direction of an external magnetic field, while it's being applied, but loses the magnetization when the field is removed. Ferromagnetic minerals, usually dispersed in a paramagnetic or diamagnetic matrix of the rock, have a very high magnetic susceptibility. The magnetic susceptibility of a rock containing more than 0,1% of ferromagnetic minerals in the total volume is dominated by their fraction. Ferromagnetic minerals may also have the ability to keep the magnetization after the external field is removed, a characteristic responsible for the remanent magnetization of rocks.

The remanent magnetization J_r is the magnetization recording of the past magnetic fields that have acted in the rock. When a magnetic field *H* applied in a rock is removed, the ferromagnetic minerals are able to keep the magnetization for a certain time *t*, on contrary to paramagnetic or diamagnetic materials. After the magnetic field removal, J_r decays exponentially, but depending on the magnetic grains size, it can be preserved through millions of years. Magnetic grains with diameters higher than 10 μm create several magnetic domains as it decreases magnetostatic energy, so that we refer to them as multi-domain (MD) grains. When magnetic grain size decreases, the number of magnetic domain decreases as well, until the grain becomes so small that dividing the grain in several magnetic domains is not energetically favorable anymore. In this case, the grain contains only one domain, and it is referred as a single-domain (SD) grain [*Dunlop and Ozdemir,* 1997; *Liu et al.,* 2012].

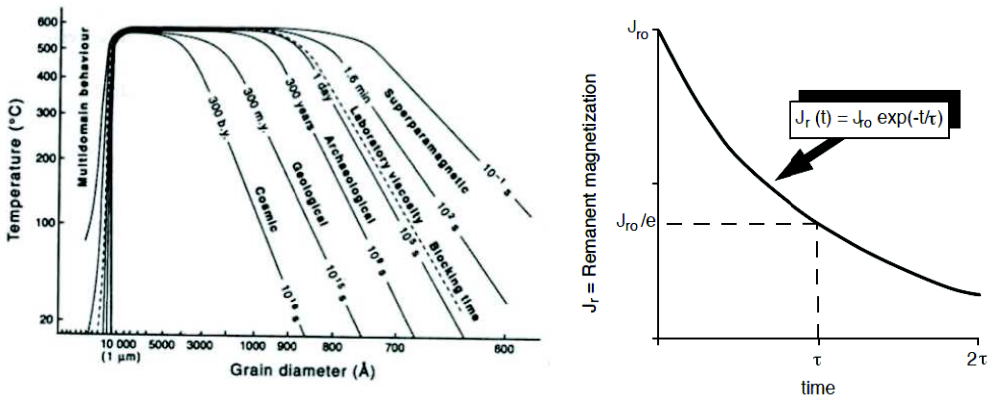

Figure 2.3 Amount of time by which a magnetic grain carry a remanent magnetization, in function of its size and temperature (from *Robert Butler*, 1992).

As we observe in Figure 2.3, MD grains do not have the ability to retain the induced magnetization for a considerable time after the removal of the magnetic field. On the other hand, SD grains may preserve a remanent magnetization for a long time. The law expressing the remanent magnetization J_r of SD grains in function of time t, also represented in Figure 2.3, is:

$$J_r = J_{r0}\, e^{\frac{-t}{\tau}}$$

Where J_{r0} is the initial remanent magnetization and τ is the relaxation time, after which J_r decays by a factor of e (J_{r0} / e), expressed as follows:

$$\tau = \frac{1}{C}\, e^{\frac{v\, h_c\, j_s}{kT}}$$

Where C is a frequency factor (~10^{-8} s^{-1}), v is the volume of SD grain, h_c is the microscopic coercive force, j_s is the saturation magnetization of the ferromagnetic grain, and kT is the thermal energy. By analyzing the equation, we observe that for a SD grain, the decrease of grain volume results in a decrease of the relaxation time. Eventually, the grain becomes so small that keeps its remanence for less than 1.5 minutes. After that limit, the grains are called superparamagnetic grains. The relaxation time also depends on temperature. It gradually decreases with the increase of temperature, but the decay is slow and hardly noticed until ~450ºC. The temperature at which a SD grain starts to exhibit a paramagnetic behavior (very low relaxation time) is called blocking temperature. Considering that the ambient temperatures in our planet are much lower than usual blocking temperatures, SD grains are

generally able to record magnetic fields to which they were exposed, for long periods of time. The remanent magnetization present in a rock before any laboratory treatment is called Natural Remanent Magnetization (NRM). The NRM acquired during the formation of the rock is called primary, and depends on the geomagnetic field and the geological nature of the process. In some rocks, secondary NRM components may be recorded subsequent to rock formation, contaminating or even destroying the primary NRM, which is the component sought in most of paleomagnetic investigations. The natural processes that produce a remanent magnetization in rocks will be summarized in the next sub-chapters.

2.2.3 Thermal Remanent Magnetization (TRM)

The most common rocks used in paleomagnetic studies are volcanic, especially basalts. They are rich in iron oxides, what generally results in very high, easily measured and stable remanent magnetizations. These rocks are formed at very high temperatures, at which the iron oxides do not exhibit a ferromagnetic behavior. During the cooling process, when the rock reaches the temperature at which its iron oxides start having ferromagnetic characteristics (Curie temperature), their magnetic moments will align with the ambient magnetic field (which is naturally the Earth's magnetic field). After the temperature cool bellow the blocking temperatures of the SD grains, generally close to Curie temperature, their relaxation time starts increasing incredibly fast, acquiring a magnetic remanence that can be stable over millions or even billions of years.

2.2.4 Detrital Remanent magnetization (DRM)

Another natural mechanism capable of producing a NRM occurs when ferromagnetic mineral grains settle into a sedimentary matrix. In theory, these grains orientate with the Earth's magnetic field during the deposition and before the consolidation of the sedimentary rock. The most used model to explain DRM (Figure 2.4) illustrate light detrital material (silts, clays) resultant from erosion, containing ferromagnetic minerals, falling in a deep water column, aligning with the geomagnetic field before settling in the bottom of the sea (or lake). Paleomagnetism in sedimentary rocks is usually more challenging than in volcanic rocks. Generally, concentration of ferromagnetic minerals in sediments is considerably lower, so that the NRM intensity is weaker and sometimes harder to detect. Additionally, several problems may affect the reliability of NRM recorded direction. Distortion during sampling (drilled cores), bioturbation (plant or animal activity in the bottom of the sea/lake that mix the sediments) or diagenesis, for example, may compromise the primary NRM. Shallowing

inclination is also a process affecting several sediment magnetic records that deserves particular attention. In marine/lacustrine sediments, it is caused by the weight of sediments deposited on top of a particular layer that shallows the inclination of the magnetic vector (Figure 2.4). For this reasons, paleomagnetic directions obtained from sedimentary rocks are usually more difficult to obtain and interpret, with higher uncertainties.

The acquisition of magnetic remanence in speleothems is a DRM, but its mechanism differs from the model illustrated in Figure 2.4. In the case of speleothems, there is not a deep column water where magnetic grains slowly fall until they reach the bottom. The magnetic grains, present in the soils above the cave, are transported by water trough fissures in the calcareous rock systems until they reach the speleothem surface. The magnetic grains align with the geomagnetic field and are locked when the calcite crystals grow and are imprisoned in the calcite matrix. This acquisition mechanism prevents speleothems from having some of the problems of lacustrine/marine sediments DRM. There is no distortion during sampling, bioturbation or shallowing inclination due to compaction since speleothems calcite matrix is more compact and solid. For this reasons, paleomagnetic directions obtained from speleothems are generally more stable, with lower errors, when compared to other sedimentary sources, despite the problem of low concentration in ferromagnetic mineral remains in some cases.

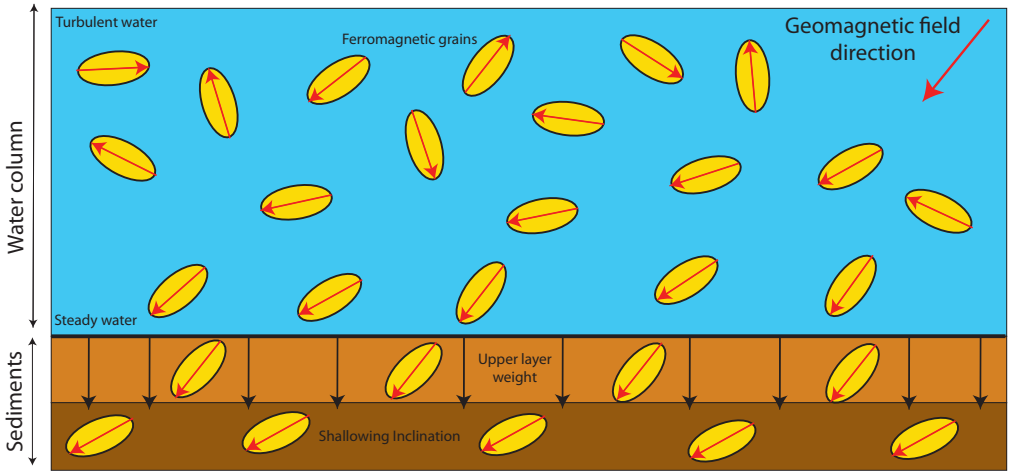

Figure 2.4 Simple model for acquisition of detrital remanent magnetization in sediments. The magnetic moments of the ferromagnetic grains tend to align with the geomagnetic field as they fall in the water column. The weight of the upper layers of sediments may affect the original magnetic direction due to shallowing inclination.

2.2.5 Chemical Remanent magnetization (CRM)

Chemical changes in rocks that result in the formation of new ferromagnetic minerals, or alteration of one ferromagnetic mineral to another, may lead to the acquisition of a new magnetic remanence, called chemical remanent magnetization (CRM). In some cases, when this alteration occurs soon after the deposition, or when there is no significant change of crystal structure (keeping the magnetic remanence of the original grains), this NRM may be considered primary. For example, red bed's hematite is thought to be formed shortly after deposition, although the time of acquisition of magnetic remanence in red sediments is still in debate. However, when CRM is acquired long after deposition, it is considered a secondary magnetic component. In marine sediments, processes of diagenesis (formation of Fe-sulfides and MnFe-oxides) may generate a secondary CRM.

2.2.6 Viscous Remanent Magnetization (VRM)

After the rock is formed and acquired the primary magnetic remanence, it is still exposed to the geomagnetic field, which is continuously changing. VRM is a remanent magnetization that is gradually acquired during this exposure to the geomagnetic field long after the formation of the rock. It is therefore considered a secondary magnetization, a contamination undesirable for paleomagnetic studies. For a better understanding, the concept of magnetic coercivity should be introduced. The coercivity of a ferromagnetic grain, expressed in the same units as the magnetic field (Tesla), is a measure of its resistance from being magnetized when exposed to a certain magnetic field. For example, a magnetic grain with a coercivity of 15 mT will retain its primary NRM if exposed to magnetic fields weaker than 15 mT, but will acquire a VRM (secondary magnetization) for higher intensity magnetic fields. In nature, as the geomagnetic field direction and intensity vary in time, the ferromagnetic grains with lower coercivities or with short relaxation times (MD grains, for example) are susceptible of being remagnetized, acquiring a VRM component. This can be resolved in the large majority of cases, as explained in the methods chapter.

2.2.7 Characteristic Remanent Magnetization (ChRM)

On contrary to the remanent magnetizations referred before, ChRM is not a particular natural process of magnetic remanence acquisition. However, its concept should be introduced since the term will be used several times. As already stated, NRM may contain more than one component. Some components (VRM for example) are easily removed as they are recorded by low coercivity grains, and can be called low-stability components. On the other hand, the

highest stability component of the NRM is usually referred in paleomagnetism as ChRM. It is not necessarily a primary NRM, because there is a possibility that the rock had been totally remagnetized. The use of this term is just to avoid the association of a principal magnetic component measured in a rock to a primary origin, what naturally and desirably happens in some cases, but it's not always true.

2.3 Speleothems and Climate

2.3.1 Paleoclimatology

Paleoclimatology is the study of the climate from the past hundreds to millions of years. Given that at that time there were no observations, scientists have been looking for natural archives (called proxies) which possess the ability to record changes of properties with time and can provide information about climate parameters, such as precipitation and temperature. Some of the most common proxies include, for example, tree rings, ice cores, sediments or corals. By studying the width, physical or chemical properties in each layer, scientists can deduce about climate conditions present when the layer formed. If correctly dated, the evolution of climate within a certain age interval can therefore be inferred.

The construction and interpretation of long-term climate records are important to understand how it has been varying through Earth's history, which is crucial to study the factors controlling the climate on our planet and what may be expected for the future. Considering the actual discussion of climate change and its acceleration due to anthropogenic factors, it is still more important to evaluate the climate before human perturbations.

2.3.2 Speleothems as a climate proxy

Speleothems have been used as a climate archives in several studies. Paleoclimate reconstructions (precipitation and temperature), information about climate variability during geomagnetic excursions [*Rossi et al.,* 2014], paleofloods due to extreme rainfall events [*Dasgupta et al.,* 2010; *Gázquez et al.,* 2014], atmospheric circulation patters in the past (such as monsoons [*Strikis et al.,* 2011], El Niño Southern Oscillation [*Zhu et al.,* 2017], North Atlantic Oscillation [*Luetscher et al.*, 2015]) and even solar activity [*Knudson et al.,* 2012; *Duan et al.,* 2014] are some examples of what has been obtained using different speleothem's climate proxies. The possibility of combine several different climate proxies parameters in a speleothem constitute a great advantage over other climate archives.

Speleothems commonly presents continuous episodes of growth, with thousands of years of duration, and the recent development of sampling and measurement techniques allow very high time resolutions which makes it possible to study the annual variability in some cases. Speleothems can also be accurately dated by U-series techniques, which is far better than any dating performed in other materials capable of holding long records, are relatively protected from erosion and are widespread around all continental areas in the world.

The most widely used climate proxies obtained from speleothems are oxygen and carbon isotopes ($\delta^{18}O$ and $\delta^{13}C$ respectively), but researchers are now obtaining alternative parameters such as growth rate variation, magnetic susceptibility, trace elements (e.g. Mg, Sr, Fe, Al, P), detrital clay-sized particles quantities in layers and even pollens. Considering there are many possible factors, including local context, controlling $\delta^{18}O$ and $\delta^{13}C$, the interpretation of their time-series are difficult and often inconclusive. There is still insufficient knowledge about the meaning of the proxy variables, but the combination of several proxies may lead to a better understanding and a improved calibration of recorded climatic signal.

2.3.3 Oxygen and Carbon Isotopes

In this work, oxygen and carbon isotope data are presented. Isotopes are chemical elements that contain the same number of protons but differ in the number of neutrons in their nuclei. There are three different oxygen isotopes: ^{16}O, ^{17}O and ^{18}O. They all have 8 protons, but ^{16}O has 8 neutrons, ^{17}O has 9 neutrons and ^{18}O contains 10 neutrons. This results in different weights between the isotopes, with those with more (less) neutrons being heavier (lighter). The same logic is valid for the carbon isotopes, which are two: ^{12}C and ^{13}C. The different weight between isotopes leads to a fractionation during natural processes that affect their relative quantities. The water phase transition processes are good examples: when ocean water evaporates, lighter ^{16}O is preferentially uptaken, while heavier ^{18}O is left behind. In condensation process (and precipitation), the heavier ^{18}O tends to fall before ^{16}O. This results in enriched ^{18}O water in areas with more evaporation than precipitation, and the opposite in areas with more precipitation. The measurement of isotope values of a sample is made in comparison with a sample with known values, called reference standard. Oxygen and carbon isotopes, expressed as per mil (‰), are defined as follows:

$$\delta^{18}O = \left(\frac{\left(\frac{O18}{O16}\right)sample}{\left(\frac{O18}{O16}\right)standard} - 1 \right) \times 1000$$

$$\delta^{13}C = \left(\frac{\left(\frac{C13}{C12}\right)sample}{\left(\frac{C13}{C12}\right)standard} - 1 \right) \times 1000$$

Oxygen isotope values in the environment depend on temperature, rainfall amount and atmospheric circulation (source of rainfall) (*McDermott,* 2004). Speleothems are formed through the precipitation of calcite dissolved in drip water sourced from rainfall that fell on the ground and infiltrated through the soil and karst system. Therefore, oxygen isotopes are trapped in speleothem's cristal structure when they form. By analyzing them we can know about past environmental conditions, since the oxygen isotope composition of the speleothem is influenced by the isotope composition of the rainfall. In a specific location, if the process controlling the isotope composition of the rain is known (temperature, rainfall amount or rain source), then a local speleothem can record changes in this process. However, the interpretation of oxygen isotope values is not so easy, since there are other processes that can influence the isotopic composition of the speleothem (*Lachniet*, 2009). Through the speleothem's formation, the release of CO_2 contained in dripwater and the precipitation of $CaCO_3$ can lead to another oxygen isotope fractionation which will change the isotopic composition of rainfall. Additionally, karst systems are often composed by large aquifers that store water for several years. The mixing of this water with the rainfall may lead to an averaged isotopic value recorded by the speleothem through many years.

Carbon isotope values are even more difficult to interpret, since they are influenced and dependent of many processes. Stable carbon isotopes found in speleothems are derived from CO_2 released by plants during photosynthesis to the soil, decay of dead plants in the soil and from dissolved $CaCO_3$ in dripwater. The photosynthetic pathway of the vegetation above the cave (C3 – used by trees and grass/shrubs in cold regions; C4 – used by shrubs and grass that grows in arid and hotter environment) strongly affects the $\delta^{13}C$ signature. As a consequence, researchers usually interpret carbon isotope values as the vegetation cover, what can be linked with climate: lower $\delta^{13}C$ is commonly thought to result from higher vegetation density driven by a warmer/wet climate, while higher $\delta^{13}C$ reflects cooler/drier conditions what drives less vegetation cover. However, several other factors possibly affects carbon isotope signal, such as the atmospheric CO_2 isotope composition, inorganic carbon derived from bedrock ($CaCO_3$ dissolved in dripwater), production of CO_2 from the soils and degassing of CO_2 during precipitation of calcite. As well as with oxygen, carbon isotopes also depend on local conditions. The percolating pathway and the time residence of water in the soil layer for example, may play an important role on $\delta^{13}C$ signature in speleothems.

2.3.4 Speleothem's magnetism and climate

In a relatively recent past, some studies have successfully linked past climate to some magnetic parameters obtained from caves. Particularly, magnetic susceptibility obtained from cave sediment sequences have been documenting known past climate events and are well correlated to other climate proxies [*Elwood et al.*, 2001; *Elwood et al.*, 2004; *Elwood and Gose*, 2006]. However, magnetism in speleothems and its relationship with climate is in early stages of development. *Bourne et al.* (2015) obtained profiles of the soft and hard components of IRM (indicative of magnetite and hematite/goethite concentrations, respectively) and compared them with Oxygen and Carbon isotope profiles from the same stalagmite, collected in Virginia (USA). They observe a significant positive correlation ($r = 0.5$) between $\delta^{18}O$ and IRM soft component (magnetite), which is interpreted as a relationship between the total flux of magnetic particles to amount of precipitation (increased precipitations enhances pedogenic magnetite production in the soils and transport to the cave). *Jaqueto et al.* (2016) conducted a similar study in a stalagmite from Brasil, and observed that generally the more negative (positive) oxygen and carbon isotope values correspond to lower (higher) values in magnetization. According to the authors, the periods with higher $\delta^{13}C$ and $\delta^{18}O$ (and higher magnetization) coincide with drier periods, what is contrary to conventional thinking that enhanced magnetite production in the soils during wetter periods controls the magnetic input in the cave. Thus, the authors suggest that magnetic concentration in the studied stalagmite is controlled by the soil erosion above the cave: drier (wetter) periods favour less (more) vegetation cover what results in more (less) erosion and more (less) magnetic particles transported to the cave by dripwaters. This interpretation is supported by evidences that changes in $\delta^{13}C$ in soils from Brasil are usually driven by changes in the relative quantities of C3 and C4 plants: in drier periods, C4 plants prevail, what increases $\delta^{13}C$ values in the soils.

In conclusion, a few recent studies introduced magnetic mineral concentration as a climate proxy that can be obtained from speleothems. The input of magnetic particles in the cave is likely to be controlled by vegetation cover and/or precipitation amount, but the local conditions may influence how they are related. More speleothems should be analyzed in order to better understand the processes that influence magnetic particles concentration and how we can relate it to climate.

3.Methodology principles

As already stated, one of the main objectives of this PhD is to study the reliability of the magnetic remanence recorded in speleothems. In this chapter, the used magnetic methods and techniques are listed, with a theoretical introduction and an explanation of how they were applied concretely in this PhD.

3.1 Alternate Field (AF) Demagnetization

In the previous chapter, there is a general description of how rocks can record a remanent magnetization. The following is summarized how we can calculate the magnetic direction recorded by a rock. There are three possible methods: Alternate field (AF) demagnetization, thermal demagnetization and chemical demagnetization (rarely used). Here, the applied method in the studied speleothem was the AF demagnetization. It is based on the application of an alternate (sinusoidal) magnetic field with linear decrease in magnitude in time. The alternate field points to opposite directions alternately, cancelling the net magnetic moment of the magnetic grains with coercivity (h_c) lower than the applied field magnitude. Thus, the magnetic remanence recorded by the magnetic grains with h_c lower than the initial (and maximum) field magnitude (H_{AF}) will be erased, while NRM carried by grains with $h_c \geq H_{AF}$ remain. The advantage of AF demagnetization method is that it is very effective in separating secondary components (VRM) from the ChRM. The method consists in starting to apply AF with weak magnitudes, in order to erase only the NRM carried by the low coercivity grains, more susceptible to acquire a VRM. The magnitude of the applied AF is progressively increased until the total magnetization is almost removed. The objective is to estimate the direction of the ChRM, the highest stability component that corresponds to the magnetization recorded at the time the rock was formed if no remagnetization has occurred in the meantime.

Figure 3.1 shows an example of AF demagnetization. The first step is to measure the magnetic vector recorded (direction and intensity) in a sample, before any laboratory experience, using a magnetometer. The result is called NRM. Then we apply to the sample successive alternate fields, with progressively higher magnitudes (called demagnetization steps), until most of the original magnetization is removed. Between each demagnetization step, the magnetic vector is measured. The results are generally displayed as illustrated in figure 3.1. The stereographic projection (figure 3.1 A) shows the evolution of the magnetic vector direction evolution during the AF demagnetization process. The magnetic declination is the angle with the North, read in clockwise direction (0 to 360º), while magnetic inclination ranges from 0º (center of the stereograph) to 90º (extremity of the stereograph) in this example, as the points are solid. If the points were opened, the magnetic inclination

would be read as negative (-90º to 0º). The orthogonal projection (figure 3.1 B) joins two different projections of the magnetic vector into a single vector component diagram: the projection of the vector onto the horizontal plane, and the projection onto a vertical plane, oriented north-south. It allows the user to read the both magnetic direction and intensity, and is especially useful to identify different magnetic components. The last graphic (figure 3.1 C) shows the evolution of the magnetization vector intensity along the process. In the example used in figure 3.1, show that magnetic declination remains nearly constant (NNE) for all demagnetization steps, but magnetic inclination decreases progressively until demagnetization step 3, stabilizing the magnetic direction on further steps. This is generally indicative of the presence of a secondary component (VRM), which in this case is completely erased after the step 3. In the orthogonal projection the presence of VRM component is clearly identified. The NRM vector is represented and corresponds to the sum of all components (VRM+ChRM), first measured before any demagnetization process (step 0). The VRM component is progressively removed as the magnitude of AF increases, until step 3. Between steps 3 and 6, the magnetic vector direction stabilizes into a well-defined direction, the high-stability component and normally assumed primary magnetization (ChRM). Naturally, the intensity of the magnetic vector decreases between steps 3 and 6 since the AF magnitude is progressively increased in each step, cancelling the magnetic moment of the grains with coercivities below that magnitude. This is also observed in Figure 3.1 C, where it is possible to notice that after step 6 the magnetic vector intensity decayed to nearly 20% of the original.

After obtaining the magnetic data with the AF demagnetization process, treatment of data is required to determine the final magnetic vector. This is usually performed by Principal Component Analysis (PCA), a rigorous quantitative technique that determines the direction of the best-fit line of a sequence of selected data points. Additionally, PCA provides maximum angular deviation (MAD) values for evaluation of the best-fit line precision. The set of data points with lower MAD values are generally chosen to determine the ChRM, provided that it contains a reasonable amount of data points. Usually, points obtained in the initial demagnetization steps are excluded from the best-fit line calculation since they are normally affected by undesirable secondary components, although it depends on the data.

The magnetic remanences of speleothem samples were measured using a JR6 spinner magnetometer (sensitivity of 2.4×10^{-6} A/m), while a LDA-3A demagnetizer induced the alternate fields for progressive demagnetization of the samples. After initial measurement of

the sample NRM, remanent magnetizations were measured after each demagnetization step (2, 4, 6, 8, 10, 12, 14, 16, 18, 20, 22 and 25 mT), totalizing 12 points. The ChRM vectors were determined with PCA technique, using the Remasoft software developed by AGICO.

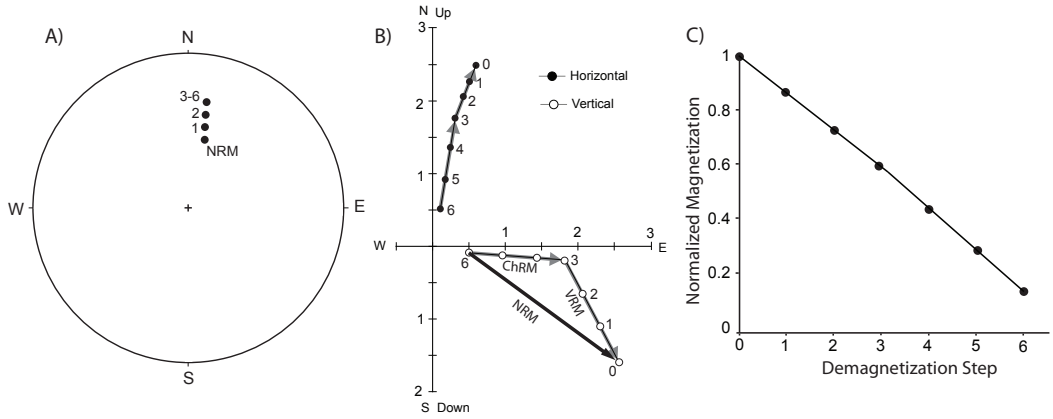

Figure 3.1 A) Equal-area projection of the magnetic vector direction during AF demagnetization process. The numbers indicate the demagnetization step. B) Horizontal (black) and vertical (white) projections of the magnetic vector. C) Magnetization of the sample (normalized) versus demagnetization step. (Figure modified from *Robert Butler*, 1992).

3.2 Isothermal Remanent Magnetization (IRM)

IRM is a remanent magnetization acquired by a rock when exposed to strong magnetic fields of short duration at constant temperature. It is generally imparted in laboratory by exposure to a magnetic field generated by an electromagnet, but secondary NRM components can be formed when a rock is struck by lightning. IRM is normally used as a technique for studying the magnetic mineralogy of a rock. It is especially useful to identify and separate low and high coercivity magnetic minerals, by analysis of IRM acquisition curves. Before imparting an IRM to a sample, any other remanent magnetization should be erased, so that in its initial state the magnetization is almost zero. The sample is then exposed to a direct magnetic field and the acquired IRM is measured, before applying another magnetic field, with increased intensity, and successively. This procedure allows building an IRM curve, representing the acquired magnetization in function of the applied magnetic field intensity. The shape of the curve will depend on the coercivity of the minerals composing the sample. If low coercivity minerals dominate its content, sample magnetization will increase faster before eventually reach magnetic saturation, SIRM (when all ferromagnetic grain have been magnetized, so that magnetization of sample can not increase). On contrary, if the content in high coercive grains is significant, the magnetization curve will increase at lower rate and the saturation may not be achieved (or only at high magnetic fields).

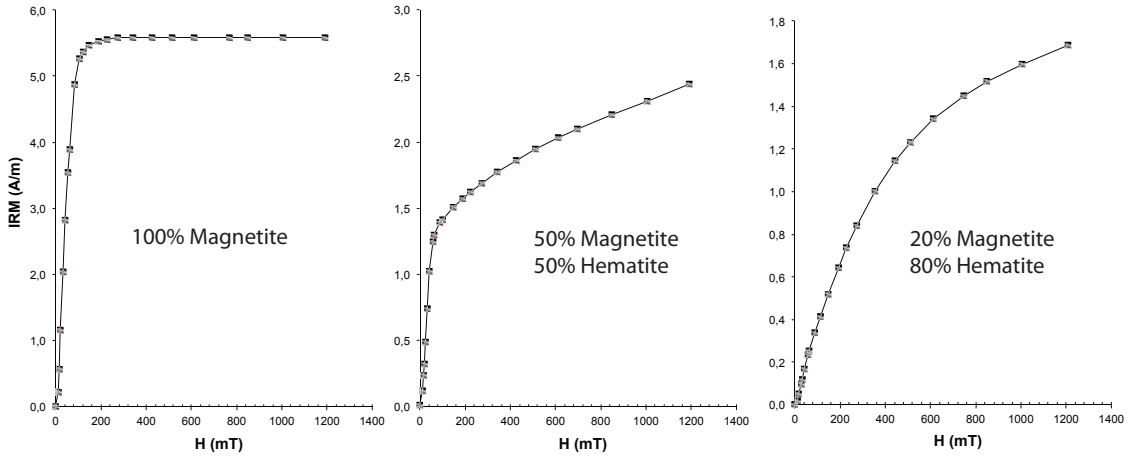

Figure 3.2 Typical IRM curves for three different magnetic mineral contribution ratios.

In Figure 3.2, three examples of IRM curves are illustrated, the first of a sample with major concentration in low coercivity minerals, the second with similar contribution of both low and high coercivity magnetic grains, and the third with stronger contribution of high coercivity grains. In the first case, the sample rapidly increases its magnetization at weaker magnetic fields and reaches SIRM. This curve shape typically corresponds to a magnetite rich sample, a low coercivity mineral that sometimes can be saturated at 100 mT fields. In the second case, we observe an early quick and strong magnetization, evidence of magnetite presence, but the curve do not stabilize and fails to reach saturation, which is indicative of a coarser magnetic mineral, generally associated to hematite (or in some cases, goethite). Finally, the third example is a case where hematite, a high coercivity mineral, dominates the magnetic contribution. The magnetization is acquired at slower rates for lower magnetic fields, and SIRM is not reached in the range of applied fields.

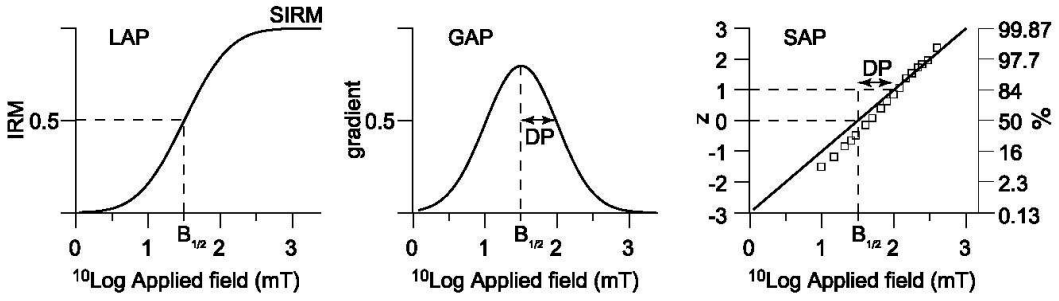

Figure 3.3 CLG treatment of a IRM acquisition curve, expressed in a linear scale (LAP), as a gradient (GAP) and in a probability scale (SAP) (*Kruiver et al.,* 2001).

The shape of the IRM curve can provide clues about the nature of magnetic mineralogy of a sample, but its treatment using Cumulative Log-Gaussian (CLG) functions allows individual separation of all magnetic components contributing to sample IRM and more information. CLG treatment is based on the IRM curve fitting versus the logarithm of the applied field. The acquisition curve is expressed in three different ways, represented in Figure 3.3: linear acquisition plot (LAP), on a linear scale; gradient acquisition plot (GAP), on a gradient scale; standardized acquisition plot (SAP), on a probability scale.

CLG analysis allows to better characterize the magnetic mineral population trough specific given parameters: i) SIRM for all components, ii) the mean coercivity of a magnetic component ($B_{1/2}$), expressed as the magnetic field at which half of the SIRM is reached, iii) dispersion parameter (DP), given by one standard deviation of the logarithmic distribution and representing the width of the distribution. Typical values of these parameters are known for each magnetic mineral, what makes CLG treatment a powerful tool for identifying magnetic minerals in a rock sample.

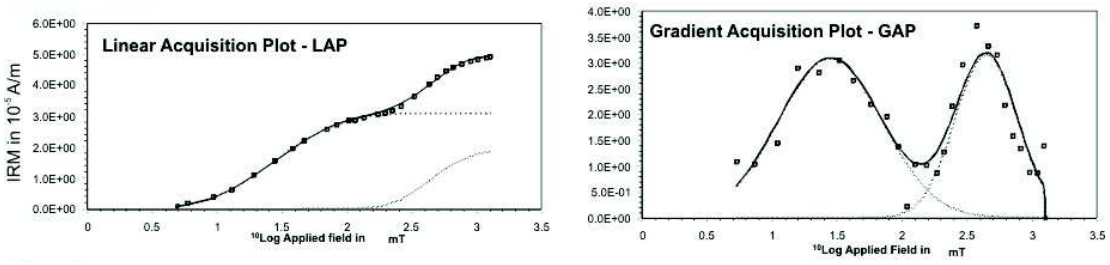

Figure 3.4 Example of CLG treatment of IRM data acquired in a orthogneiss sample. Two magnetic components were identified, probably corresponding to magnetite and goethite (from *Kruiver et al.,* 2001).

A practical example of CLG treatment is illustrated in Figure 3.4. The points are the IRM data while the curves represent the model considered to better fit the data. In this case, two magnetic components are clearly identified. The first component is a low coercivity phase, with $B_{1/2}$ ~1.5, while the second component is a hard coercivity component, with $B_{1/2}$ ~2.7 and shorter DP. The parameter values for the component 1 are typical for magnetite, while the component 2 is more characteristic of goethite, although not far from the values of hematite. Note that CLG allows the identification of minerals in unsaturated samples, and also estimates the contribution (%) of each component.

In the laboratory of magnetism of Instituto Dom Luiz, University of Lisbon, IRM acquisition is performed using an impulse magnetizer (model IM-10-30). As already stated, magnetic fields with progressively increased intensity are applied to the sample. Between applications

of the magnetic fields, magnetization acquired by the sample is measured using the JR6 spinner magnetometer. In the studied speleothem samples, the applied fields range between 0 and 1000 mT, and the number of data points is recommended to be at least 30, more concentrated at the lower fields, while the sample does not reach saturation. CLG treatment is performed using software developed by *Kruiver et al.* (2001) with the help of the program Max UnMix [*Maxbauer et al.,* 2016]. The IRM data (intensity of applied field and correspondent acquired IRM) is uploaded, and the software calculates and displays the LAP, GAP and SAP graphics. Then, the user try to find the model that better fits the data, by estimations on the number of components, their SIRM, $B_{1/2}$ and DP. Program Max UnMix has the advantage of providing uncertainties of the chosen model, and also suggests an improved model, with lower uncertainty, based on an initial guess of the user. It is is more time consuming, so that in this PhD the chosen program was the software from by *Kruiver et al.* (2001), but some samples were also analyzed by Max UnMix program to compare results and in some cases improve estimations.

3.3 Anhysteretic Remanent Magnetization (ARM)

ARM is a laboratory induced magnetization, by applying a weak direct magnetic field (DC) in the presence of a decaying AF. The physical principle is similar to AF demagnetization: the AF is responsible to cancel the magnetic moments of magnetic grain with coercivity lower than the AF magnitude (H_{AF}), but in ARM the presence of a DC field will induce a magnetization in its direction. In resume, acquisition of ARM curves follows the next steps: 1) Demagnetize the sample to have an initial magnetization close to zero, as recommended for IRM, 2) Define a constant DC field that will be the same in every magnetization applied during the process, 3) Progressively increase the AF intensity, similar to AF demagnetization process, and measure the acquired ARM between each step. The result is a remanent magnetization acquired by the sample due to DC field over the range of coercivities below the peak of the applied AF.

ARM is strongly dependent on the magnetic grain size, so it is commonly used to characterize them and consequently the magnetic domains of a rock. Since ARM acquisition is a process similar to the acquisition of NRM, especially TRM, it is also used as a laboratory analog to study NRM acquisition. Particularly, ARM is sometimes used as a substitute for laboratory TRM to estimate paleofield intensities, eliminating the need of heating the sample and the risk of subsequent chemical alterations. In sediments, ARM is also a normalizing factor used for determination of relative paleointensities (RPI). In this PhD, ARM is used not

only as a normalizing factor, but also to test pseudo-Thellier method in speleothems for RPI estimation. The ARM was imparted in the LDA-3A demagnetizer and measured on JR6 spinner magnetometer.

3.4 Anisotropy of Magnetic Susceptibility (AMS)

Magnetic susceptibility χ has been already defined as the "magnetizability", or a measure of how easily a rock is magnetized when exposed to an external field. However, in nature the intensity of magnetization is not uniform in all directions, which is called anisotropy of magnetic susceptibility. AMS generally occurs due to the crystalline structure of the minerals, resulting a magnetization in specific directions (magnetocrystalline anisotropy) or when the induced magnetization is preferentially oriented along the long axis of the grains (shape anisotropy).

Some techniques to measure and describe the preferential directions of magnetization and the magnitude of anisotropy of a rock have been developed. AMS is determined by applying a magnetic field to a sample and measure the acquired magnetization in six different directions. This allows describing magnetic susceptibility as a second order symmetric tensor that can be geometrically represented as an ellipsoid with three principal axes: the direction of maximum (K_1), intermediate (K_2) and minimum (K_3) susceptibility (Figure 3.5 a). The mean susceptibility K_m is defined by the arithmetic mean of the directional susceptibilities:

$$K_m = \frac{K_1 + K_2 + K_3}{3}$$

Several parameters can also be defined to evaluate the magnetic fabric of a rock, for example:

- P (anisotropy degree): $\boldsymbol{P} = \frac{\boldsymbol{K_1}}{\boldsymbol{K_3}}$
- L (Lineation): $\boldsymbol{L} = \frac{\boldsymbol{K_1}}{\boldsymbol{K_2}}$
- F (Foliation): $\boldsymbol{F} = \frac{\boldsymbol{K_2}}{\boldsymbol{K_3}}$
- T (Shape parameter): $\boldsymbol{T} = \frac{\mathbf{2\ln(K_2) - \ln(K_1) - \ln(K_3)}}{\mathbf{\ln(K_1) - \ln(K_3)}}$

The anisotropy degree P is defined by the ratio of maximum and minimum susceptibilities. Parameters L, F and T are useful to obtain the shape of the magnetic susceptibility ellipsoid. The ellipsoid of an isotropic fabric would be a perfect sphere ($K_1=K_2=K_3$). An oblate fabric has low values of parameter L and high values of F ($K_1 \approx K_2 > K_3$), the opposite of a prolate fabric ($K_1 > K_2 \approx K_3$), as shown by Flinn diagram (Figure 3.5 b). If the three principal

susceptibilities are significantly different, the magnetic fabric is triaxial ($K_1>K_2>K_3$). The T parameter is useful to distinguish oblate from prolate fabrics by the Jelinek diagram (Figure 3.5 c), since positive (negative) values correspond to oblate (prolate) fabrics (*Jelinek,* 1981).

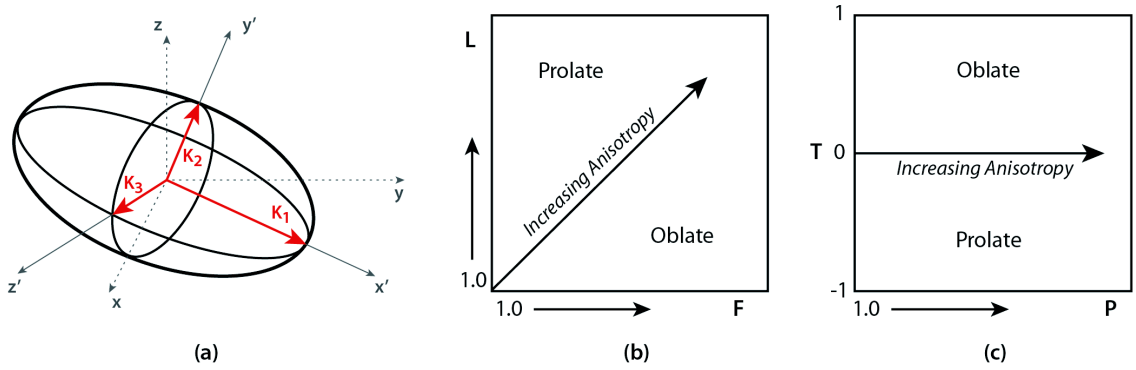

Figure 3.5 (a) Magnetic susceptibility ellipsoid represented in an arbitrary coordinate system, with the three principal axes K_1, K_2 and K_3. (b) Finn diagram, relating parameters L and F. (c) Jelinek diagram relating shape parameter T and the degree of anisotropy P *(image retired from PhD thesis of Marta Neres)*.

Directions of the principal susceptibilities can be plotted in a stereographic projection, similarly to paleomagnetic directions. K_1, K_2 and K_3 are represented by squares, triangles and circles, respectively.

Anisotropy of magnetic susceptibility was measured in several samples during the PhD in the laboratory of magnetism of Instituto Dom Luiz, Faculty of Sciences of University of Lisbon, using a MFK1 Kappabridge from AGICO. The data was processed by Anisoft software, also developed by AGICO.

3.5 Anisotropy of Anhysteretic Remanent Magnetization (AARM)

Magnetic susceptibility is calculated based on the magnetization of a sample while exposed to a magnetic field. As already explained, in the presence of an external field, paramagnetic and diamagnetic material contributes to the magnetic signal. In most cases, this is not a problem since the presence of a reasonable amount of ferromagnetic minerals (at least 0.1% of total volume) overcomes the signal of para-diamagnetic contributions. However, in the case of speleothems, concentrations of ferromagnetic minerals can be very low, and the matrix is calcite (diamagnetic), so that the anisotropy of magnetic susceptibility may not reflect the anisotropy of the ferromagnetic mineral, but the anisotropy of the calcite matrix instead. In order to overcome this difficulty, the anisotropy study of a remanent magnetization is conducted, since ferromagnetic minerals are the only contribution possible in this case. It is possible to determine the anisotropy of isothermal remanent magnetization

(AIRM), but in this work anisotropy of anhysteretic remanent magnetization (AARM) has been chosen because generally ARM is a better analogue to natural processes leading to acquisition of a NRM.

AARM data was obtained by magnetizing the sample with the same field in six different directions using a LDA-3A demagnetizer and measuring the recorded ARM with a JR6 spinner magnetometer (Figure 3.6). The AARM ellipsoid is represented exactly the same way as for AMS, with the same parameters and interpretation, but in the case of AARM data only the preferential orientation of ferromagnetic minerals present in the sample is measured, excluding contributions of paramagnetic or diamagnetic components.

Figure 3.6 Equipment used for magnetic and paleomagnetic data acquisition. a) JR6 spinner magnetometer. b) LDA-3A demagnetizer. c) MFK1-FA Kappabridge. d) ASC impulse magnetizer, model IM-10-30.

4. The effect of speleothem surface slope on the remanent magnetic inclination

Summary

The first months of the PhD focused on rock magnetic and paleomagnetic data acquisition and treatment of a speleothem from the Algarve, previously studied by Font et al. (2014). Preliminary data show that the speleothem recorded a high intensity and stable magnetization. The main objective is now to study the influence of the slope of the calcite layers of the speleothem on the orientation of the recorded magnetization. A first experience consisted in measuring the magnetization and anisotropy of magnetic susceptibility of individual cubic samples of a standard size (2x2x2cm) collected in a slice cut along the frontal side of the speleothem, called SPAIII (Figure 4.1). The sampling has been performed trying to include the same growth lines of the speleothem into each specimen in order to minimize age error among samples. Results suggest that the inclination of the magnetization is strongly affected by the slope of the calcite layers and are described in section 4.1. However, the use of cubic samples of 2 cm wide limits the number of samples used for analysis as well as the temporal resolution. In particular, samples do not include exactly the same number of calcite layers, making their comparison poorly accurate. In this case, differences observed in the recorded magnetic inclinations can be interpreted as the result of secular variation of the Earth's magnetic field rather than the influence of the slope of the calcite layers. In order to overcome this problem, small cylindrical samples (1.1 cm in diameter and ~ 2 cm in height) were sampled from the frontal face of the speleothem, named SPAIV (Figure 4.9). In addition to paleomagnetic analysis, I performed anisotropy of magnetic susceptibility and anisotropy of anhysteretic remanent magnetization analysis in order to link the recorded magnetic inclination with the orientation of the magnetic particles trapped in the calcite layers. Results, published at *Journal of Geophysical Research (JGR)* and presented in section 4.2, confirm that the inclination of the remanent magnetization is influenced by the slope of the speleothem surface, through a physical mechanism of particles rolling. This finding provides new clues to better understand the mechanism of acquisition of magnetization in speleothems and addresses a critical problem concerning the reliability of paleomagnetic data acquired in speleothem.

4.1 Preliminary Results

4.1.1 Geological Settings and Sampling

The stalagmite SPAIII was collected in the Excentricas Cave, located in the Peral-Moncarapacho karstic aquifer (area of 44 km^2) in Algarve, Southern Portugal. Detailed mineralogical data, magnetic properties and carbon and oxygen isotopic compositions are documented in *Font et al*., [2014].

For the purpose of the present study, the vertical plane of the stalagmite SPAIII was oriented in situ (in the cave; geographic coordinates of 37°06' N, 7°46'W) with a magnetic compass (Strike=168º; Dip=0º). Sub-sampling for paleomagnetic measurements was made by cutting individual cubic specimens of 2x2x2 cm^3 from sub-horizontal top to laterally strongly dipping calcite growth layers (Figure 4.1). A total of 5 "sites" or lines (called SPAIII.A to SPAIII.E; Figure 4.1) were subsampled, each one recording a specific time span, with a total of 31 samples (4 to 8 samples per site).

4.1.2 Methods

The magnetic measurements were performed at the Paleomagnetism Laboratory of the Institute Dom Luiz, Faculty of Sciences of the University of Lisbon, Portugal. Magnetic mineralogy was studied by analyzing the IRM curves of the samples. It was acquired by magnetizing the samples between 0 and 1000 mT (27 points) with an impulse magnetizer Model IM-10-30 (Figure 3.6 d) and the acquired IRM was measured using a JR6 spinner magnetometer, with sensitivity of $2.4x10^{-6}$ A/m (Figure 3.6 a). Anisotropy of magnetic susceptibility was also obtained with the MFK1-FA kappabridge with a field of 200 A/m and a frequency of 976 Hz. Magnetic remanence was measured with the JR6 spinner magnetometer after step-wise alternating field (AF) demagnetization using an LDA-3A demagnetizer. Characteristic Remanent Magnetization (ChRM) was calculated based on Principal Component Analysis [*Kirschvink, 1980*] and Fisher statistic [*Fisher, 1953*] by using the software Remasoft 6.0 (AGICO). The values of calcite growth inclination were estimated relative to horizontal plane, which is also called dip, by using the software Adobe Illustrator. The final value of the calcite growth inclination is given by the mean of the angles measured in the front face and in the back face of the cubic specimens. Finally, the age of the different lines (A to E) were estimated by interpolation of the corrected ^{230}Th ages [*Ghaleb et al., 2014*] using the algorithm StalAge [*Scholz and Hoffmann, 2011*] (more details in appendix section).

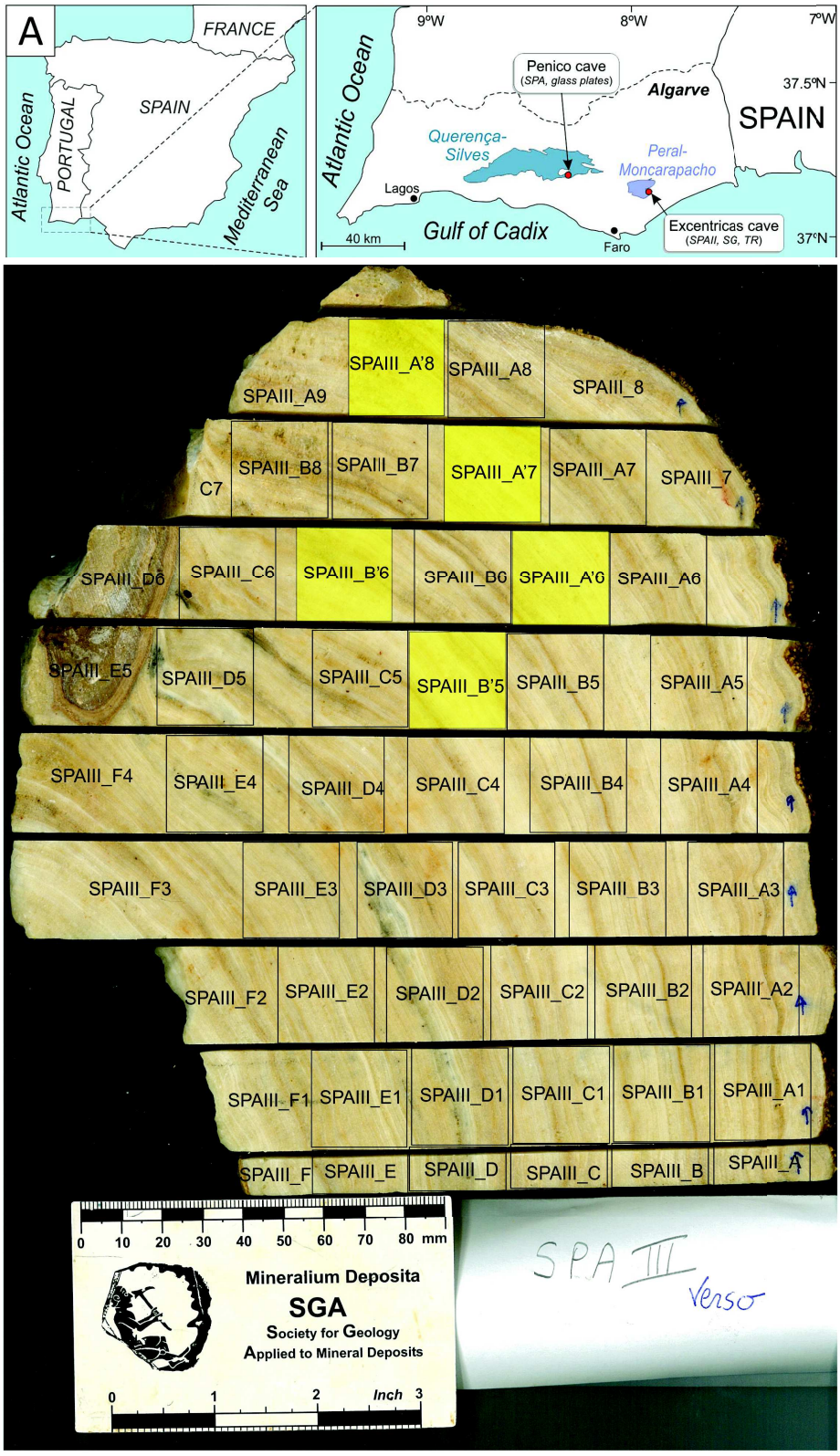

Figure 4.1 Location of the cave where the studied speleothem (SPA) was collected and sampling plan for the slice used in this chapter (SPAIII). The slice was cut in cubic samples (2x2x2 cm), trying to encompass the same growth lines (age).

4.1.3 Results and Discussion

4.1.3.1 Magnetic mineralogy

IRM curves have been acquired to analyze magnetic mineralogy and how it varies along the speleothem under study. In Figure 4.2 a, it is observed that IRM curves are very similar for all samples, with a strong magnetization in weak field, reaching more than 90% of saturation (SIRM) when exposed to a field intensity of 100 mT. After unmixing the IRM curves by CLG treatment, resumed in Table 4.6 (appendix II), it is possible to identify three magnetic components (Fig. 4.2). The first component is a low coercivity phase (mean coercivity $B_{1/2}$ of ~ 23.5 mT), contributing between 80-90% of the total SIRM and with relatively weak dispersion (DP ~ 0.24). The second component is a medium-high coercivity component ($B_{1/2}$ ~ 87 mT) with a very weak dispersion (DP ~ 0.19), but only contributing between 2 and 9% of total SIRM. A third very high coercive component ($B_{1/2}$ ~ 500/600 mT) is observed and contributes to 7 to 13% of the total remanence. These values are compatible with magnetite, hematite and goethite, respectively, and confirm previous results obtained by Font et al. (2014). The similarity of the shape of the normalized IRM curves observed in all samples suggests that the nature of the magnetic carriers is mostly the same in the whole speleothem.

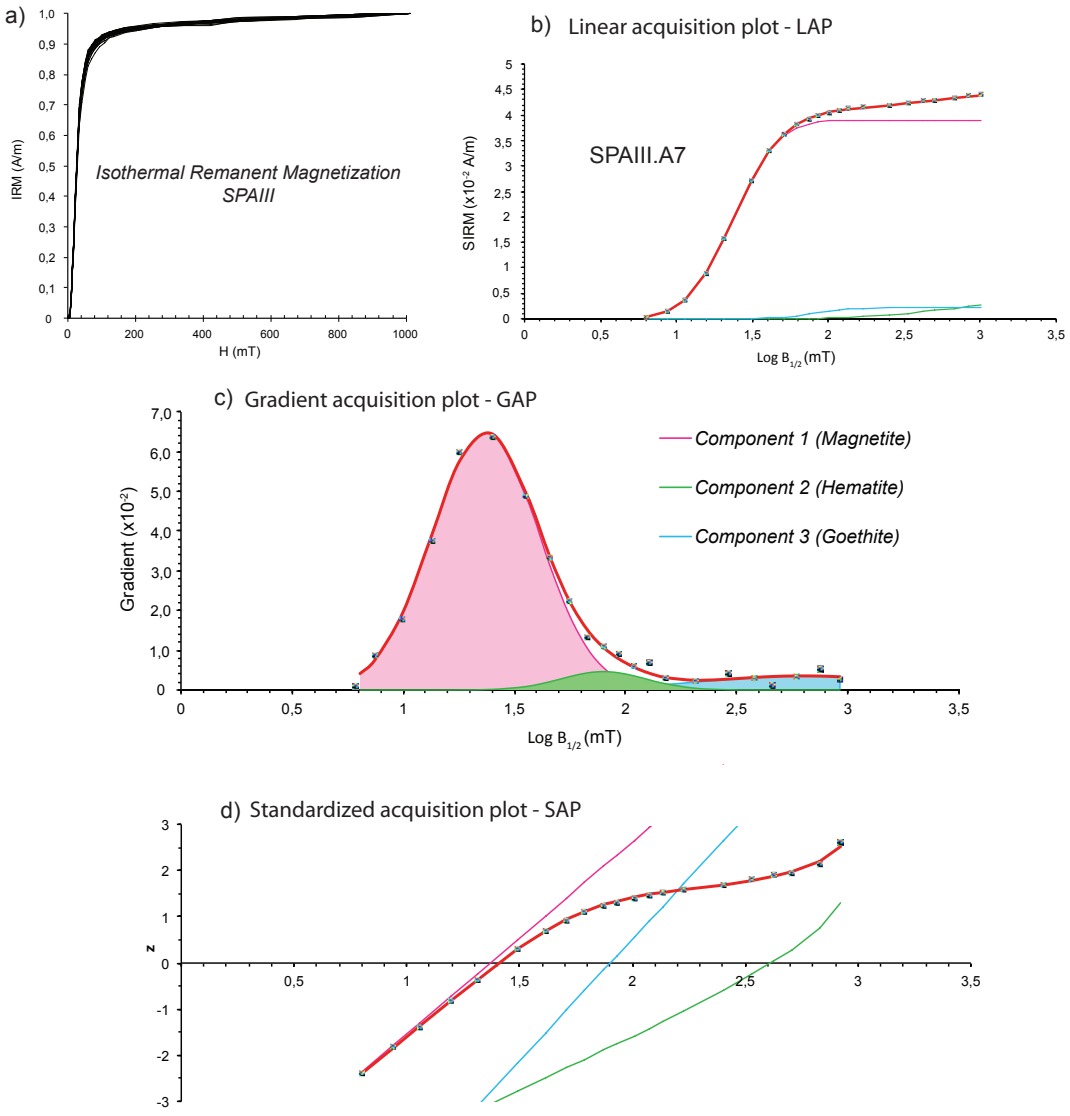

Figure 4.2 Normalized IRM acquisition curves of all samples (a) and example of an IRM curve analyzed by the Cumulative Log-Gaussian from sample SPAIII.A7: linear acquisition plot (b), gradient acquisition plot (c) and standardized acquisition plot (SAP).

4.1.3.2 Anisotropy of magnetic susceptibility (AMS)

AMS data has been conducted in order to study the magnetic fabric of the speleothem. The mean susceptibility K_m alternates between negative and positive values (18 positive and 17 negative). The parameter P (degree of anisotropy) abruptly increases in cases where magnetic susceptibility is near zero. A similar behavior has been already documented for quartz and salt samples [*Hrouda*, 1986; *Machek et al.,* 2014], which also have very low magnetic susceptibility or even negative values. In nature, almost all rocks have positive magnetic susceptibility, but in cases where the rock is composed by a diamagnetic matrix and contain

very low concentration of iron oxides, magnetic susceptibility can be negative. This is the case of some samples of SPAIII with negative magnetic susceptibility: the presence of iron oxides detected by IRM analysis and SEM is unequivocal, but speleothems are constituted (more than 99%) of calcite, which is diamagnetic, and in some cases the presence of ferromagnetic minerals is not high enough to overcome the diamagnetic susceptibility. The calculation of parameters P, L and F is not reliable for negative or close to zero susceptibilities, explaining the observed odd values (Table 4.1). Particularly, parameter P tends to infinite values when susceptibility is closer to zero (Figure 4.3 b). For this reason, it is recommended the use of parameters Δk ($\Delta k = k_1 - k_2$) and U ($U = (2 k_2 - k_1 - k_3) / (k_1 - k_3)$) to quantify the degree of anisotropy and ellipsoid shape, respectively, for samples having very low or negative values of magnetic susceptibility [*Hrouda*, 1986; *Hirt and Almqvist,* 2012].

The maximum and intermediate eigenvectors (k_1 and k_2) directions are dispersed within a large region, while the minimum eigenvector (k_3) is well clustered, with a WNW direction and inclinations ranging between 17 and 66º (Figure 4.3 a). This distribution suggests an oblate fabric, where it is difficult to distinguish the maximum and intermediate magnetic susceptibility axis, but the minimum axis direction is well defined ($k_1 \approx k_2 > k_3$). The susceptibility difference Δk, used to measure the degree of anisotropy, lies between 7.12×10^{-7} and 11.1×10^{-7} with exception of two outliers with lower Δk that coincides with the two samples with K_m closer to zero (Figure 4.3 c). The U parameter values are all strongly positive ($0.31 < U < 0.986$), which confirms the oblate magnetic fabric (Figure 4.3 d).

When analyzing the AMS data variation along a single calcite growth layer, a striking correlation ($R^2 = 0.95$) between the inclination of k_3 and the calcite layer dip is observed (Figure 4.4). In fact, k_3 inclination is almost perpendicular to the surface of the calcite growth layers, with k_1 and k_2 concordant with the surface plane of the speleothem. Therefore, the magnetic fabric somehow mimics the shape of the speleothem. Usually, the crystallization of calcite in speleothems occur perpendicular to the surface, in the same direction of k_3, following the direction of the c-axis corresponding to the longest axis. Similar AMS results in speleothems have been reported by *Zhu et al.* (2012).

Table 4.1 Summary of AMS data collected from speleothem SPAIII. *M* represents the mass of the cubic sample, *CLD* is the calcite layer dip, *Inc* K_3 is the inclination of the minimal susceptibility axis, *L* is the lineation parameter, *F* is the foliation parameter, *P* is the degree of anisotropy, *U* is the shape anisotropy, *Δk* is the susceptibility difference and K_m is the mean susceptibility.

Sample	m (g)	CLD(º)	Inc K_3(º)	L	F	P	U	Δk	K_m (x10^{-6})	Error (%)
SPAIII_A1	26,209	81,5	17	1,012	1,23	1,245	0,883	8,67621E-07	4,11	0,5887
SPAIII_A2	26,11	82,5	23	1,028	1,212	1,246	0,724	8,90722E-07	4,17	0,754
SPAIII_A3	26,488	78	21	1,061	-0,844	-0,895	0,946	2,33735E-07	0,11	6,4801
SPAIII_A4	26,985	73	28	1,041	-50,649	-52,74	0,922	8,87567E-07	0,57	2,7848
SPAIII_A5	28,414	71	33	1,039	12,17	12,648	0,918	9,61662E-07	0,71	3,0406
SPAIII_A6	26,135	57,5	40	1,099	-5,062	-5,565	0,847	7,12116E-07	0,42	6,2835
SPAIII_A'6	26,575	52	48	1,187	1,022	1,213	0,795	1,0234E-06	-5,19	0,9804
SPAIII_A7	28,007	48	50	1,165	-0,681	-0,793	0,875	1,74134E-07	0,08	5,7692
SPAIII_A'7	27,876	35,5	56	1,252	1,022	1,28	0,795	9,38482E-07	-3,69	0,426
SPAIII_A8	28,873	32	63	1	1,013	1,013	0,95	8,58264E-07	65,02	0,0173
SPAIII_A'8	27,301	32,5	66	1,047	1,103	1,155	0,33	7,85E-07	5,50	1,119
SPAIII_B1	26,958	80	20	2,124	1,008	2,14	0,986	8,97274E-07	-1,09	1,817
SPAIII_B2	27,744	76	24	1,535	1,019	1,564	0,933	9,50809E-07	-2,01	0,3198
SPAIII_B3	27,946	72	31	1,497	1,029	1,541	0,893	9,72416E-07	-2,14	0,6493
SPAIII_B4	26,779	67	32	1,018	1,552	1,58	0,902	8,88731E-07	2,11	0,9349
SPAIII_B5	27,144	57	44	1,397	1,041	1,454	0,821	9,3528E-07	-2,40	1,4052
SPAIII_B6	26,788	43	55	1,551	1,069	1,659	0,79	8,6708E-07	-1,64	1,6135
SPAIII_B'6	26,925	38	56	1,334	1,213	1,618	0,31	1,11172E-06	-2,30	4,9126
SPAIII_B7	28,498	33	62	1,043	2,765	2,883	0,875	8,26503E-07	0,97	1,7384
SPAIII_B8	28,45	28,5	53	1,005	1,079	1,085	0,861	7,27076E-07	9,03	0,184
SPAIII_C1	26,678	80	19	1,504	1,014	1,525	0,947	8,75366E-07	-1,97	0,8453
SPAIII_C2	25,379	75	27	1,448	1,028	1,488	0,886	7,78812E-07	-1,87	0,6772
SPAIII_C3	27,267	68	31	2,463	1,054	2,595	0,933	8,77855E-07	-0,85	3,605
SPAIII_C4	28,116	58	41	1,619	1,08	1,749	0,786	9,68312E-07	-1,65	1,7283
SPAIII_C5	27,425	38,5	53	1,026	1,299	1,332	0,8	8,42134E-07	3,07	1,5539
SPAIII_C6	28,131	32	54	1,006	1,053	1,059	0,794	7,86358E-07	13,82	0,2097
SPAIII_D1	26,17	79,5	20	1,036	2,187	2,266	0,875	8,34407E-07	1,20	1,5481
SPAIII_D2	27,909	73,5	26	1,052	3,382	3,559	0,861	8,49624E-07	0,88	2,3577
SPAIII_D3	25,869	65	31	1,03	2,815	2,901	0,91	7,74124E-07	0,91	1,2401
SPAIII_D4	27,502	50,5	46	1,023	6,065	6,205	0,946	8,63418E-07	0,73	3,1193
SPAIII_D5	25,853	30	60	1,496	1,018	1,524	0,93	8,9341E-07	-2,01	1,5223
SPAIII_E1	26,215	78	22	1,458	1,031	1,504	0,876	9,1891E-07	-2,15	1,2618
SPAIII_E2	27,141	68	22	1,289	1,011	1,303	0,925	9,13045E-07	-3,33	0,6615
SPAIII_E3	26,942	56	42	1,235	1,03	1,272	0,777	8,96215E-07	-3,62	0,8696
SPAIII_E4	24,427	38,5	55	1,215	1,007	1,224	0,935	8,47591E-07	-4,07	0,3716

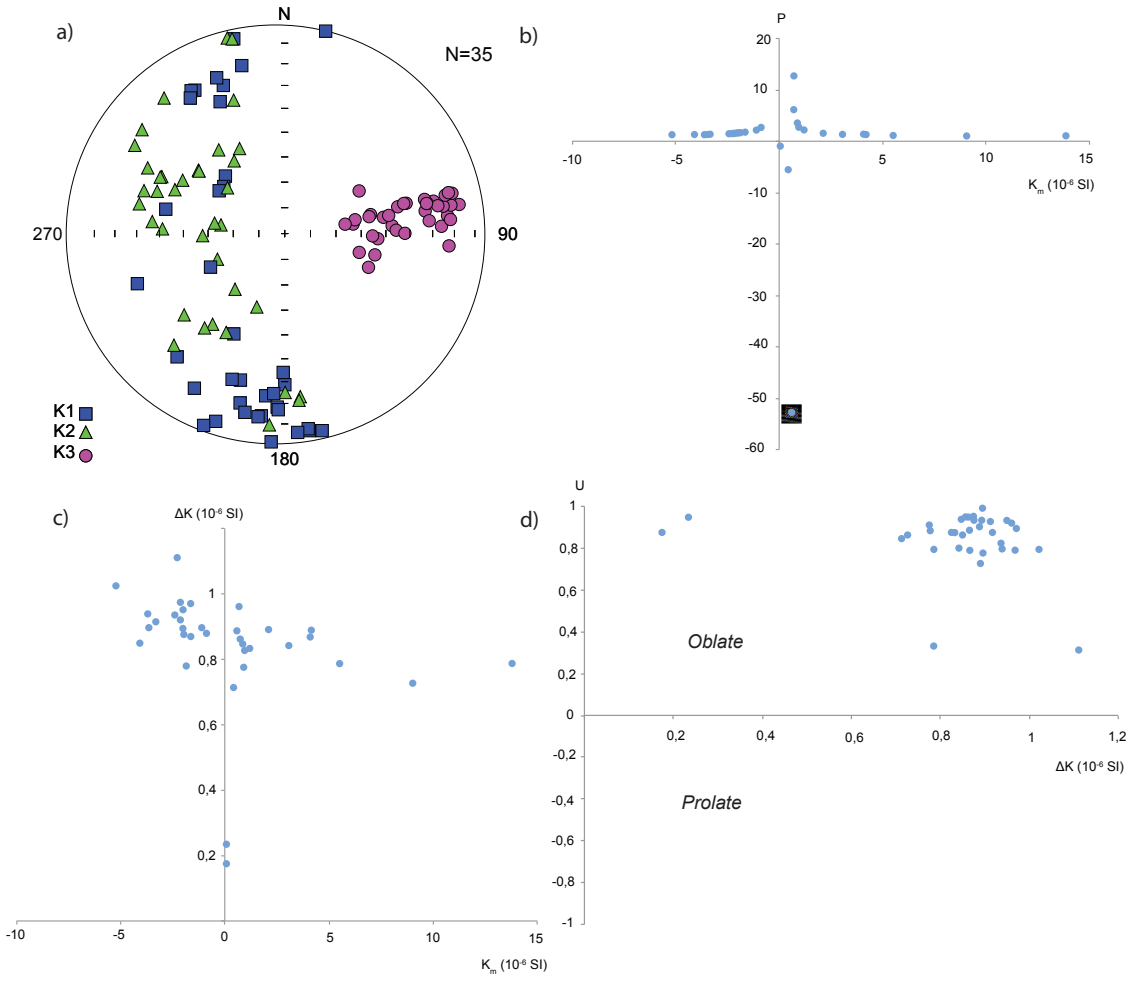

Figure 4.3 a) Representation of the three principal axis of magnetic susceptibility directions, k_1 (blue squares), k_2 (green triangles) and k_3 (pink circles), in a stereographic projection. b) Parameter P vs mean susceptibility (K_m). c) Susceptibility difference (Δk) vs mean susceptibility. d) U parameter vs Susceptibility difference.

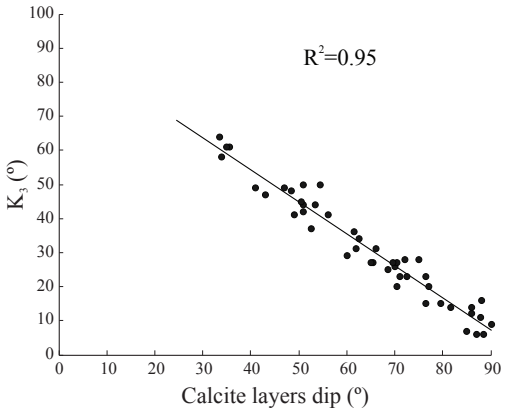

Figure 4.4 k_3 inclination in function of the calcite layer dip, showing a very strong linear correlation.

4.1.3.3 Paleomagnetic data

NRM intensities are relatively high and range between $0.76x10^{-3}$ and $2.53x10^{-3}$ A/m. After cleaning of a weak (VRM) magnetization below 6 mT, orthogonal projections show stable and well-defined remanent magnetization directions pointing to the origin (Figure 4.5). The median destructive field (MDF) is included between 10 to 15 mT, indicating the presence of a low coercive phase (magnetite). After AF demagnetization at 30 mT, more than 90% of the remanence was cleaned, suggesting that magnetite is the main carrier of the remanent magnetization recorded in these samples, as also evidenced by IRM analysis. Sample-based magnetic directions have declination values varying between 354.2º and 2.5º and inclination ranging from 38.4º up to 53.4º, with low (0.7º to 2.5º) maximum angle deviation (MAD) values.

One of the disadvantages of speleothems in paleomagnetism is usually the low concentration of ferromagnetic minerals, which make it difficult to measure stable paleomagnetic directions. However, the speleothem under study has a relatively high concentrations of ferromagnetic minerals previously identified by *Font et al.* (2014) based on IRM acquisition curves and now confirmed with the newly IRM data presented in section 4.4. This results in relatively high NRM intensities, which allowed determining stable paleomagnetic directions, with very low MAD values. These results are very positive indicators of their reliability.

The paleomagnetic vector for each sample and its variation in function of time and along each line, representing the same time interval, were analyzed. A tendency has been detected for the magnetic inclination to decrease from the top to base of the speleothem, as the calcite layers become steeper (Figure 4.6). For this reason, magnetic declination and inclination have been plotted in function of the calcite layer dip for each line (Figure 4.7). Magnetic declination does not depend on the calcite layer dip. Conversely, magnetic inclination has significant negative correlations ($R^2 \sim 0.43$-0.96) with the dip of the calcite growths. Magnetic inclination decreases linearly with the dip of the calcite growth bedding, with a maximum difference of 4 to 9º. Such correlation is systematically observed in the case of the five lines (A to E) and suggests a close relationship between the dip of the calcite growths and the corresponding magnetic inclination. This effect has already been hypothesized before, but it has never been proven. Previous paleomagnetic studies in speleothems [e.g. *Latham et al.,* 1982*; Latham et al.,* 1986; *Latham et al.,* 1989; *Morinaga et al.,* 1989*; Lean et al.,* 1995*; Openshaw et al.,* 1997]) compared magnetic

inclination values in the central (horizontal layers) and lateral sides (vertical layers), but have not found significant differences, at least higher than the paleomagnetic directions calculation uncertainty. However, the stalagmites studied by the authors did not have the best shape to perform such study, since the thickness of the calcite layers located at the top of the speleothem is much higher than the thickness of the calcite layers located on the borders of the speleothem. Additionally, they only compared two or three samples spanning similar ages, which is insufficient. SPAIII present a very particular shape, since the thickness of the calcite layers varies few along the entire speleothem, making easier the comparison of samples having the same age and the same number of individual calcite layers. It was possible to compare 4 to 8 samples along a specific layer (Figure 4.6), making it especially suitable for the study of the effect of the slope of the calcite layers on the recorded magnetic remanence.

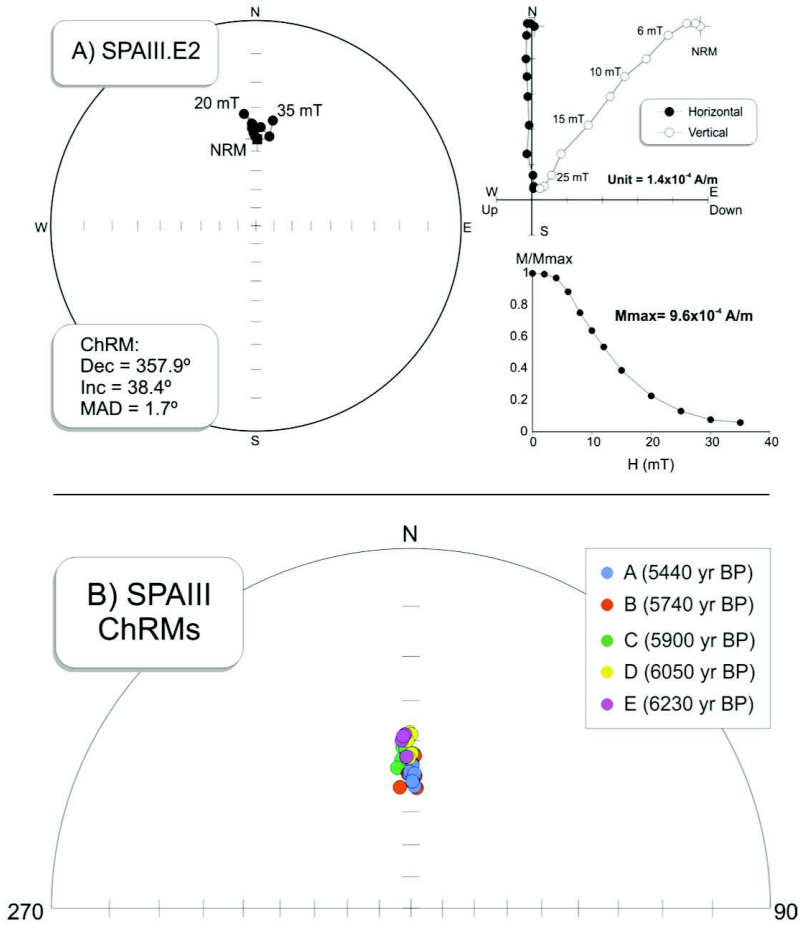

Figure 4.5 A) Stereographic and orthogonal projections and remanence intensities during Alternating Field (AF) cleaning of sample SPAIII_E2. B) Stereographic projections of the Characteristic Remanent Magnetizations (ChRMs) obtained in all specimens. The colors correspond to the different lines.

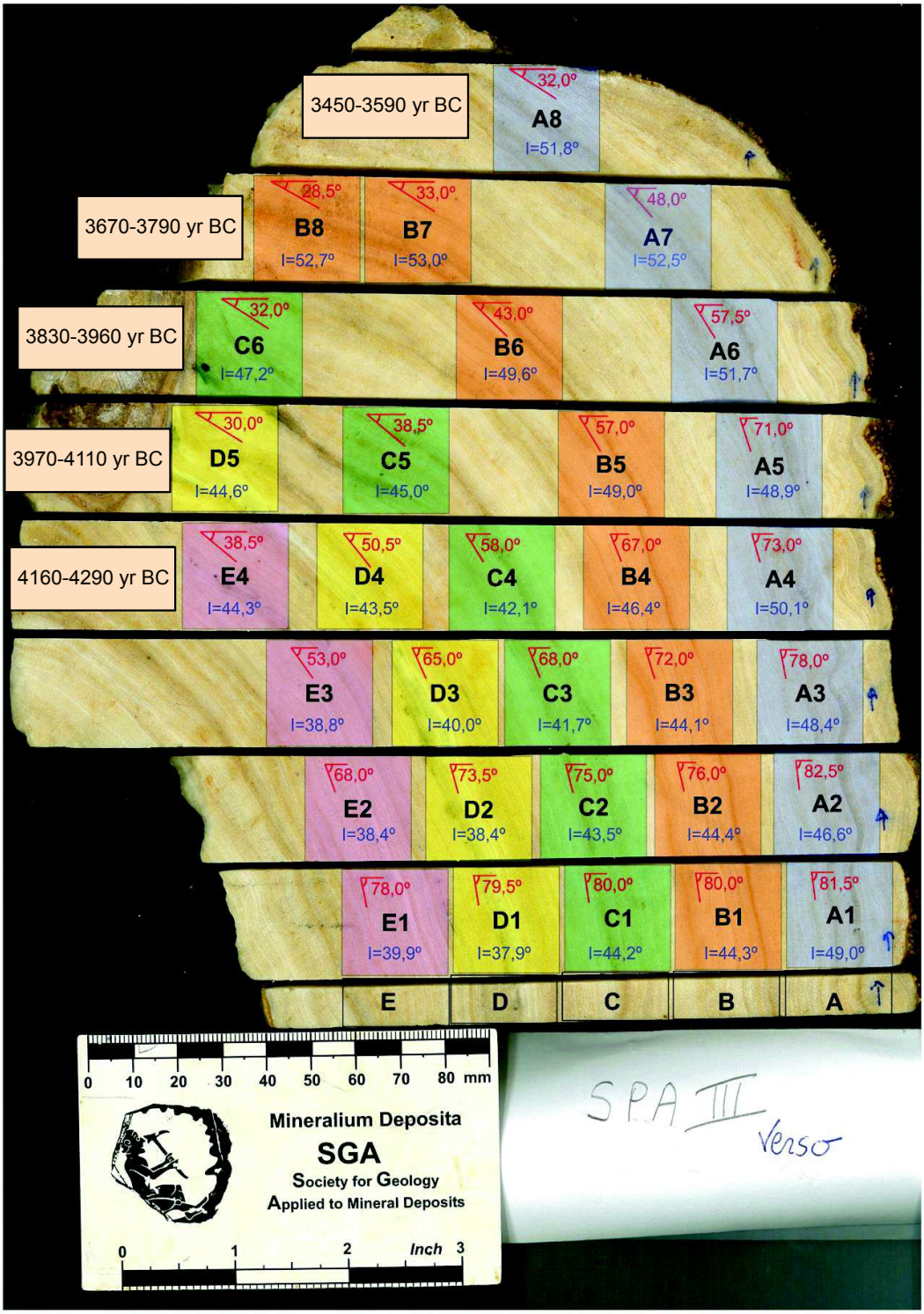

Figure 4.6 Selected samples for preliminary paleomagnetic study. Five lines (each with a darker calcite layer as reference) were used to reconstruct the recorded geomagnetic field in the age interval encompassed by the speleothem. Magnetic inclination and the calcite layer dip for each sample are displayed.

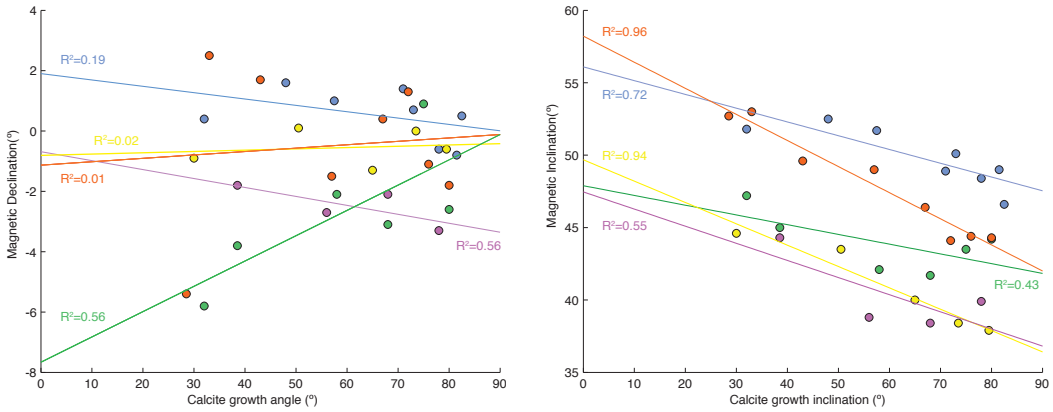

Figure 4.7 Magnetic declination (left) and inclination (right) in function of the estimated angle of the calcite growth layers with the horizontal plane. The correlation factor (R^2) is shown for each line.

Despite the evidence of a shallowing inclination effect in the studied speleothem, the recorded paleomagnetic directions were compared to a paleosecular variation curve obtained from the global model *SHA.DIF.14K* [*Pavón-Carrasco et al.,* 2014]. Magnetic declination and inclination for five different ages (corresponding to the five studied lines, A to E) are represented in Figure 4.8. The site-based mean declinations (Figure 4.8 A) and inclinations (Figure 4.8 B) are consistent with the *SHA.DIF.14K* model for the age interval (~4220-3430 yrs BC), falling into the area within 95% confidence interval of the model, with exception of the declination in line C (slightly above). Particularly, during this time interval, *SHA.DIF.14K* magnetic inclination exhibits a characteristic trend that increased from ~32º up to 57º, which is well corroborated by the newly found data showing the same trend. Magnetic inclination recorded in individual samples with the most sub-horizontal (A8, B8, C6, D5, E4) and vertical (A2, B1, C1, D1, E1) calcite growth laminae were also represented in Figures 4.8 C and 4.8 D. Concerning samples featured by sub-horizontal calcite layers, sample-based magnetic inclinations are included in the 95% confidence interval of the *SHA.DIF.14K* model. In addition, the square of confidence of each sample, calculated based on both the age uncertainty estimated by the age model calculated by StalAge algorithm and their MAD value, overlaps the curve predicted by the model. Conversely, samples belonging to the most vertical calcite layers systematically show lower values compared to the model. The magnetic inclination values of line A and B is even lower than the 95% confidence interval, and no overlap between the square of confidence and the PSV model curve is noted.

We concluded that the magnetic inclination recorded in the SPA speleothem depends on the slope of the calcite layer. However, and as pointed before, the accuracy of the data is biased

by the fact that cubic samples are too large comparing to the very small individual calcite layers and may not necessarily include the same time interval. For this reason, new paleomagnetic data were acquired on smaller cylindrical samples and are presented below [*Ponte et al.,* 2017].

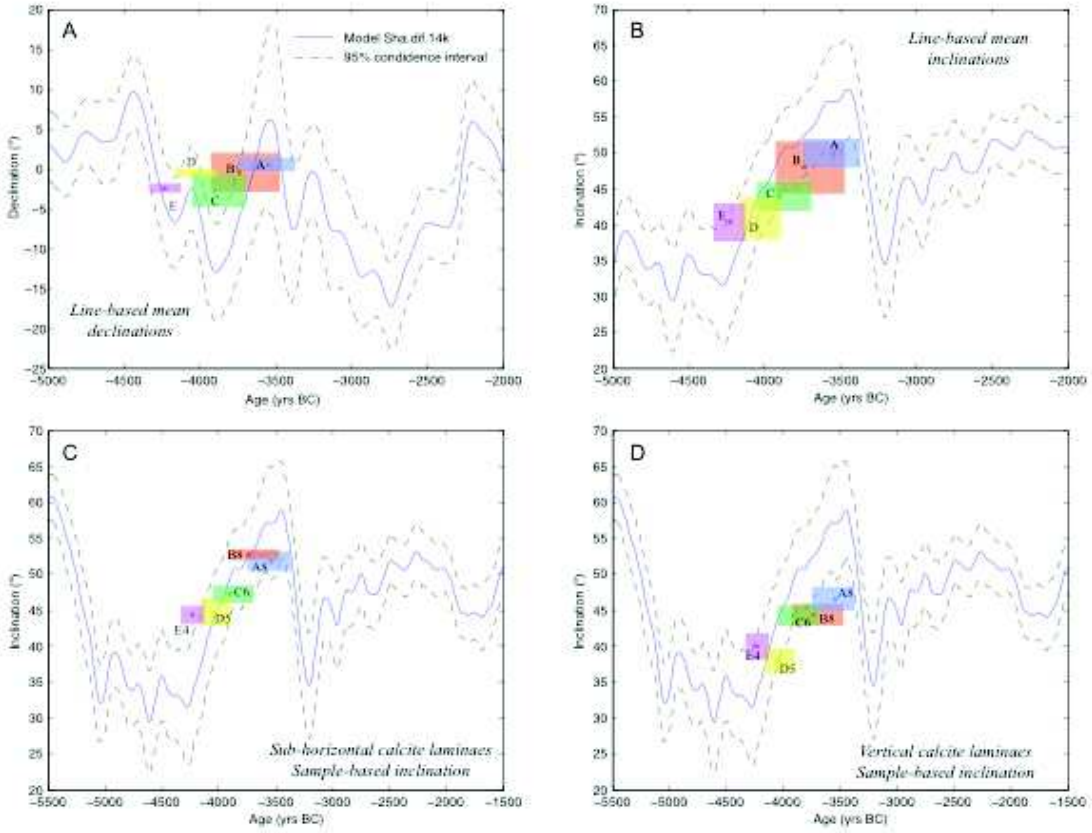

Figure 4.8 Comparison of the SPAIII paleomagnetic data with the SHA.DIF.14K model [*Pavón-Carrasco et al.,* 2014]. The errors, represented by squares, are estimated based upon model age uncertainty given by StalAge [*Scholz and Hoffmann,* 2011] and standard deviation (A and B) or maximum angular deviation (MAD) (C and D). Site-based mean declination (A) and inclination (B) values showing a reliable correlation with the SHA.DIF.14K model. Magnetic inclination value for specimen with sub-horizontal (C) and sub-vertical (D) calcite growths. A systematic offset is observed in the case of vertically oriented layers.

Table 4.2 Site based mean ChRMs in geographic coordinates (Dec = Magnetic declination; Inc = Magnetic inclination; n is the number of samples used for ChRM calculation; R is the vector length of the additionof unit vectors; K is the precision parameter and a95 is the 95% confidence interval).

	ChRMs					
Site	n/N	Dec (deg)	Inc (deg)	R	K	a95
SPAIII.A	8	0,5	49,8	8,00	1613,0	1,4
SPAIII.B	8	-0,5	48,0	7,98	403,8	2,8
SPAIII.C	6	-2,7	44,0	6,00	1001,7	2,1
SPAIII.D	5	-0,5	40,9	4,99	704,4	2,9
SPAIII.E	4	-2,5	40,4	4,00	865,2	3,1

4.2 The effect of speleothem surface slope on the remanent magnetic inclination

Published in:

Ponte, J. M., E. Font, C. Veiga-Pires, C. Hillaire-Marcel, and B. Ghaleb (2017), The effect of speleothem surface slope on the remanent magnetic inclination, *J. Geophys. Res. Solid Earth*, 122, doi:10.1002/2016JB013789.

https://agupubs.onlinelibrary.wiley.com/doi/10.1002/2016JB013789

The effect of speleothem surface slope on the remanent magnetic inclination

J. M. Ponte[1], E. Font[1], C. Veiga-Pires[2], C. Hillaire-Marcel[3], B. Ghaleb[3]

[1] IDL-FCUL, Instituto Dom Luís, Faculdade de Ciências, Universidade de Lisboa, Portugal

[2] CIMA-FCT, Universidade do Algarve, Faro, Portugal

[3] GEOTOP, Université du Québec, Montreal, Canada

(This sub-chapter is presented in a paper format, as published in *Journal of Geophysical Research*, Ponte et al., 2017, DOI: 10.1002/2016JB013789)

Abstract

Speleothems are of interest for high-resolution reconstruction of the Earth's magnetic field. However, little is known about the influence of speleothem morphologies on their Natural Remanent Magnetization (NRM) record. Here we report on a high-resolution paleomagnetic study of a dome-shaped speleothem of Middle Holocene age from southern Portugal, with special attention to the anisotropy of magnetic susceptibility (AMS) and anisotropy of anhysteretic remanent magnetization (AARM). To assess the potential influence of the slope of the speleothem surface on the recorded remanent magnetization, we compare magnetic directions and AMS and AARM fabrics from sub-horizontal to gradually sub-vertical calcite growth layers collected in a transversal cross-section of the speleothem. A linear correlation is observed between magnetic inclinations, calcite laminae slope and AARM k_1 inclination. The AMS fabric is mostly controlled by calcite crystals, with direction of the minimum axes (k_3) perpendicular to laminae growth. Magnetic inclinations recorded in inclined and vertical calcite growth layers are underestimated when compared to a global paleosecular variation (PSV) model. After extrapolating magnetic inclinations to the horizontal, the corrected data better fit the PSV model, but are still lower than the predicted magnetic inclinations, suggesting that inclination shallowing affects the entire speleothem. We suggest that speleothem morphology exerts a critical role on the magnetic inclination recording, which is controlled by the Earth's magnetic field but also influenced by particle rolling along the sloping surfaces. These observations open new avenues for reconstructing high-resolution paleomagnetic secular variations records from speleothems and provide new insights into their NRM acquisition mechanisms.

4.2.1 Introduction

Speleothems are high-resolution archives of the Earth's climate and the intensity of its magnetic field [*Latham et al.,* 1979; *Morinaga et al.,* 1986; *Martin,* 1990; *Lascu and Feinberg,* 2011*; Osete et al.,* 2012*; Strauss et al.,* 2013*; Font et al.,* 2014; *Bourne et al.,* 2015*; Jaqueto et al.,* 2016; *Lascu et al.,* 2016]. However, little is known about the influence of the slope of calcite growth layers of speleothems on the orientation of recorded Natural Remanent Magnetisation (NRM). Pioneer paleomagnetic studies suggested that the difference of the magnetic inclination recorded along the speleothem surface is not large enough to assess whether they are due to the slope or to the measurement error [e.g. *Latham et al.,* 1982*; Latham et al.,* 1986; *Latham et al.,* 1989; *Morinaga et al.,* 1989*; Lean et al.,* 1995*; Openshaw et al.,* 1997]. More recently, *Zhu et al.* [2012] applied Anisotropy of Magnetic Susceptibility (AMS) and Anisotropy of Isothermal Remanent Magnetization (AIRM) techniques in two speleothems and concluded that the orientation of ferrimagnetic minerals in speleothems are not controlled by the speleothem growth laminae, but by the geomagnetic field. To unravel the potential effect of the speleothem's morphology on the recorded NRM vector directions it is therefore useful to consider the variation of the direction of the primary (detrital) magnetization along a speleothem at a high temporal/spatial resolution. This is not straightforward because speleothems generally contain very low amounts of magnetic particles within the diamagnetic calcite matrix. Such a limitation can be solved by using large (2x2x2cm) paleomagnetic samples. However, taking into account that the thickness of annual lamination is generally of a millimetrical scale, this solution results in a low temporal resolution.

The aim of this study is to examine the potential influence of calcite growth patterns on the NRM directions using a well-dated, high growth rate Mid-Holocene speleothem (~ 3200-4500 yrs BC) collected from the Algarve region, in southern Portugal. This speleothem, already studied by *Font et al.*[2014], carries a primary (detrital) remanent magnetization due to detrital magnetite and maghemite and exhibits high values of remanent magnetization of the order of 10^{-3} A/m. Such properties allowed us to collect relatively small specimens but with a high temporal and spatial resolution. Detailed U-Th measurements [*Ghaleb et al., 2014*] provided a robust age model, using StalAge algorithm for interpolations [*Scholz and Hoffmann, 2011*]. On these grounds, paleomagnetic data could be compared with a reference model of paleosecular variations.

4.2.2 Geological setting and Sampling

The karst system investigated is developed in Jurassic limestones from the sedimentary sequence of the Algarve basin, southern Portugal. These consist in reef and bioclastic carbonates capped by Terra Rossa soils. Laterally, the limestones are replaced by a nearshore facies with either silex nodule layers or sandstones with siliceous-fossil rich pockets [*Terrinha et al.*, 2013]. The SPA speleothem was collected in the *Excentricas Cave* (geographic coordinates of 37°06' N, 7°46'W), located over the large Peral-Moncarapacho karstic aquifer of Algarve, Southern Portugal. The *Excentricas cave* lies over the Querença-Silves aquifer system (Cerro da Cabeça). The region is dominated by a Mediterranean climate with a mean annual precipitation below 500 mm generally falling in autumn and spring and a mean annual temperature of 18° C. The area depicts a scrubland vegetation cover with sparse shrubs and small trees (*Querqus coccifera*, *Ilex aquifolium*, etc).

The studied speleothem shows parallel banding, with no layer showing anomalous detrital minerals accumulation or even dissolution, suggesting that growth was almost continuous along the studied profile. The speleothem has also a peculiar shape, because the growth layers do not become thinner and condensed along the sides of the speleothem (Figure 4.9). It corresponds to a dripstone with a conical shape and tapered form, similar to mammiform speleothem [*Hill and Forti*, 1997]. Detailed mineralogical data, magnetic properties and carbon and oxygen isotopic compositions from a portion of the speleothem under study (named SPAII) are documented in *Font et al*. [2014].

Sub-sampling for U-Th dating was achieved on a 1 cm-thick slice cut along the growth axis of the stalagmite. For paleomagnetic analysis, the sampled section of the speleothem was thoroughly oriented using a magnetic compass. As illustrated by Figure 4.9 A, the strike and dip of the vertical section are N80º and 90º, respectively. Small cylindrical specimens of approximately $2cm^3$ in volume (1.1cm in diameter and 2cm in length) were subsequently drilled in the laboratory perpendicularly to the oriented face of the speleothem and named SPAIV (Figure 4.9 B) (samples SPAIII being the focus of another study). The orientation of the specimens was reported by a vertical line pointing to the top of the cylinder as illustrated in Figures 4.9 C and 4.9 D. The final declination value of the cylindrical specimens is Nº168, considering a correction of the local declination of ~-2º (N80º+90º-2º), with a dip of 0º. Specimens were collected from the top of the speleothem (where calcite laminae are inclined to sub-horizontal) to the laterally strongly dipping calcite growth layers (Figure 4.9 B). A total of six horizons or "lines" (called SPAIV.3-5-7-9-11-13; Figure 4.9) were selected, each

one recording a specific time span, leading to a total of 48 samples (8 samples per line; Figure 4.9 B).

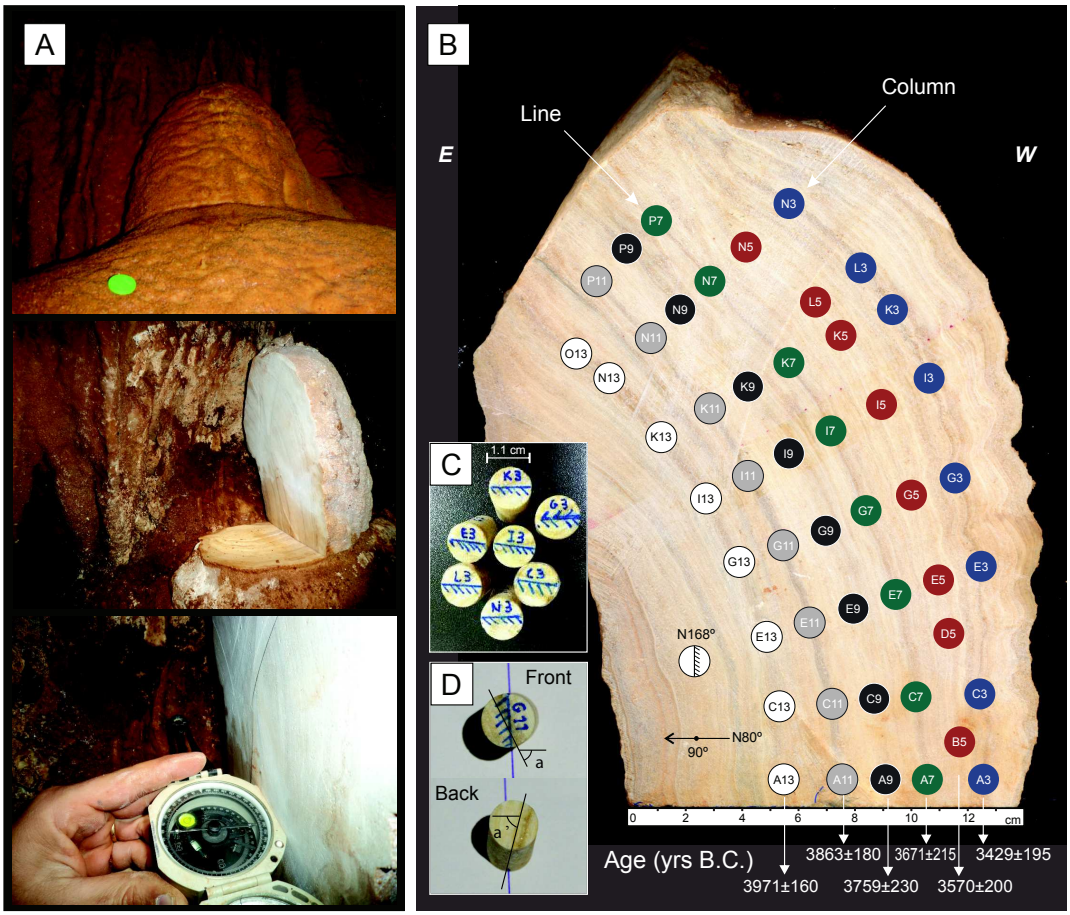

Figure 4.9 A) Photographs of speleothem under study before cutting (top), after cutting and replacement in its original position (center), and orientation of the vertical plane with a magnetic compass (bottom). B) Vertical face of the speleothem with location of the cylindrical SPAIV specimens (1.1×~2cm) collected for subsequent paleomagnetic measurements. Samples are distributed along lines corresponding to calcite growth layers of a similar age, and columns that represent the temporal variations. Each line includes a reference calcite growth layer (darker). Ages Before Christ (BC) and associated errors have been determined by interpolation of corrected ^{230}Th ages for dated layers using the StalAge algorithm [*Scholz and Hoffmann,* 2011]. C) Cylindrical specimens and their respective orientation. D) The dip of calcite laminae is calculated based on the mean of the angles measured on the front (a) and back sides (a') of the specimen.

4.2.3 Methods

The U-series measurements for age determination were performed at the Radiochronology laboratory of the GEOTOPO-UQAM-McGill research Center, Canada. Each half or cm-thick subsample of about 2 to 4 g was grinded in an agate mortar for subsequent U-series isotope measurements. The sample powders were dissolved using nitric acid in a Teflon™ beaker into which a weighted amount of calibrated mixed spike ^{233}U-^{236}U-^{229}Th had been placed and

evaporated slowly to dryness. After the dissolution around 10 mg of iron-carrier was added and the solution was then left over night for spike-sample equilibration. U and Th were co-precipitated with $Fe(OH)_3$ by adding ammonium hydroxide drop by drop until reaching pH 8-9. The precipitate was recovered by centrifugation and washed twice with deionized water, then dissolved in 6N HCl. U-Th separation was performed on a 2 ml AG1X8 anionic resin volume. The thorium fraction was recovered though elution with 6N HCl, and the U and Fe fraction, with water. The U fraction was purified on a 0.2 ml U-Teva™ (Elchrom industry™) resin volume. Fe was eluted with 3N HNO_3 and the U fraction with 0.02N HNO_3. After drying, Thorium purification was carried out on a 2 mL AG1X8 resin in 7N HNO_3 and eluted with 6N HCl. U-Th measurements were performed using a multi-collector inductively mass spectrometry Nu instrument ™ (MC-ICP-MS). ^{236}U-^{235}U-^{234}U-^{233}U and ^{232}Th-^{230}Th-^{229}Th were measured on the ion counter (IC0) in peak switching mode for uranium and thorium isotopes, respectively. ^{238}U was not measured but calculated from $^{235}U/^{236}U$ ratios, assuming a constant $^{238}U/^{235}U$ mass ratio (137.88). Knowing $^{236}U/^{233}U$ of the spike, mass bias corrections in atomic mass unit (amu^{-1}) were calculated and used to correct measured ratios between uranium isotopes and between thorium isotopes. In order to get a direct insight into isotopic properties of contaminating detrital fractions eventually transported into the cave and incorporated into speleothem calcite layers, clay fractions (< 2μm) from soils overlying the karts system (Terra Rossa) were sampled and pooled. The above U-Th chemical extraction procedures were used for the clay fraction, except at early sample dissolution stage, for which we used a mixture of concentrated HF and HNO_3. After total evaporation, 2 ml of HCl supersaturated with H_3BO_4 were added, and the solution was evaporated to dryness, prior to re-dissolution with HCl 6M. The overall analytical reproducibility was estimated from replicate measurement of a uraninite standard Hu-1. Precision is usually better than ±0.5% for uranium results and around 1 % for thorium in young samples at two sigma levels.

Finally, detrital values of U/Th ratio determined from Terra Rossa soils and the stratigraphical ordering of samples as proposed by [*Hellstrom, 2006*] similarly corrected ^{230}Th ages. One of the layers was also sampled several times for the setting of an isochron age also in accordance with other correction methods [*Ghaleb et al., 2014*]. Model ages of the 6 lines of samples were finally estimated by interporlation between corrected ^{230}Th ages and using the algorithm StalAge [*Scholz and Hoffmann, 2011*] (Figure 4.10).

Magnetic measurements were performed at the Paleomagnetism Laboratory of the Instituto Dom Luis, Faculty of Sciences of the University of Lisbon, Portugal. The magnetic

remanence was measured using a JR6 spinner magnetometer (sensitivity of 2.4×10^{-6} A/m) after step-wise alternating field (AF) demagnetisation using a tumbling LDA-3A demagnetizer device. Characteristic Remanent Magnetization (ChRM) was calculated based on Principal Component Analysis [*Kirschvink, 1980*] and Fisher statistics [*Fisher, 1953*] using the software Remasoft 6.0 (AGICO) software.

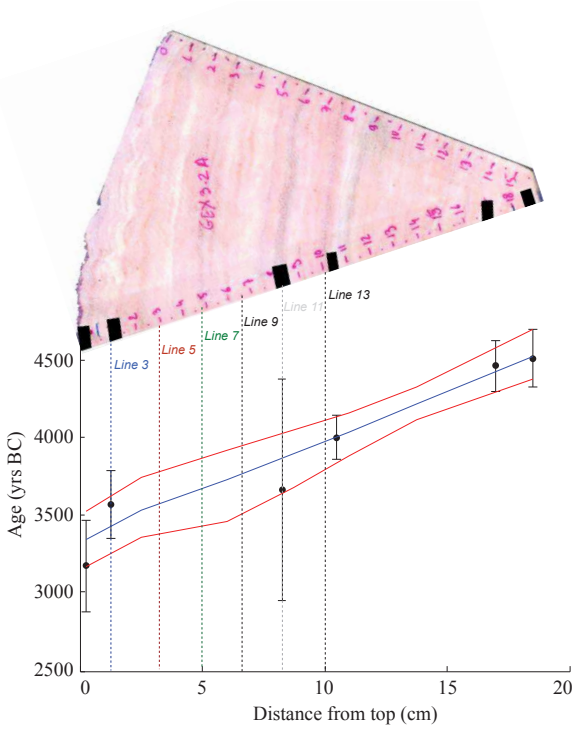

Figure 4.10 Age model for SPAIV obtained from the StalAge algorithm [*Scholz and Hoffmann,* 2011]. The blue and red lines represent the estimated ages and their upper and lower 95% confidence limits, respectively. The vertical dashed lines correspond to each sample line (see Figure 4.9). The black points represent the input data as corrected ^{230}Th ages and their respective errors.

Low field anisotropy of magnetic susceptibility (AMS) was measured with a MFK1-FA Kappabridge (AGICO), with a field of 200 A/m and a frequency of 976 Hz. Data were analyzed by using the Anisoft 4.2 software of AGICO. The magnetic anisotropy is represented by an ellipsoid whose geometry is given by its principal axes, or eigenvectors K_{max} (k_1) ≥ K_{inter} (k_2) ≥ K_{min} (k_3) of the corresponding AMS tensor [*Tarling and Hrouda, 1993*]. The susceptibility difference ΔK ($\Delta K = k_1 - k_3$) and the shape parameter U ($U = (2 k_2 - k_1 - k_3) / (k_1 - k_3)$) are preferentially used for samples having very low or negative values of magnetic susceptibility [*Hrouda*, 1986; *Hirt and Almqvist,* 2012].

Anisotropy of Anhysteretic Remanent Magnetization (AARM) was performed following the method of *McCabe et al.* [1985]. This technique is useful for sedimentary rocks that have low (or negative) bulk susceptibility values, as in this case, and isolates the contribution of the ferromagnetic minerals. AARM is obtained by a combination of a DC magnetic field of 0.5 mT and an alternating field (AF) magnetic field of 50 mT. Samples were previously demagnetized using AF of 50 mT using a LDA-3A demagnetizer. Remanence was measured with the JR6 spinner magnetometer. The procedure was repeated for 6 different orientations and data were treated using the software Anisoft 4.2 (AGICO). AARM is represented by an

ellipsoid defined by the three principal axes (minimum, intermediate and maximum susceptibility axes). The anisotropy degree is evaluated by the P parameter ($P = k_1 / k_3$) and the shape is defined by the T parameter ($T = 2 (\ln (k_2) - \ln (k_3)) / (\ln (k_1) - \ln (k_3)) - 1$).

Slopes (dips) of calcite growth layers *vs* the horizontal plane were calculated based on the mean between the angles measured on the front and the back faces of each cylindrical sample as illustrated by figure 4.9 D.

The coefficient of determination R^2 has been determined using the most general definition, $R^2 = 1 - (SS_{residual}/SS_{total})$, where SS_{total} is the total sum of squares and $SS_{residual}$ is the sum of squares of residuals.

4.2.4 Results

4.2.4.1 U-Th dating and age model

The studied speleothem was first analyzed for its ^{14}C content. Result yielded conventional ages ranging from 6048 ±45 to 4836 ± 47 years (±1σ) [*Veiga-Pires et al., 2011*]. However, since cave $^{14}CO_2$ offsets with atmospheric CO_2 are not known and might have varied through time, U-series measurements were made in order to obtain ^{230}Th ages. The precise U-series dating of this speleothem revealed to be challenging, due to its low total U-content (mean ~ 115 ppb) and relatively abundant contaminating detrital fraction, illustrated by a mean ^{232}Th content of ~ 12 ppb. Several corrections have been proposed in literature in order to estimate the U strictly co-precipitated within calcite and its in-grown daughter ^{230}Th isotope, to be used for calculating sample ages. The isotopic composition of the contaminating fraction is generally considered uniform in U-Th dated speleothems or, at least, within given growth layers, and estimated from ^{232}Th-contents strictly inherited with this fraction. The detrital-source isotopes are quantified (i) assuming a mean crustal isotopic composition (i.e., [Th]/[U] ~ 3.8), or (ii) through the calculation of theoretical isotopic ratios yielding stratigraphically ordered corrected ages, or (iii) based on the isotopic composition of clay fractions in soils overlying the karst system or (iv) using an isochron approach. All methods yielded compatible results within standard deviations, the latter three with more precise final age estimates. They range from 4.52 ± 0.19 ka (bottom) to 3.08 ± 0.24 (top) ka (Figure 4.10). These corrected ages were then used as input values into the StalAge algorithm developed especially for determining age models in speleothems [*Scholz and Hoffmann, 2011*]. The resulting age model (Figure 4.10) was used to attribute an age (with given uncertainty) to each of the studied lines (Figure 4.9 B).

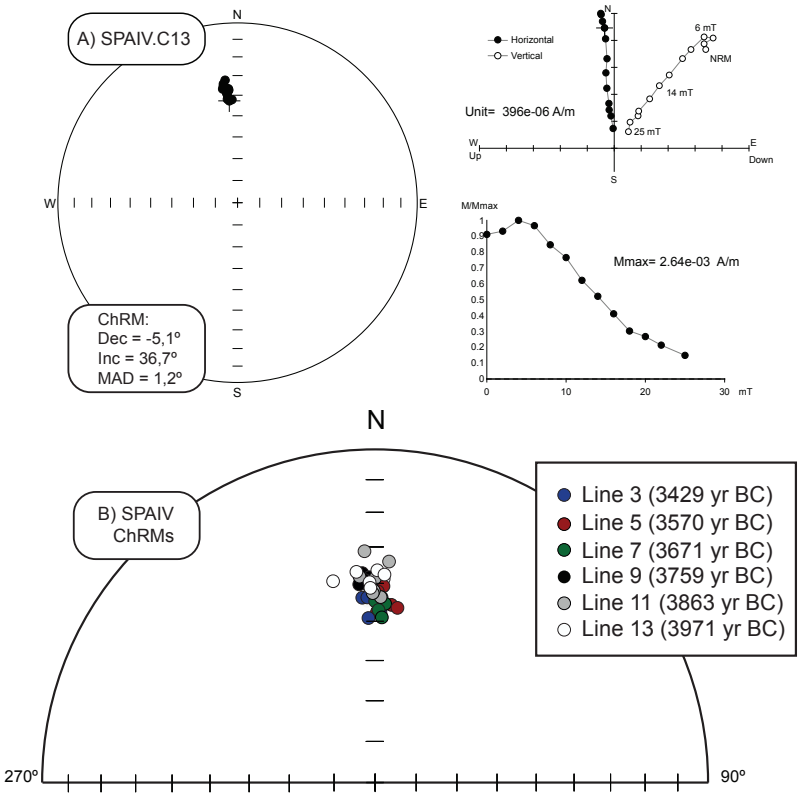

Figure 4.11 A) Stereographic and orthogonal projections and remanence intensities during alternating field (AF) cleaning of sample SPAIV_C13. After cleaning a viscous remanent magnetization below 6 mT, the orthogonal projection shows a unidirectional magnetic vector pointing to the origin. B) Stereographic projections of the Characteristic Remanent Magnetizations (ChRMs) obtained from all specimens; the colors correspond to the different lines.

4.2.4.2 Paleomagnetism

Paleomagnetic results are summarized in Figure 4.11 and in Table 4.3. NRM intensities are relatively high and range between $0.88x10^{-3}$ and $2.98x10^{-3}$ A/m, in agreement with previous data [*Font et al.,* 2014]. After cleaning of a weak (viscous) magnetization below 6 to 8 mT, orthogonal projections show stable and well-defined remanent magnetization directions trending to the origin (Figure 4.11 A). After AF demagnetization at 25 mT, about 90% of the remanence was cleaned. The median destructive field (MDF) ranges between 10 to 15 mT, confirming the presence of a low coercive phase (magnetite) as previously described by *Font et al*. [2014]. Sample-based magnetic directions are well clustered within a region from 348.2º to 5.2º in declination and from 31.4º up to 49.1º in inclination (Figure 4.11 B).

Table 4.3 Paleomagnetic, AMS and AARM data. Dec. and Inc. represents the magnetic declination and inclination respectively; MAD is the maximum angular deviation; NRM is the natural remanent magnetization intensity; K_m is the mean magnetic susceptibility; ΔK is the susceptibility difference and U correspond to the shape anisotropy parameter obtained from AMS measurement; P and T correspond to anisotropy degree and shape parameters, respectively; Inclination of k_3 (AMS) and k_1 (ARM) axis are also indicated.

							AMS				AARM			
Specimen	Calcite layer dip (º)	NRM (A/m)	Dec (º)	Inc (º)	MAD (º)	AF demag.	Km (SI)	ΔK	U	k3 (º)	Km (SI)	P	T	k1 (º)
SPAIV_A3	90	2,76E-03	-4	43,7	1,8	7 ; [8, 20]	5,24E-06	7,44E-07	0,189	9	7,03E-05	1,034	0,116	42
SPAIV_C3	88,5	2,33E-03	-2,4	43,7	1,7	7 ; [8, 20]	3,93E-06	9,53E-07	0,63	6	7,20E-05	1,045	-0,237	7,8
SPAIV_E3	79,5	2,04E-03	2	43,7	2,5	7 ; [6, 18]	2,23E-06	7,96E-07	0,739	15	5,85E-05	1,036	0,306	59,3
SPAIV_G3	77	2,49E-03	0,6	44,6	1,8	6 ; [8, 18]	4,53E-06	8,38E-07	0,435	20	7,17E-05	1,027	-0,077	7,8
SPAIV_I3	66	1,60E-03	0,9	45,9	1,3	8 ; [6, 20]	7,08E-07	8,27E-07	0,936	31	5,15E-05	1,037	-0,026	44
SPAIV_K3	56	2,01E-03	1,4	47,4	0,8	7 ; [10, 22]	1,49E-06	9,31E-07	0,903	41	5,89E-05	1,03	-0,378	57,6
SPAIV_L3	48,5	1,76E-03	1,8	47,7	1,4	8 ; [8, 22]	-1,09E-06	6,57E-07	0,945	48	5,12E-05	1,056	0,535	42,5
SPAIV_N3	35,5	1,66E-03	-2,3	49,1	2	8 ; [4, 18]	3,76E-06	1,43E-06	0,515	61	6,88E-05	1,047	-0,437	54,6
SPAIV_B5	77	1,11E-03	-2,8	40,3	3,7	5 ; [4, 12]	-	-	-	-	3,22E-05	1,055	-0,547	48,7
SPAIV_D5	81,5	1,27E-03	3,7	41,2	2	6 ; [6, 16]	-4,63E-06	1,44E-06	0,514	14	3,26E-05	1,047	-0,366	45
SPAIV_E5	72,5	1,33E-03	-0,3	42,3	1,5	7 ; [6, 18]	-7,32E-06	1,27E-06	0,725	23	3,56E-05	1,06	-0,594	64,3
SPAIV_G5	75	9,90E-04	1,1	42,1	2	5 ; [8, 16]	-9,18E-06	1,09E-06	0,79	28	2,94E-05	1,013	-0,562	62,4
SPAIV_I5	65,5	1,19E-03	-0,1	44,1	2,2	7 ; [8, 20]	-7,26E-06	1,24E-06	0,919	27	5,28E-05	1,039	0,064	76,7
SPAIV_K5	52,5	9,69E-04	0,4	48,4	2,1	6 ; [6, 16]	-7,95E-06	1,05E-06	0,696	37	3,11E-05	1,093	-0,396	85,7
SPAIV_L5	53,5	9,49E-04	0,8	46,2	2,3	6 ; [6, 16]	-8,31E-06	1,14E-06	0,562	44	2,83E-05	1,074	-0,135	55,1
SPAIV_N5	43	8,81E-04	7,3	46,1	1,7	5 ; [8, 16]	-8,96E-06	1,73E-06	0,37	47	2,84E-05	1,072	-0,315	57,5
SPAIV_A7	87	2,08E-03	1,7	44	2,5	8 ; [6, 20]	9,44E-08	2,29E-07	0,451	6	5,14E-05	1,054	-0,051	80,4
SPAIV_C7	85	1,82E-03	0,3	43,6	2,4	8 ; [6, 20]	9,69E-06	1,55E-06	0,357	7	4,61E-05	1,036	-0,376	63
SPAIV_E7	70,5	1,91E-03	0	44,4	1	8 ; [6, 20]	-7,16E-07	1,21E-06	0,249	20	5,00E-05	1,04	-0,616	39,8
SPAIV_G7	71	1,88E-03	0	44,2	1,9	8 ; [6, 20]	1,76E-06	1,15E-06	0,281	23	4,40E-05	1,067	-0,088	28,1
SPAIV_I7	62,5	1,88E-03	3,5	45,1	1,8	8 ; [6, 20]	2,08E-06	8,66E-07	0,66	34	4,92E-05	1,063	-0,4	62,4
SPAIV_K7	49	1,87E-03	0,9	46,5	1,7	8 ; [4, 18]	-1,01E-06	8,85E-07	0,88	41	5,31E-05	1,044	-0,725	62,6
SPAIV_N7	51	2,00E-03	0,7	46,4	1,9	8 ; [6, 20]	5,18E-06	9,02E-07	0,079	42	6,34E-05	1,058	-0,482	59,8
SPAIV_P7	34	2,03E-03	2,4	48,7	1,7	8 ; [6, 20]	4,50E-06	1,20E-06	0,003	58	6,65E-05	1,054	-0,072	58,2
SPAIV_A9	88	1,30E-03	-3,5	37,1	2,4	7 ; [6, 18]	-1,97E-06	5,18E-07	0,924	16	3,38E-05	1,054	0,15	57,8
SPAIV_C9	86	1,28E-03	0,3	38,9	1,9	7 ; [6, 18]	-4,52E-06	9,13E-07	0,415	14	3,72E-05	1,057	-0,067	27,4
SPAIV_E9	65	1,19E-03	-1,6	38,3	2,1	7 ; [6, 18]	-5,37E-06	9,13E-07	0,63	27	3,43E-05	1,171	0,445	48,1
SPAIV_G9	70	1,18E-03	-3	39	1,8	7 ; [6, 18]	-5,58E-06	8,78E-07	0,814	26	3,26E-05	1,037	-0,524	41,3
SPAIV_I9	61,5	1,32E-03	-2,1	40,4	1,7	7 ; [6, 18]	-5,25E-06	1,01E-06	0,768	36	3,72E-05	1,042	-0,253	38,3
SPAIV_K9	51	1,60E-03	-4,6	40	2,2	7 ; [6, 18]	-3,48E-06	1,14E-06	0,658	50	4,62E-05	1,071	0,089	68,9
SPAIV_N9	54,5	1,16E-03	0,8	41,8	2,2	6 ; [6, 16]	-4,81E-06	7,63E-07	0,839	50	3,89E-05	1,059	-0,592	54,2
SPAIV_P9	35	9,99E-04	-2,5	44,7	2,4	6 ; [6, 16]	-2,72E-06	6,30E-07	0,795	61	4,24E-05	1,067	-0,265	68,4
SPAIV_A11	84	1,05E-03	-2,5	31,4	3	8 ; [6, 20]	3,38E-05	1,09E-06	0,67	12	6,06E-05	1,047	0,106	17,1
SPAIV_C11	76,5	1,65E-03	-4,3	38	2,7	7 ; [8, 20]	3,61E-05	1,15E-06	0,714	15	7,72E-05	1,061	-0,243	67,2
SPAIV_E11	68,5	1,45E-03	0,1	39,8	1,4	7 ; [6, 18]	2,90E-06	8,44E-07	0,697	25	6,88E-05	1,064	0,67	13
SPAIV_G11	70,5	1,66E-03	3,6	34	3,5	7 ; [4, 16]	3,79E-06	7,89E-07	0,849	27	7,29E-05	1,055	-0,287	39,7
SPAIV_I11	60	1,60E-03	-1,6	40,8	1,6	7 ; [6, 18]	4,19E-06	1,22E-06	0,077	29	8,53E-05	1,055	-0,654	50,3
SPAIV_K11	51	1,51E-03	1,7	43,6	2,6	6 ; [8, 18]	4,88E-06	9,94E-07	0,867	44	8,31E-05	1,037	-0,486	47,1
SPAIV_N11	50,5	1,80E-03	-0,4	41,9	2	7 ; [6, 18]	7,63E-06	9,14E-07	0,771	45	9,49E-05	1,072	0,274	38,5
SPAIV_P11	33,5	2,28E-03	-0,7	42,6	2,9	6 ; [6, 16]	2,31E-05	5,59E-07	0,549	64	1,54E-04	1,099	-0,249	67,5
SPAIV_A13	87,75	1,71E-03	-11,8	38,3	3,2	5 ; [12, 20]	8,58E-06	1,34E-06	0,561	11	8,61E-05	1,038	0,553	4,5
SPAIV_C13	76,5	2,64E-03	-5,1	36,7	1,2	7 ; [8, 20]	8,22E-06	1,20E-06	0,605	23	9,11E-05	1,071	-0,162	62,3
SPAIV_E13	72	2,87E-03	0,7	36,1	2,1	8 ; [6, 20]	6,55E-06	1,45E-06	0,924	28	8,63E-05	1,073	0,137	19
SPAIV_G13	69,5	2,89E-03	2,6	37,6	1,5	8 ; [6, 20]	6,57E-06	1,06E-06	0,719	27	8,12E-05	1,114	-0,313	35,9
SPAIV_I13	62	2,37E-03	2,5	38,5	2,3	8 ; [6, 20]	4,77E-06	1,25E-06	0,521	31	7,49E-05	1,101	-0,745	54,5
SPAIV_K13	47	2,19E-03	-2,6	39,4	2,2	8 ; [6, 20]	3,27E-06	2,28E-06	0,263	49	7,50E-05	1,067	-0,778	69,4
SPAIV_N13	41	2,98E-03	-1,5	41,3	1,6	8 ; [6, 20]	6,44E-06	1,31E-06	0,714	49	7,92E-05	1,07	-0,256	55,8
SPAIV_O13	37	2,31E-03	-4,4	42,2	2,1	6 ; [6, 16]	-	-		-	6,55E-05	1,06	0,065	77,3

Maximum angle deviation (MAD) values are low (0.8º to 3.7º). The recorded magnetic inclinations decrease from the top to the base of the speleothem, a pattern verified in all six lines (Figure 4.12 A) and evidenced by the striking correlations ($0.67<R^2<0.97$) between the magnetic inclination and the dip angle of the corresponding calcite laminae. The trend is very similar in four of the studied lines (3, 7, 9 and 13) and slightly higher in lines 5 and 11.

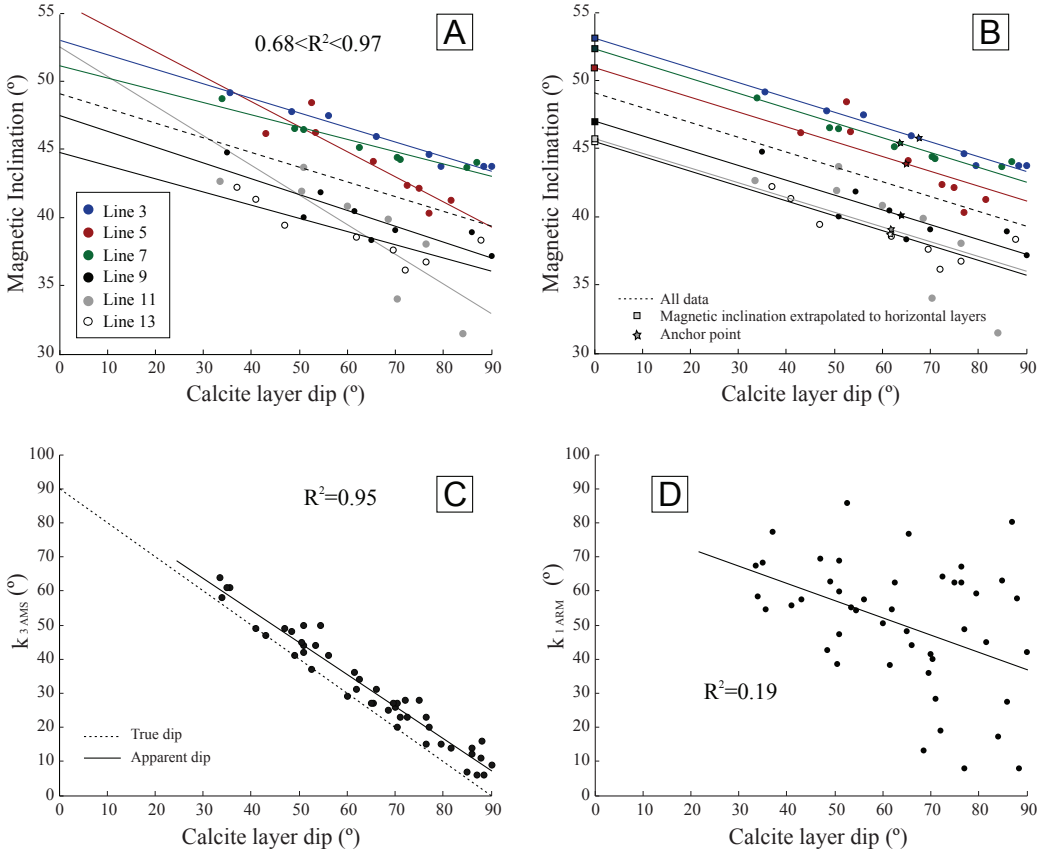

Figure 4.12 (A) Remanent magnetic inclination as a function of the calcite layer dip. The dashed line represents the linear regression considering all data. (B) Same data but with the trend line corrected by using the slope of the linear regression calculated in (A). The anchor points (stars) are defined by the sample based mean magnetic inclination and the mean calcite layer dip of each line. Extrapolated magnetic inclinations for horizontal calcite layer is obtained at calcite dip = 0º. (C) $k_{3\,AMS}$ and (D) $k_{1\,ARM}$ inclinations in function of the calcite layer dip. The determination coefficient (R^2= 1- ($SS_{residual}/SS_{total}$)) is also shown.

4.2.4.3 Anisotropy of Magnetic Susceptibility

The AMS data are illustrated in Figure 4.13 and in Table 4.3. The bulk susceptibility ($K_m = [k_1 + k_2 + k_3] / 3$) varies from -9.18×10^{-6} to 3.61×10^{-5} SI and includes 18 samples with negative values and 28 samples with positive values (Figure 4.13 A). These values are slightly higher than the magnetic susceptibility of pure calcite (K_m= -12.1x10^{-6} SI [*Schmidt et*

al., 2006] or K_m= -15x10^{-6} SI [*Borradaile and Jackson,* 2010]), pointing towards a major contribution of diamagnetism due to calcite and a few, but significant, contribution of para- and/or ferromagnetic minerals to the bulk susceptibility.

The AMS eigenvectors ($k_1 \geq k_2 \geq k_3$) are clustered within elongate 95% confidence regions (Figure 4.13 B). Parameters k_1 and k_2 are confined within an NW-SE great circle, while k_3 is oriented NE-SW and has inclination values ranging from nearly horizontal to 70º (Figure 4.13 B).

The susceptibility difference ΔK varies from 2.29x10^{-7} to 2.28x10^{-6} SI (Figure 4.13C). The mean value of ΔK is 1.05x10^{-6} SI, comparable to the reference value of 1.1x10^{-6} SI of calcite [*Schmidt et al.,* 2006]. The U parameter is positive for all samples, confirming the oblate fabric suggested by the orientation of the AMS ellipsoid (Figure 4.13 D).

The oblate shape and the gradually decreasing k_3 inclinations with respect to the calcite layer inclination points to a fabric that mimics the shape of the speleothem, i.e. where the magnetic foliation (k_1- k_2) is concordant with the surface of the speleothem with k_3 perpendicular to it. Such a feature is strengthened by the very strong positive correlation (R^2=0.95) between k_3 inclination and the dip of the calcite layers (Figure 4.12 C). Samples from the base of the speleothem (vertical layers) display the highest k_3 inclinations, while the samples located at the top (sub-horizontal layers) are nearly vertical. However, the inclination of the k_3 susceptibility eigenvector is systematically steeper (by over 10° in some cases) than the complement to the calcite layer dip (90°-calcite layer dip) (Figure 4.12 C), which suggests that the measured calcite layer angle is an apparent dip rather than the true dip, or that the orientation of the AMS ellipsoid is slightly influenced by the orientation of the AARM ellipsoid (i.e. orientation of the ferromagnetic particles).

The striking correlation between k_{3AMS} and the calcite layer dip suggests that a close relationship exists between the orientation of the AMS fabric and the crystallographic orientation of the calcite crystals, similarly to what has been shown by *Zhu et al.* [2012]. The crystallisation of calcite crystals in speleothems follows the direction of the c-axis, which corresponds to the longest axis perpendicular to the bedding plane. This orientation corresponds to the k_{3AMS} axes measured in this study.

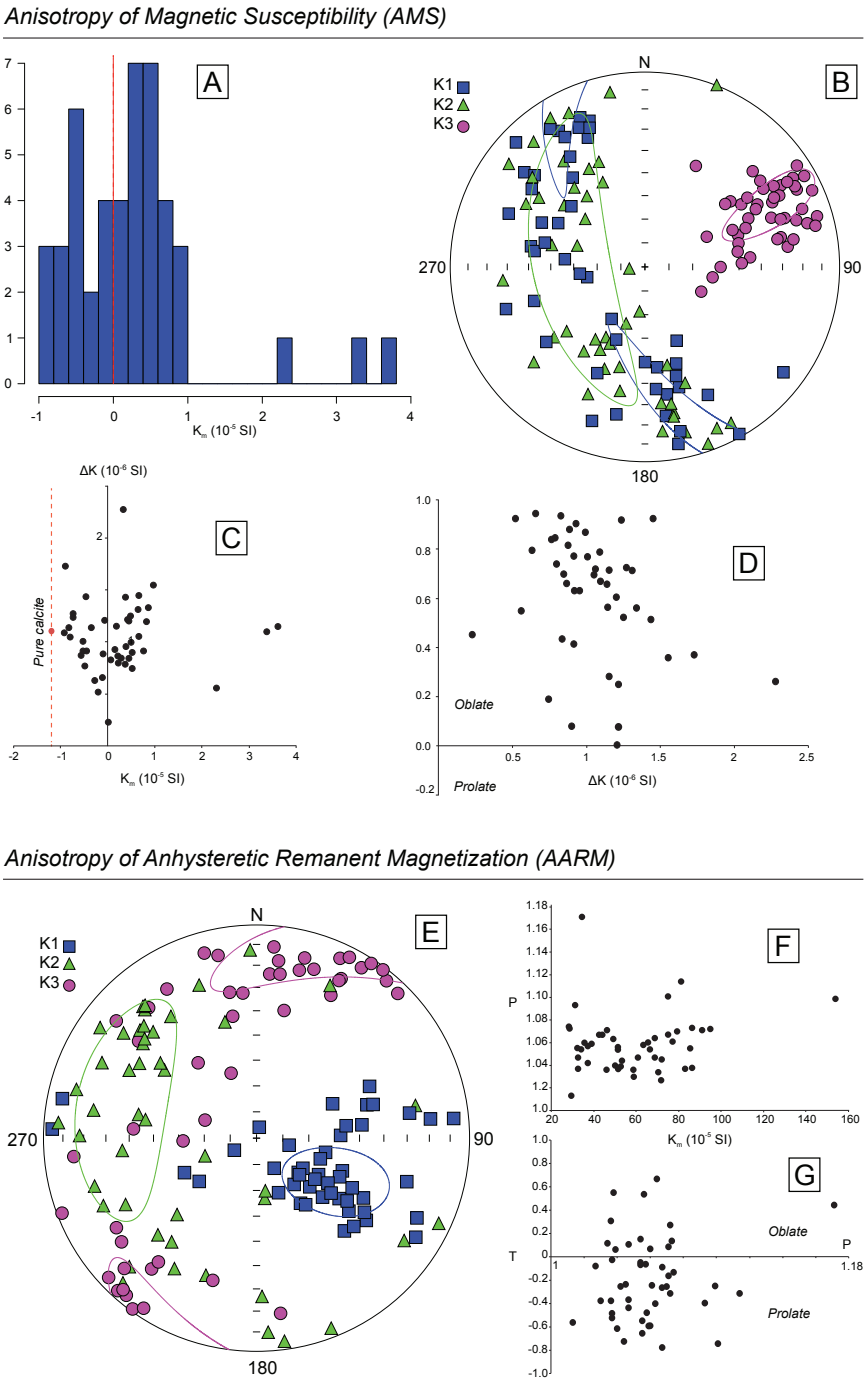

Figure 4.13 AMS and AARM data of the SPAIV speleothem. A) Histogram of the mean magnetic susceptibility B) Representation of the three principal axis of magnetic susceptibility: k_1 (squares), k_2 (triangles), k_3 (circles). C) Susceptibility difference (ΔK) versus bulk susceptibility (K_m) diagram. The red point in ΔK-K_m represent the reference value for pure calcite [*Schmidt et al*., 2006]. D) Shape anisotropy (U) versus ΔK; oblate and prolate domain are also shown. E) Representation of the three principal axis of anhysteretic magnetic remanence: k_1 (squares), k_2 (triangles), k_3 (circles). F) P parameter (anisotropy degree) versus bulk susceptibility diagram. G) Shape parameter (T) versus anisotropy degree parameter (P).

4.2.4.4 Anisotropy of Anhysteretic Remanent Magnetization

AARM data are illustrated in Figure 4.13 and Table 4.3. Most of the maximum remanent anisotropy axes (k_{1ARM}) are preferentially distributed within the SE quadrant of the stereographic projection, and show variable inclinations ranging from 40 to 80º (Figure 4.13 E-G). The intermediate and minimum axes (k_{1ARM} and k_{2ARM}) are more dispersed, but distributed along a NE-SW great circle (Figure 4.13 E).

The samples exhibit a weak ARM anisotropy, with P ranging from 1.013 to 1.114, at the exception of sample E9 that shows a P of 1.171 (Figure 4.13 F). Despite this low anisotropy, the fabric is a dominantly prolate (more than 70% of the samples), while some samples exhibit an oblate fabric, as shown by T values ranging from -0.778 to 0.670 (Figure 4.13 G). k_{1ARM} are not close to the horizontal plane but are rather steeply inclined (Figure 4.13 E). More exactly, sub-horizontal calcite layer has higher values of k_{1ARM} inclination (60-80º), while sub-vertical calcite layer exhibits shallower k_{1ARM} inclinations (Figure 4.13 D). This suggests that the orientation of the AARM ellipsoid (i.e. orientation of the ferromagnetic particles) depend on the slope: the steeper the slope is, the shallower the k_1 axes. Interestingly, samples located at the top of the speleothem, where the slope is shallower (~35º), show a lower dispersion of the $k_{1\ ARM}$ (55º to 75º) than in the case of samples located at the bottom (dip of 90º) for which $k_{1\ ARM}$ ranges from 5º to 80º (Figure 4.13 D). Such a gradual increase in the $k_{1\ ARM}$ dispersion suggests that the distance travelled by ferromagnetic minerals from the top to the bottom, as the water drops travel down the speleothem's surface, has a strong influence on the orientation of the AARM ellipsoids (see below).

4.2.5 Discussion

The new paleomagnetic data presented above indicates that the main magnetic carrier of the speleothem investigated in the present study is a low coercive phase, probably corresponding to magnetite and/or maghemite. Data corroborates previous results by *Font et al.* [2014], who pointed to the presence of a primary (detrital) remanent magnetization carried by pedogenic magnetite/maghemite based on detailed rock magnetic properties and microscopic observations. In contrast to most examples from the literature, the present SPAIV speleothem has rather high NRM intensities (~10^{-3} A/m) linked to the presence of a terrigenous detrital fraction also labelled by high detrital Th contents. The speleothem under study has a peculiar curved shape, in which the thickness of the calcite laminae remains nearly constant along the

growth surface. Both peculiarities provide the means to document with accuracy the influence of the speleothem shape on the recorded Earth´s Magnetic field.

In order to assess the influence of the speleothem's morphology on the recorded magnetic directions, SPAIV sample-based magnetic directions were compared with the dip angle of the corresponding calcite layers (Figure 4.12 A). As already mentioned, the results show a striking linear correlation (R^2>0.68) between the recorded magnetic inclination and the dip of the calcite layer (Figure 4.12 A): the steeper the calcite layer, the shallower the inclination of the NRM vector (Figure 4.14).

The inclination error observed in the studied speleothem can also be also evidenced by comparing the present data with the SHA.DIF.14k geomagnetic field model [*Pavón-Carrasco et al,* 2014]. The SHA.DIF.14K model is exclusively based on archaeomagnetic and lava flow data, and thus immune from possible influence of biased inclination data from sedimentary rocks. We analyzed the variation of the magnetic inclination of the speleothem under study between ~3970 yrs BC (line 13 on Figure 4.9) and 3430 yrs BC (line 3), and we considered the three following cases: i) nearly vertical layers (column C + sample B5 on Figure 4.9); ii) intermediate-steep (dip~65-75º) layers (column I); and iii) the top of the speleothem where calcite layer dip varies from 35º to 50º (column N). Results are illustrated in Figure 4.15. All lines show a trend comparable to the reference model within the interval of 3500-4000 yrs BC. The rate at which magnetic inclinations vary during this time interval is similar in the three cases (column B5-C, I and N) and comparable to the characteristic increase of the Earth's magnetic field inclination observed in the SHA.DIF.14k model during the studied time-interval. This suggests that the remanent magnetization recorded by the speleothem is primary and provides a robust record of the Earth's magnetic field at the time of deposition. However, the magnetic inclinations from the speleothem are underestimated (below the 95% confidence interval) compared to the SHA.DIF.14K model and are gradually displaced from the reference curve as the calcite dip increases (Figure 4.15).

The speleothem investigated has no horizontal layer at the top, but since the relation between the remanent magnetic inclination and the calcite layer dip is linear (Figure 4.12A), we attempted to extrapolate the data to the horizontal (dip of 0º in Figure 4.12 B). We first assume that the influence of the speleothem surface slope at any point should be the same for all lines, because calcite layers are mostly parallel in the speleothem under study (Figure 4.9). However, the linear regressions have slightly different slopes in Figure 4.12 A, mostly due to measurement errors of the magnetic inclination (ex. Line 11). For this reason, we calculate a

mean variation rate of the magnetic inclination as a function of the speleothem surface slope based on all data (48 samples) (dashed line in Fig. 4.12 A-B). Subsequently, the trend line is anchored to the point defined by the sample based mean magnetic inclination and mean calcite layer dip of each line (Figure 4.12 B). With this approach, the influence of samples affected by measurement errors is minimized. The final extrapolated magnetic inclinations are obtained when considering a calcite dip layer value of 0º. Finally, we compared the extrapolated magnetic inclinations with the SHA.DIF.14K model to check for the validity of our approach. The resulting corrected PSV curve shows a better correlation with the SHA.DIF.14k model than original data (Figure 4.15). Inclination values are slightly lower than the mean inclinations given by the model but are within the 95% confidence envelope. These observations confirm our inference about the critical influence of the speleothem shape on the recorded magnetic inclinations and highlight the need to further investigate this effect in future studies on speleothem magnetism.

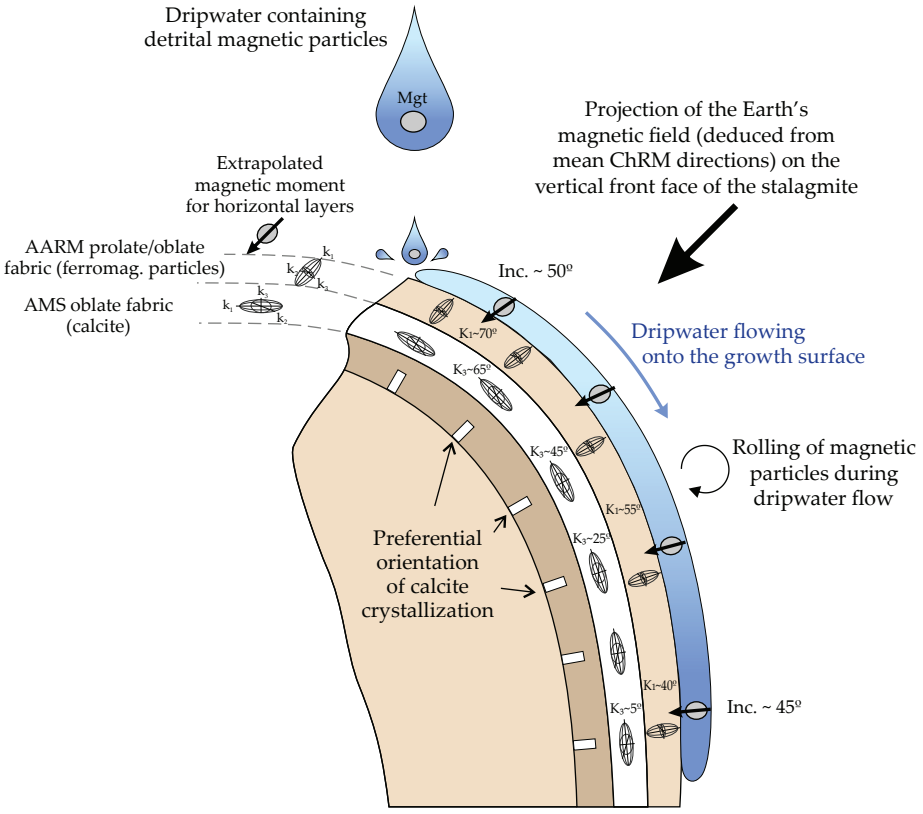

Figure 4.14 Conceptual model of the orientation of the magnetic grains when dripwater flows along the speleothem surface. The reported values of $k_{3\ AMS}$, $k_{1\ ARM}$ and magnetic inclinations are based on the present data set. Mgt = Magnetite grains.

The process by which sediments (including speleothems) acquire a detrital remanent magnetization (DRM) is a very complex and not completely understood mechanism. Less is known in the case of speleothem [*Lascu and Feinberg*, 2011]. Paleomagnetic inclinations in sedimentary rocks are frequently suspected of being too shallow, and the recognition and correction of shallow bias has been the focus of numerous investigations [e.g., *Verosub*, 1977; *Tauxe and Kent*, 2004; *Tauxe et al.*, 2008]. Since the early 1950s, a number of laboratory experiments simulated the deposition of sediments in an attempt to investigate the origin of the inclination error observed in sediments [see *Bilardello*, 2013 for a comprehensive review]. Their results indicated that particle size and shape (anisotropy), gravity, viscosity, water current, surface slope angle, intensity and direction of the ambient magnetic field, and magnetic interactions between magnetic particles are the main factors controlling the acquisition of a DRM. Some inclination error also occurs during post-depositional remanent magnetization acquisition by processes of compaction, slumping, bioturbation and water-filled voids allowing rotation of the magnetic minerals within the sediment matrix. However, such effects are insignificant in the case of speleothems, where burial and compaction are negligible, and where the time lag between the deposition of the magnetic particles and their immobilization by calcite precipitation is minimal [*Lascu and Feinberg*, 2011]. This leaves the ambient field, gravity, particle shape and size, slope and magnetic interactions as the main possible factors controlling the acquisition of DRM in speleothems.

The influence of the shape and orientation of the magnetic grains along the speleothem surface were studied here by using AMS and AARM techniques. AMS experiments showed the presence of an oblate fabric, with k_3 varying from nearly horizontal to strongly dipping (~65º) depending on the location at the base or the top of the speleothem, respectively (Figure 4.14). However, it is not possible to unequivocally distinguish whether the AMS signal is controlled by calcite and/or by ferromagnetic particles. Previous studies of natural and synthetic calcite show that the fabric is dominantly oblate [*Schmidt et al.*, 2006; *Zhu et al.*, 2012]. In the case of speleothems having few or no detrital components, the k_3 is generally perpendicular to the speleothem surface and corresponds to the direction of the crystallographic axis of the calcite crystals [*Zhu et al.*, 2012]. In the present case, the speleothem has a significant amount of detrital material [*Font et al.*, 2014], as also observable by the reddish colour of the speleothem. A significant amount of ferromagnetic grains is indicated by the rather high values of the NRM (~10^{-3} A/m) (this study) and saturation

isothermal remanent magnetization (SIRM~10^{-1}-10^{-2} A/m; [*Font et al.,* 2014]). However, the very low bulk susceptibility values, close to zero, strongly questioned the contribution of ferromagnetic minerals to the AMS signal. *Rochette* [1988] and *Schmidt et al.* [2006] observed that the AMS fabric changes from oblate to prolate when paramagnetic and/or ferromagnetic minerals are present, hence when their signal overcomes the negative susceptibility of calcite. In this case, the AMS fabric remains oblate independently of whether the K_m is positive or negative (Figure 4.13), suggesting that calcite is the main carrier of the AMS signal. This is consistent with the strong correlation of k_3 versus growth layer angle (R^2=0.95; Figure 4.12 C). We thus conclude that the variations of k_3 are representative of the shape of the speleothem (i.e. of the slope of the growing surface) and not of the orientation of the ferromagnetic particles, similarly to what has been shown by *Zhu et al.* [2012].

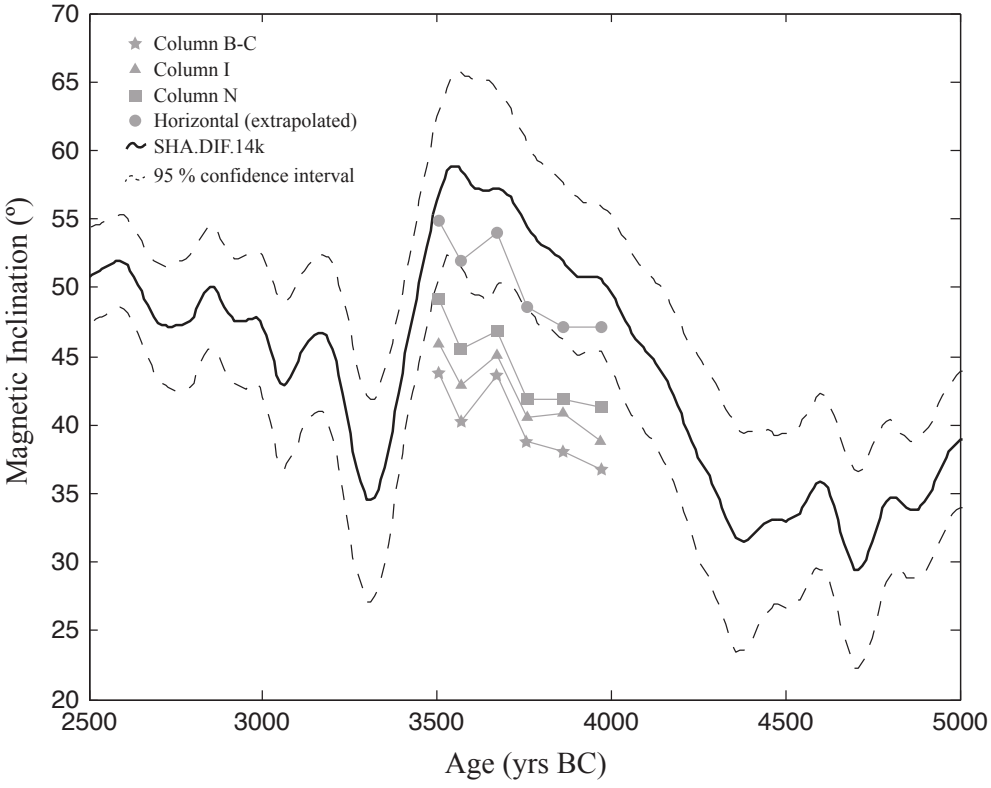

Figure 4.15 Comparison of the SPAIV magnetic inclinations with the SHA.DIF.14K model [*Pavón-Carrasco et al.,* 2014] calculated with respect to the speleothem age and for the cave's coordinates. The compared data refer to magnetic inclinations obtained from the samples in the column B-C (calcite dip angle ~ 75-85º), in column I (calcite dip angle ~ 65-75º), in column N (calcite dip angle ~ 35-50º), and extrapolated values to the horizontal layers (see text for more details).

AARM results differ strongly from those obtained by AMS techniques (Figure 4.13). AARM fabric presents a predominantly prolate shape (70% of the samples) with some samples having an oblate fabric (30%). $k_{1\ ARM}$ are relatively well-clustered into the SE quadrant, and most samples exhibit a very low degree of anisotropy (P). Such difference in the fabrics reinforces the evidence that AARM is carried by significant amounts of ferromagnetic particles, while AMS is essentially controlled by calcite. The relatively low degree of anisotropy (P<1.114) suggests a near-spherical shape of the magnetic minerals, typical of detrital magnetite grains. The fabric is preferentially prolate, with a minor contribution of oblate shapes. Inclination of the $k_{1\ ARM}$ axes shows a significant correlation with the calcite layer dip (Figure 4.12 D and 4.14). Independently of the shape (oblate or prolate) of the fabric, samples located at the top (horizontal layers) of the speleothem show $k_{1\ ARM}$ of ~70º, while samples located at the base (vertical layers) show $k_{1\ ARM}$ ~40º (Figure 4.14). This suggests that i) the particle shape has no or little control on the observed shallowing of the remanent inclination and ii) the latter is indeed controlled by the orientation of the magnetic minerals along the speleothem surface.

The first point has been investigated by *King* [1955], *Griffiths et al.* [1960] and *Bilardello* [2013], who conducted deposition experiments with spherical and platy particles under different conditions. Contrarily to the model of *King* (1955), who proposed that inclination error is mostly due to platy magnetic particles that would flatten due to gravity and align with the horizontal surface, *Griffiths et al.* [1960] suggested that rolling of the spherical particles as they encounter the substrate could also generated shallow inclination. More recently, *Bilardello et al.* [2013] and *Bilardello* [2013] have shown that sphere alone may lead to significant amounts of shallowing, and that this shallowing is also dependent on the ambient magnetic field.

Assuming that the particle shape has no influence on the shallowing of the inclination error, we suggest that the orientation of the magnetic particles along the surface of the speleothem under study is controlled by the interplay between the intensity/direction of the Earth's magnetic field during precipitation, gravity, and the slope of the speleothem surface. Gravity alone cannot explain the subsequent inclination errors, otherwise $k_{1\ ARM}$ would be vertical (parallel to the slope) at the bottom of the speleothem, which is not the case (Figure 4.12 D and 4.14). On the other hand, under the proviso that the magnetic inclinations provided by the SHA.DIF.14K are true, the direction of the Earth's magnetic field at the time of calcite precipitation alone cannot explain the observed remanent magnetic inclinations, which are

~5º lower in the extrapolated horizontal layer than in the SHA.DIF.14K model (Figure 4.15). This scenario (i.e. the case of the horizontal layer) is comparable to the experiment of *Bilardello et al.* [2013], who conducted a laboratory experiment using spherical magnetic grains settled in a tube. Considering field inclination of 30º and 60º, the authors obtained inclination shallowing of 7-20º, values compatible to our case study. Based on a newly developed numerical model, *Bilardello et al.* [2013] also suggested that particle collision during settling combined with both rolling and slipping (translation) are consistent with the experimental results. This model would also explain why the orientations of the magnetic particles evidenced by the orientation of $k_{1\ ARM}$ are much more scattered at the bottom of the speleothem than the top. As gravity preferentially acts on the sub-vertical slope at the bottom and/or the ferromagnetic grains roll more because of the increased travel distance, the directions of $k_{1\ ARM}$ become more scattered and shallow [*Jezek* et al., 2012; *Bilardello et al.*, 2013].

These findings are illustrated in Figure 4.14. Note that the difference observed between the magnetic inclination measured at the bottom and the top of the speleothem differ from ~5º, whereas the difference observed between the $k_{1\ ARM}$ is more than 30º. This corroborates the observation of *Jackson et al.* [1991] who suggested that the orientation of the long axes of the ferromagnetic particles is mainly controlled by physical mechanism (rolling in this case), while the orientation of the magnetic moment is mainly controlled by the geomagnetic field. The increased misalignment of the magnetic particles results in a net distribution of magnetic moments that is shallower than the orientation of the ambient geomagnetic field.

Although our findings are specific to the speleothem investigated, whose shape is not common, it provides important insights into the NRM acquisition mechanisms in speleothems. Accordingly, it is also strongly recommended to study horizontal layers collected in the center of the speleothems, in agreement to what has been done in recent paleomagnetic studies [e.g., *Osete et al.*, 2012; *Lascu et al.*, 2016], where shallowing effect is suggested to be minor. However, further investigations are urgently needed to evaluate the extent of the shallow inclinations and improve the representativeness of paleomagnetic data in speleothems.

4.2.6 Conclusions

Our results show that the recorded magnetic inclinations in the speleothem under investigation are strongly influenced by its shape. Comparing the obtained magnetic inclinations with a global paleosecular variation model (PSV) indicates that magnetic inclinations move gradually away from the PSV curve as the surface slope increases. The best fit between our data and the PSV model is obtained when extrapolating magnetic inclinations to the horizontal.

Although the studied speleothem contains significant amounts of detrital particles (including ferromagnetic grains), its AMS signal is dominantly carried by diamagnetic calcite, attested by negative bulk magnetic susceptibility, and corresponds to an oblate fabric where k_3 represents the crystallographic direction of the calcite growths and thus mimics the shape of the speleothem. On the other hand, the orientation of the AARM ellipsoid is perpendicular to the calcite layers and its orientation varies according to the slope of the layers, i.e. the steeper the slope, the shallower the $k_{1\ ARM}$. Although the remanent magnetic directions recorded in the speleothem under study are mainly controlled by the ambient geomagnetic field, inclination error may result from the influence of physical mechanism, such as particle rolling and slipping during transport along the slope. Increased misalignment of the ferromagnetic particles results in a net distribution of directions that is shallower than that of the ambient geomagnetic field. Contrarily to previous studies suggesting that speleothem shapes had no influence on the remanent magnetization, the present data provide the first and undisputable piece of evidence against this conclusion. Our data also suggest that inclination error may occur even in horizontal layers, and this aspect should deserve more attention in forthcoming paleomagnetic studies of speleothems.

4.3 Appendix I (Dating)

The reconstruction of the paleosecular variation curve recorded on the studied speleothem requires a precise dating of the samples. A slice of the speleothem has been dated using the U-Th disequilibrium method, but the contamination of detrital Thorium (in higher content on darker layers) lowers the precision, making it necessary to apply correction methods. The results are resumed in Table 4.4 and Figure 4.16, with the ages before and after correction. The uncorrected ages range between 6678 and 13247 yrs BP, but the stratigraphy principle is not corresponded since the age is not growing continuously from the top to the bottom (age inversion), as it should. After applying both corrections, the age inversion only occurs for the detrital fraction method between 1.25 and 8.25 cm depths, where age decreases from 5513 to 5381 yrs BP. The dating of the layer at the depth of 8.25 cm is problematic since its very dark (see Figure 4.16), with more concentration in detrital material and therefore higher contamination in detrital thorium, resulting in higher errors. Results from detrital fraction and stratigraphic method are very similar, with slightly higher uncertainty in the latter. However, the stratigraphic method constrains the ages to avoid age inversions, so that I have chosen the corrected ages obtained from the stratigraphic method to reconstruct the paleosecular variation.

Table 4.4 Dating results of the speleothem in six points (yrs BP): uncorrected ages, corrected ages using stratigraphic $^{232}Th/^{238}U$ method and corrected ages using measured detrital fractions with less than 2 μm.

Depht (cm from top)	Uncorrected age (yrs BP)	Corrected Age (Stratigraphic method)	Corrected Age (detrital fraction method)
0,25	7961 ± 238	5180 ± 296	5080 ± 244
1,25	7281 ± 195	5577 ± 217	5513 ± 191
8,25	13247 ± 519	5670 ± 716	5381 ± 536
10,50	6678 ± 138	6011 ± 142	5984 ± 136
17,00	7339 ± 157	6474 ± 164	6438 ± 155
18,50	7335 ± 181	6523 ± 186	6489 ± 179

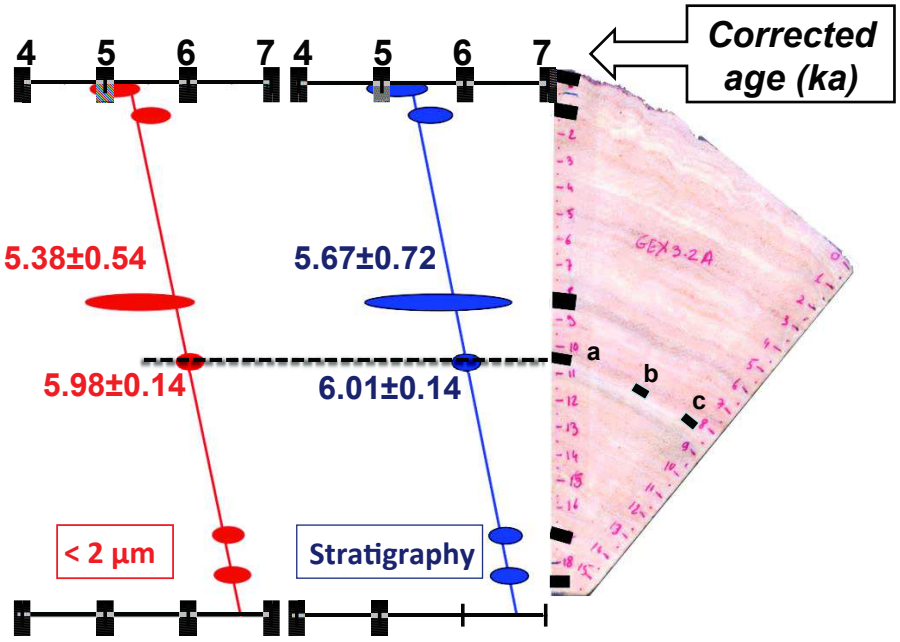

Figure 4.16 Determination of the speleothem age after correction of dating by to different methods: Stratigraphic $^{232}Th/^{238}U$ and detrital fraction < 2 µm.

As referred before, the speleothem had been dated only in six specific points, which do not necessarily coincide with the "lines" used for the paleomagnetic study documented in this chapter. For this reason, one of the objectives at the beginning of the PhD was to determine the age of the studied "lines", to reconstruct the paleosecular variation recorded in the speleothem and compare it to PSV models or paleomagnetic data. The first challenge stems from the fact that dating has been performed on another slice of the speleothem. The darker/lighter calcite layers of the slice in which dating has been done (GEX3.2A) could be easily identified and associated in the slice used in this study (SPAIII). For example, the line D (Figure 4.17 - SPAIII.D1 to SPAIII.D5) follows a lighter calcite layer (next to a darker layer) that corresponds to the 10.5 cm depth of the dated slice (Figure 4.17). With the first challenge exceeded, the next step would be to estimate an age for the lines A to E. In order to achieve this objective, an algorithm specifically developed by *Scholz and Hoffmann* (2011) for speleothems has been used, the StalAge.

StalAge has been designed to construct speleothem age models, based on U-series ages and their uncertainties. It is applicable to problematic datasets, with outliers, age inversions, hiatuses and large changes in growth rates. The algorithm is written in the open source statistical software R and the input consists in a .txt file with the U-series data, with the depths and corresponding age and uncertainty. The user is also asked to insert in another text

file the depths at which the algorithm returns the exact calculation of the age and their upper/lower 95% confidence limit in an output file, as a complement of the final age model graphic for the whole age interval with the calculated age curve and the upper/lower limits with 95% confidence drawn. The final age model is calculated with a Monte Carlo simulation fitting ensembles of straight lines to sub-sets of the age data, after analysis of outliers, age inversions and other possible features. For the age model used during the PhD, the input file contains the ages corrected by the stratigraphic method. Another input file with several depths, including those estimated for the lines A to E, was also created, so that StalAge returned an output file with the estimation of the ages and the respective 95% confidence levels (Table 4.5).

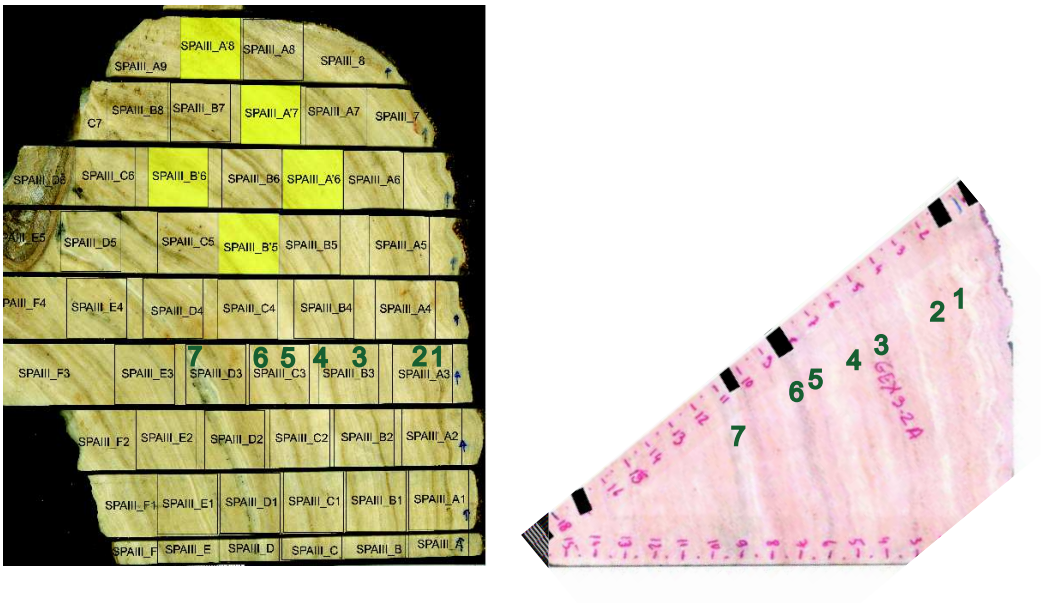

Figure 4.17 Pictures of SPAIII (the slice used for paleomagnetic analysis in this chapter) and GEX3.2A (the slice of the speleothem used for dating). The numbers associate referenced darker calcite layers from GEX3.2 to SPAIII, what allowed to transpose the ages of GEX3.2A to SPAIII.

The age model for the studied speleothem, obtained using the algorithm StalAge (Figure 4.18), is crucial for the interpretation of magnetic and paleomagnetic results. It allows estimating the age in every point of the speleothem, which makes it possible to analyze the variation of data in time and compare it to another dated results from other investigations.

Table 4.5 Output table of the StalAge algorithm applied to U-series data of the studied speleothem. The estimated age, with 95% confidence upper and lower limits, for the corresponding depth are returned.

Depth (cm)	Age (yrs BP)	Upper limit	Lower limit
0,25	5353	5523	5167
1,25	5441	5628	5260
2,15	5519	5723	5334
2,5	5545	5751	5357
3,1	5582	5785	5390
4,05	5633	5823	5421
5	5684	5867	5435
5,75	5727	5908	5450
6,5	5771	5950	5488
7,35	5822	5994	5564
8,25	5876	6037	5653
9,25	5936	6081	5736
10	5983	6116	5795
10,75	6033	6155	5862
11,5	6084	6197	5936
13,75	6233	6336	6128
14,75	6297	6404	6194
18,5	6543	6711	6402

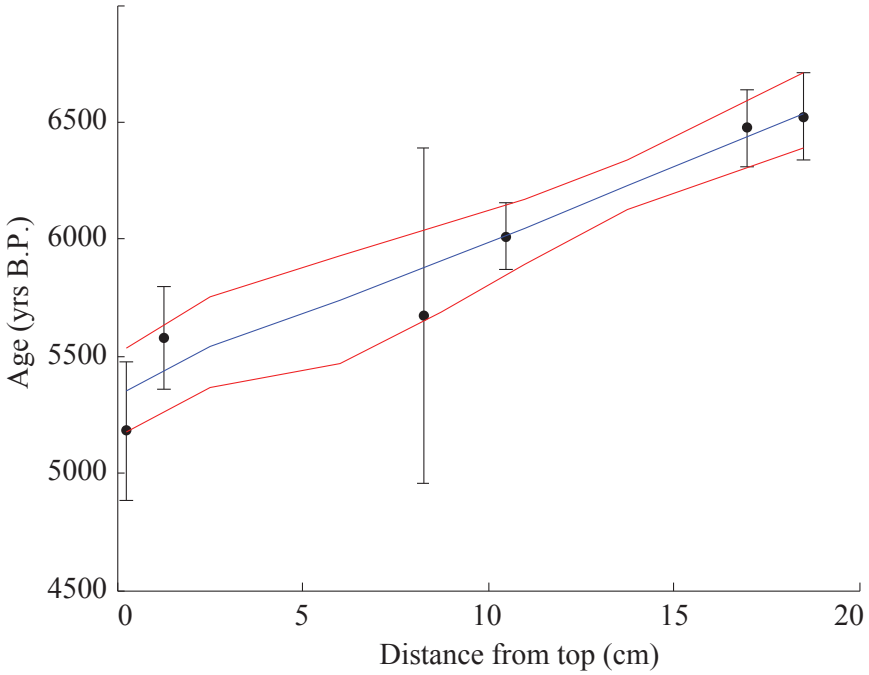

Figure 4.18 Age model proposed by algorithm StalAge. The black dots and respective error bars represent the input data, while the lines represent the estimated age (blue) and their upper/lower limits (red) with 95% confidence.

4.4 Appendix II (Table with unmixing of IRM curves of SPAIII, cubic samples)

Table 4.6 Unmixing results of IRM curves obtained for each sample. SIRM, coercivity, dispersion parameter and contribution of each component is given.

Sample	Component 1				Component 2				Component 3				Total SIRM	S-RATIO
	SIRM (A/m)	$\log(B_{1/2})$	DP	Cont (%)	SIRM (A/m)	$\log(B_{1/2})$	DP	Cont (%)	SIRM (A/m)	$\log(B_{1/2})$	DP	Cont (%)		
SPAIII_A1	4,20E-02	1,38	0,23	85,71	3,00E-03	1,95	0,15	6,12	4,00E-03	2,70	0,40	8,16	4,90E-02	0,932
SPAIII_A2	3,85E-02	1,37	0,22	83,70	4,00E-03	1,87	0,18	8,70	3,50E-03	2,75	0,45	7,61	4,60E-02	0,933
SPAIII_A3	3,75E-02	1,37	0,23	86,61	2,50E-03	1,90	0,18	5,77	3,30E-03	2,75	0,47	7,62	4,33E-02	0,929
SPAIII_A4	3,70E-02	1,37	0,22	86,05	2,50E-03	1,92	0,19	5,81	3,50E-03	2,80	0,45	8,14	4,30E-02	0,930
SPAIII_A5	3,95E-02	1,37	0,23	85,13	2,50E-03	1,91	0,20	5,39	4,40E-03	2,79	0,50	9,48	4,64E-02	0,926
SPAIII_A6	3,65E-02	1,38	0,24	85,88	2,50E-03	1,92	0,19	5,88	3,50E-03	2,80	0,45	8,24	4,25E-02	0,923
SPAIII_A7	3,90E-02	1,37	0,24	86,28	2,20E-03	1,90	0,19	4,87	4,00E-03	2,80	0,45	8,85	4,52E-02	0,923
SPAIII_A8	6,00E-02	1,38	0,25	89,29	1,70E-03	1,96	0,20	2,53	5,50E-03	2,80	0,45	8,18	6,72E-02	0,924
SPAIII_B1	3,30E-02	1,38	0,24	86,39	1,90E-03	1,97	0,18	4,97	3,30E-03	2,80	0,45	8,64	3,82E-02	0,927
SPAIII_B2	3,07E-02	1,38	0,24	87,22	1,50E-03	1,95	0,20	4,26	3,00E-03	2,80	0,45	8,52	3,52E-02	0,919
SPAIII_B3	3,10E-02	1,37	0,24	84,93	2,00E-03	1,94	0,20	5,48	3,50E-03	2,80	0,45	9,59	3,65E-02	0,921
SPAIII_B4	3,03E-02	1,37	0,24	87,57	1,50E-03	1,95	0,20	4,34	2,80E-03	2,80	0,45	8,09	3,46E-02	0,920
SPAIII_B5	4,00E-02	1,37	0,24	86,39	2,30E-03	1,93	0,19	4,97	4,00E-03	2,80	0,45	8,64	4,63E-02	0,915
SPAIII_B6	3,00E-02	1,36	0,23	83,80	2,50E-03	1,90	0,20	6,98	3,30E-03	2,80	0,50	9,22	3,58E-02	0,925
SPAIII_B7	4,23E-02	1,38	0,24	84,10	3,00E-03	1,95	0,17	5,96	5,00E-03	2,75	0,50	9,94	5,03E-02	0,926
SPAIII_B8	5,80E-02	1,37	0,23	82,86	4,00E-03	1,93	0,19	5,71	8,00E-03	2,75	0,50	11,43	7,00E-02	0,922
SPAIII_C1	3,10E-02	1,38	0,24	80,52	2,50E-03	1,95	0,15	6,49	5,00E-03	2,50	0,80	12,99	3,85E-02	0,930
SPAIII_C2	2,90E-02	1,37	0,23	83,82	2,30E-03	1,93	0,20	6,65	3,30E-03	2,80	0,45	9,54	3,46E-02	0,925
SPAIII_C3	3,55E-02	1,37	0,24	85,96	2,30E-03	1,93	0,16	5,57	3,50E-03	2,80	0,50	8,47	4,13E-02	0,926
SPAIII_C4	3,40E-02	1,36	0,23	83,33	3,00E-03	1,95	0,20	7,35	3,80E-03	2,80	0,45	9,31	4,08E-02	0,922
SPAIII_C5	5,05E-02	1,37	0,24	87,37	2,50E-03	1,96	0,19	4,33	4,80E-03	2,75	0,45	8,30	5,78E-02	0,917
SPAIII_C6	7,75E-02	1,37	0,24	89,08	2,00E-03	2,01	0,16	2,30	7,50E-03	2,75	0,45	8,62	8,70E-02	0,921
SPAIII_D1	3,70E-02	1,38	0,24	86,25	2,20E-03	1,94	0,20	5,13	3,70E-03	2,80	0,50	8,62	4,29E-02	0,930
SPAIII_D2	3,96E-02	1,37	0,24	88,20	1,80E-03	1,99	0,17	4,01	3,50E-03	2,80	0,45	7,80	4,49E-02	0,927
SPAIII_D3	3,67E-02	1,38	0,24	88,43	1,80E-03	1,99	0,18	4,34	3,00E-03	2,80	0,45	7,23	4,15E-02	0,926
SPAIII_D4	3,88E-02	1,38	0,24	88,38	1,60E-03	1,93	0,16	3,64	3,50E-03	2,80	0,45	7,97	4,39E-02	0,927
SPAIII_D5	2,95E-02	1,38	0,24	85,51	1,50E-03	1,93	0,19	4,35	3,50E-03	2,80	0,45	10,14	3,45E-02	0,928
SPAIII_E1	2,58E-02	1,38	0,24	86,87	1,30E-03	1,97	0,19	4,38	2,60E-03	2,80	0,50	8,75	2,97E-02	0,927
SPAIII_E2	2,45E-02	1,38	0,24	85,66	1,60E-03	1,92	0,18	5,59	2,50E-03	2,80	0,45	8,74	2,86E-02	0,924
SPAIII_E3	2,33E-02	1,38	0,24	87,27	1,20E-03	1,92	0,19	4,49	2,20E-03	2,80	0,45	8,24	2,67E-02	0,927
SPAIII_E4	1,95E-02	1,38	0,24	83,69	1,30E-03	1,90	0,18	5,58	2,50E-03	2,80	0,45	10,73	2,33E-02	0,923

4.5 Appendix III (Correction of magnetic inclinations)

If the magnetic inclination recorded in the studied speleothem is biased by the calcite layer dip, this effect should be corrected to obtain a more realistic magnetic field direction at the time of formation. In the paper, it was suggested that only central samples (with horizontal layers) should be sampled. However, speleothem SPA does not have horizontal calcite layers, so a correction method should be applied. But how? Most speleothems grow much faster in the center, in the area where the drip water falls, resulting in a strong convergence of the growth lines in the lateral sides. This does not allow researchers to sample several specimens in the same growth line, with different slopes. Nevertheless, the speleothem under study exhibits a particular shape, which allowed collecting 8 specimens along each growth line. After analyzing the evolution of the magnetic inclination recorded in samples along the same growth layer, it is concluded that the decrease in magnetic inclination with the calcite layer dip is linear in a first approximation (see figure 4.12). By using the rate at which magnetic inclination decreases with the dip of calcite layers (the slope of the linear regression), it is possible to obtain a corrected magnetic inclination for hypothetical horizontal layers by linear extrapolation. In this method, the corrected magnetic inclination (for hypothetical horizontal layer) is obtained by summing the product of the linear regression slope and the calcite layer dip (the same as the rotation angle necessary to put the calcite layers in horizontal position) to the recorded magnetic inclination. For an easier understanding, an example is given, for the sample SPAIV.K3:

Recorded magnetic inclination = 47.4º

Calcite layer dip = 56º

Linear regression slope = 0.1

Corrected magnetic inclination = 47.4 + 0.1 x 56 = 53º

In the example of SPAIV.K3, the recorded magnetic inclination is 47.4º, and the calcite layer dip is 56º, so that a rotation of 56º is needed to put the growth layers in horizontal position. The rate at which the magnetic inclination varies with the calcite layer dip is approximately 0.1 (the slope of linear regression), what means that for an increase of the calcite layer dip of 10º, the magnetic inclination decreases 1º. This means that for a rotation of 56º to the

horizontal position (calcite layer dip = 0º), the magnetic inclination increases 5.6º, so that the corrected magnetic inclination is 53º (47.4º + 5.6º).

The calculation of the linear regression slope can be done in two different ways: based on all points (magnetic inclination vs calcite layer dip) of all measured samples or based on the points of a single growth layer (or "line"). In the first case, there is a single slope value applied in the correction of all samples, while in the latter case a specific slope is calculated for each line. I opted to the first option, since a linear regression slope calculated based on 48 samples is more robust than six different slopes (for the six lines) based on 8 points. Using the 48 samples to calculate the slope diminish the influence of a few "outliers" (points that deviate from the observed linear pattern). On the other hand, there is no guarantee that calcite layers dip influences the magnetic inclination the same way in all lines. There may be other factors, such as the detrital input (evidenced by the darker/lighter calcite layers), that may possibly change the influence of the calcite layer dip on the remanent magnetic direction. For this reason, the proposed correction for the magnetic inclination is based on two fundamental assumptions:

1. The relationship between magnetic inclination and calcite layer dip is linear.

2. The influence of the calcite layer dip on the recorded magnetic inclination is the same in the whole speleothem.

The applied correction is specific for the speleothem under study. In other speleothems, the magnetic inclination may not be affected by the calcite layer dip, or it may change in a different rate. Additionally, it can be only used in speleothems where a reasonable number of specimens can be sampled along a single growth line. However, for the SPA speleothem this correction may approximate the measured magnetic inclinations to the real values. Some corrections for shallowing inclination in sediments have been proposed before [*Jackson et al.,* 1991], but the acquisition of magnetic remanence processes were quite different from the ones occurring in speleothem. The correction proposed in this chapter is only a first attempt correction of the biased magnetic inclinations and should be improved in the future. The advances in the knowledge about the acquisition of magnetic remanence in speleothems are fundamental to understand how the calcite layer dip may influence magnetic inclination and help developing a more robust correction method in the future.

4.6 Appendix IV (Sampling and measurement of cylindrical samples)

The need to increase the resolution of the paleomagnetic data lead to the sampling of cylindrical specimens with diameter of 1.1 cm, instead of the cubic samples (~2x2x2 cm) used before. A new slice (SPAIV) of the speleothem was drilled following a carefully designed plan (see Figure 5.1) in order to make the best use of the space available, with two premises to be fulfilled: each line follow the same calcite growth line and each column is nearly perpendicular to the calcite layer dip. Initially, the lines 3, 5, 7, 9, 11 and 13 were used (Figure 4.9) to study the influence of calcite layer dip on recorded remanent magnetization (results described in this chapter), but for the reconstruction of the paleosecular variation (next chapter), data from 15 lines and 17 collumns were collected. The drilling process was made in a mechanical laboratory at University of Lisbon, using a Metalik PK203, where a cylindrical drill was attached to perforate the slice in the chosen, previously marked points. The speleothem aspect after sampling is shown in Figure 4.19.

The greatest difficulty in using small cylindrical samples concerns to the sample holders in the magnetic/paleomagnetic devices used in measurements, prepared for cylindrical samples with 2 cm of diameter or cubic samples with 2 cm size. After several tries, some of them unsucessfull due to high values of magnetization of the holders, which could interfere with magnetic data by masking/changing speleothem's signal, the solution was to cut a solid polystyrene foam cube that fits in the plastic cubic box used for the cubic sample holder. To insert the cylindrical sample, a hole in the middle of the polystyrene foam must be done with the size of the cylinders, ensuring the sample does not move during measurements when JR6 Spinner magnetometer rotates (Figure 4.20). All the holder's adaptations during the PhD were made using polystyrene foam, since it was the substance found with lower magnetizations.

Figure 4.19 Sampling of the slice SPAIV used in this chapter with a small (~1.1 cm of diameter) cylindrical drill.

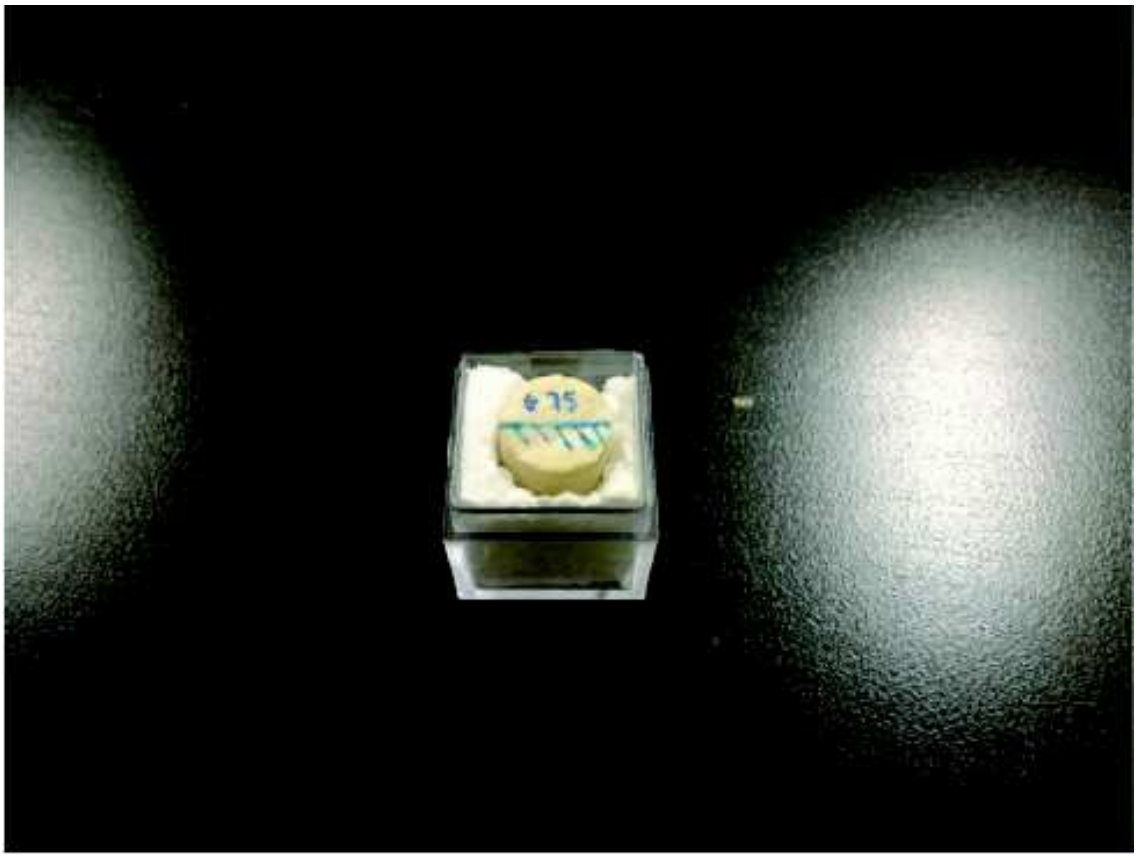

Figure 4.20 Sample holder used for cylindric samples: cubic box (2x2x2 cm) with polystyrene foam fixing the sample.

5. Reconstruction of paleosecular variation

Summary

In the chapter 5, I demonstrated the influence of the calcite layer dip on the recorded magnetic inclination. However, this aspect does not compromise speleothems as valid magnetic recorders. By avoiding sampling on the lateral sides of the speleothem (where calcite layers are more inclined) or by correcting the measured magnetic inclination, it is possible to obtain a reliable paleosecular variation curve. In this chapter, a complete reconstruction of the secular variation recorded in the studied speleothem is presented, by collecting paleomagnetic data from 102 cylindrical samples, distributed along 15 different lines (ages) between approximately 4100 and 3300 yrs BC. The data are compared with several PSV models and contemporaneous paleomagnetic data from volcanic rocks, archaeological objects and speleothems. Additionally, I provide relative paleointensity data still scarce in speleothems, using two different methods (one is used for the first time in speleothems). Results, published at *Geochemistry, Geophysics and Geosystems (G^3)* reinforce the idea that speleothems are good recorders of direction and intensity of the Earth's magnetic field. Additional data and discussion that has not been included in the paper are presented at the end of the chapter.

Speleothems as magnetic archives: paleosecular variation and a relative paleointensity record from a Portuguese speleothem

J. M. Ponte[1], E. Font[1,2], C. Veiga-Pires[3], C. Hillaire-Marcel[4]

[1] IDL-FCUL, Instituto Dom Luís, Faculdade de Ciências, Universidade de Lisboa, Lisbon, Portugal

[2] Departamento de Ciências da Terra, Faculdade de Ciências e Tecnologia, Universidade de Coimbra, 3000-272 Coimbra, Portugal

[3] CIMA-FCT, Universidade do Algarve, Faro, Portugal

[4] GEOTOP, Université du Québec, Montreal, Canada

(This chapter is presented in a paper format, as published by *Geochemistry, Geophysics and Geosystems, G*^{3}; Ponte et al., 2018, DOI: 10.1029/2018GC007651)

Abstract

We provide a high-resolution and complete paleomagnetic study from a middle-Holocene (~4100-3300 yrs BC) dome-shaped speleothem (SPAIV) from Algarve, Portugal. Our results show that the SPAIV speleothem carries a primary and stable remanent magnetization, for which directions are similar to other speleothems from the western Alps. Magnetic declination and inclination curves are also comparable to current paleosecular variation models (SHA.DIF.14k, CALS10k.1b and pfm9k.1a), one of them (SHA.DIF.14k) fitting better with the present data set. Relative paleointensity was estimated using two different methods: conventional normalization of NRM by ARM and IRM, and the pseudo-Thellier method, which is being tested here for the first time in a speleothem. Both methods show similar results, with a minimum intensity peak at ~3850 yrs BC. This low relative intensity is observed in all samples pertaining to the same respective calcite laminae. These results suggest that high growth rate speleothems are good high-resolution recorders of the direction and intensity of the Earth's magnetic field.

5.1 Introduction

Reconstructing Earth's short-term magnetic field behavior is crucial for understanding dynamo processes occurring in the Earth's outer core. Paleomagnetic data are commonly obtained from three main sources: marine or lake sediments, volcanic rocks and archaeological objects. High sedimentation rate marine or lacustrine sequences provide a continuous record of the geomagnetic field, but present potential biases due to distortion during sampling, and depositional or post-depositional effects such as bioturbation, compaction, diagenesis, etc. Lava flow and archaeological artefacts record a thermal remanent magnetization of the last time they cooled below Curie temperature, which is generally more stable than sediment magnetization. However, they only yield instantaneous records of the magnetic field. More recently, speleothems have been explored as potential archives of the Earth's magnetic field. These karstic deposits have been described as reliable earth magnetic field recorders [*Latham et al.,* 1979, 1982, 1986, 1989; *Morinaga et al.,* 1986, 1989; *Martin,* 1990; *Lean et al.,* 1995; *Openshaw et al.,* 1997; *Osete et al.*, 2012; *Font et al.,* 2014; *Lascu et al.,* 2016; *Ponte et al.,* 2017]. Within the last few years, research on speleothem magnetism has grown particularly, with some focus on the magnetic fabric [*Zhu et al.,* 2012], mineralogy and relations with climate [*Bourne et al.,* 2015; *Jaqueto et al.,* 2016; *Zhu et al.,* 2017], and on the origin of the recorded remanent magnetization [*Strauss et al.,* 2013; *Font et al.,* 2014; *Ponte et al.,* 2017]. As illustrated in these papers, the remanent magnetization is generally detrital in origin and carried by pedogenic magnetite transported by water from soils into karsts through rock fissures. During their deposition within the calcite laminae in the speleothem, these detrital magnetic grains align with the ambient magnetic field and are rapidly encapsulated by precipitation of calcite shortly after deposition, leading to an efficient record of the earth's magnetic field [*Lascu and Feinberg*, 2011]. Speleothems may thus provide very high resolution and relatively continuous record of the ancient magnetic field, depending on calcite deposition rates and processes, without being affected by effects such as bioturbation or compaction. On the other hand, such paleomagnetic data from speleothems can be biased by the slope of the speleothem surface. Some previous studies of such depositional influences on magnetizations recorded off the growth axis of stalagmites were not conclusive [e.g., *Latham et al.,* 1979, 1982, 1986, 1989; *Morinaga et al.,* 1986, 1989; *Lean et al.,* 1995; *Openshaw et al.,* 1997]. In a previous study [*Ponte et al.*, 2017], we have demonstrated that magnetic inclination decreases with steepening slope down a stalagmite periphery. This effect has to be further tested, but can nonetheless be corrected using a linear correlation between calcite dip and magnetic inclination [*Ponte et al.,* 2017], or can be

minimized when measuring in the most horizontal calcite layers along the growth axis of the speleothem.

Although speleothems are considered as good recorders of the Earth's magnetic field direction, little is known about their capability to record relative paleointensities. *Osete et al.* (2012) reported the first relative paleointensity (RPI) record in a speleothem from Cobre Cave in northern Spain and recognized the previously reported low RPI values of the Blake geomagnetic excursion, with a notable relative maximum peak just after the first reversal. *Lascu et al.* (2016) provided detailed geomagnetic record, including a low relative paleointensity level, of the Laschamp geomagnetic excursion in an accurately dated (U-Th) speleothem from North America. In front of these recent advances in the field of speleothem magnetism, further examination of their reliability as time-series recorders of paleosecular variations and paleointensity are needed. Here, we report on additional directional (PSV) data in a radioisotopic well-dated speleothem (named SPAIV; dated 4500-3200 yrs BC by the U-Th method) collected in Algarve (Portugal), previously studied by *Font et al.* (2014) and *Ponte et al.* (2017), and compared them with contemporaneous archaeomagnetic, volcanic and speleothem data from Spain and Italy, as well as three different PSV models (*CALS10k.1b*, *SHA.DIF.14k and pfm9k.1a*). We also calculate relative paleointensity data based on the normalization of natural remanent magnetization (NRM) by isothermal (IRM) and anhysteretic (ARM) remanent magnetization, and on pseudo-Thellier method, a method that has not yet been tested on speleothems. Our results provide new insights about the potential of speleothems to record high-resolution and accurate paleomagnetic data, and about how they may contribute to improve PSV models.

5.2 Geological Settings

The SPAIV speleothem was collected in the Excentricas Cave, located above the Peral-Moncarapacho Jurassic karstic aquifer of the Algarve basin, southern Portugal (geographic coordinates of 37°06' N, 7°46'W). The speleothem was orientated in-situ using a magnetic compass and has been subsequently cut in several slices in the laboratory. The speleothem was dated at ~4500 to 3200 yrs BC by U-Th disequilibrium method, and the age model was calculated using StalAge algorithm [*Scholz and Hoffmann*, 2011]. More details about dating are available in *Veiga-Pires et al.* (2011), *Ghaleb et al.* (2014) and *Ponte et al.* (2017). Detailed rock magnetic, mineralogical and geochemical data are provided in *Font et al.* (2014). Preliminary paleomagnetic data of 48 specimens distributed along six growth layers are provided in Ponte et al. (2017). Here, we used the same specimens as described in *Ponte et al.* (2017) and augmented the sample collection by collecting 54 additional samples along

nine growth layers, giving a total of 102 specimens distributed along 15 growth layers dated from 4100 to 3300 yrs BC (Figure 5.1). This new sampling results in an increase of temporal resolution, which is fundamental for secular variation reconstruction. Considering that the speleothem SPAIV encompasses approximately 800 yrs, the time span is ~50 yrs per sample.

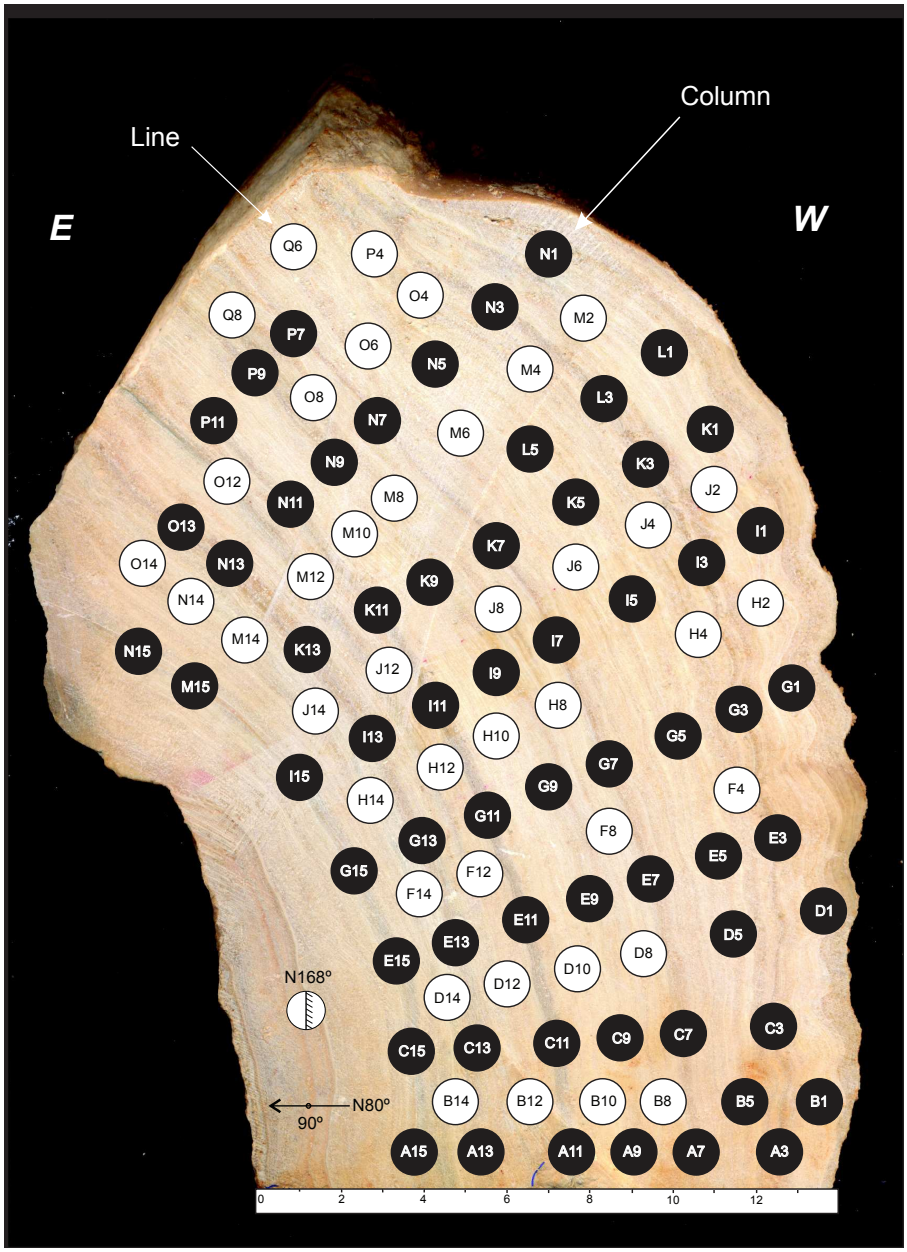

Figure 5.1 Vertical face of the speleothem with location of the cylindrical SPAIV specimens collected for subsequent paleomagnetic measurements. Samples are distributed along lines corresponding to calcite growth layers of a similar age, and columns that represent the temporal variations. Cylindrical specimens and their respective orientation are also shown. The face of the speleothem block is approximately oriented E-W, with a declination of N80º and a vertical inclination. Individual cylindrical specimens of 1.1 cm in diameter and 2 cm in height were drilled perpendicularly to the E-W oriented face of the block, with a declination of N168º (80º+90º-2º; -2º being the correction of the local magnetic declination in Algarve at the time of sampling).

5.3 Methods

Magnetic measurements were performed at the Paleomagnetism Laboratory of the Instituto Dom Luiz, Faculty of Sciences of the University of Lisbon, Portugal. The magnetic remanence was measured using a JR6 spinner magnetometer (sensitivity of 2.4×10^{-6} A/m) after step-wise alternating field (AF) demagnetisation using a LDA-3A demagnetizer. The AF field was increased progressively with steps of 2 mT up to 100 mT. Characteristic Remanent Magnetization (ChRM) was calculated based on Principal Component Analysis [*Kirschvink, 1980*] and Fisher statistics [*Fisher, 1953*] using the software Remasoft 6.0 (AGICO) software. Reconstruction of paleointensity data from sedimentary sequences has always been challenging, because paleointensity is strongly influenced by variations in magnetic grains size and concentration, as well as viscous remanent magnetization (VRM) (see review from *Tauxe, 1993*). For this reason, two different methods were used: normalization of NRM by a ferromagnetic concentration dependent parameter, namely isothermal (IRM) and anhysteretic (ARM) remanent magnetization in order to account for changes in grain size and concentration, and the pseudo-Thellier method (*Tauxe et al.,* 1995) to also eliminate VRM contribution. The results for the normalization methods are expressed as the average of the RPI values calculated for the samples belonging to the same growth line (Figure 5.1). Considering the low number of samples per line (3 to 8) and consequently the low number of measurements considered in the mean, the uncertainty Δx_{avg} was calculated according to the formula $\Delta x_{avg} = \Delta x/\sqrt{N}$, where N is the number of samples used in the mean and Δx is given by $(x_{max} - x_{min}) / 2$, where x_{max} and x_{min} are the maximum and minimum values respectively.

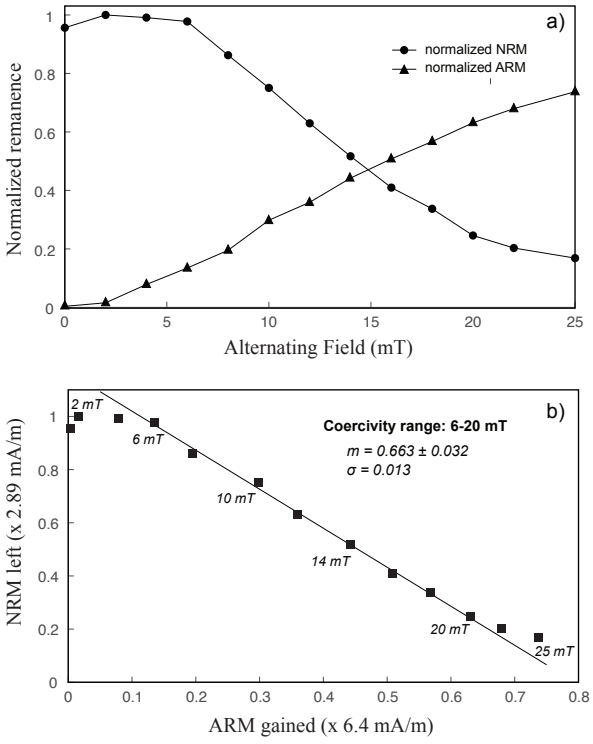

Figure 5.2 Example of the pseudo-Thellier method applied in sample SPAIV.G13. (a) Stepwise AF demagnetization and ARM acquisition curves. The values are normalized by their maximum values (ARM maximum of 6.4×10^{-3} A/m after applied an alternating field with 100 mT of intensity). (b) Arai plot: NRM intensity left after AF demagnetization steps vs ARM gained at the same peak field. Paleointensity estimate (m) corresponds to the best fit slope through the points which better define a line (6-20 mT), calculated by the least squares method. The uncertainty of m reflects the 95% confidence interval and σ is the standard error of the slope.

For comparison between different methods, RPI values were normalized by the mean value of the respective RPI data set. IRM acquisition was performed using an impulse magnetizer (model IM-10-30) by application of a magnetic field with 100 mT, which is strong enough to saturate most magnetite grains, the main magnetic carrier present in these samples, while hematite and goethite have a low contribution to the total saturation remanence (<14%) (*Font et al.*, 2014). Anhysteretic remanent magnetization (ARM) was imparted by a combination of a progressively increased AF field (the same intensities used during AF demagnetization process) and a constant DC field of 0.05 mT using a LDA-3A demagnetizer coupled to an AMU-1A anhysteretic magnetizer. The pseudo-Thellier method, based on paleointensity determination techniques using thermally blocked remanences developed by *Thellier and Thellier* (1959) and improved by *Coe et al.,* (1978), is illustrated in Figure 5.2. Relative paleointensity corresponds to the slope of the NRM left after AF demagnetization versus ARM intensity gained at the same peak field. The best fit slope *m* was determined using linear regression on the data points that best lie along a line. For each sample, the set of consecutive points with lowest standard deviation of slope (σ), with a representative number of points, was chosen to estimate the RPI (m). The slope and its standard deviation σ were estimated using the LINEST function of Microsoft Excel. A 95% confidence interval for the RPI values was also calculated by the product of σ and the t-student value. The t-value of the Student's t-distribution was determined using the T.INV function in Excel, based on the number of degrees of freedom that characterizes the distribution (number of points – 2). In the example shown in Figure 5.2b (SPAIV.G13), RPI is calculated choosing the coercivity window between 6 and 20 mT. For fields weaker than 6 mT the data do not exhibit a linear behavior, due to the contribution of a VRM component. Pseudo-Thellier method has been tested in columns G-H and M-N, in order to have two distinct temporal records of relative paleointensity with the highest resolution.

5.4 Results

5.4.1 Paleomagnetism

Paleomagnetic data are provided in 5.1 and 5.3 (appendix II). NRM intensities vary between $7.01x10^{-4}$ and $3.01x10^{-3}$ A/m, which are relatively high compared to other speleothem documented in the literature. The characteristic remanent magnetization (ChRM) is obtained after cleaning a weak viscous remanence between 4 and 6 mT in most of samples (Figure 5.3). In some specimens, such as SPAIV.K3, the viscous component was erased with slightly higher AF field of 8 mT. The directions of the ChRM are stable and point to the origin of the orthogonal projection. More than 90% of the remanent magnetization is erased after applying an AF of 25 mT. The median demagnetization field (MDF) is between 10 and 15 mT, indicating the presence of low coercivity ferromagnetic minerals. All characteristic remanent magnetic directions point towards North (declinations of -18º to 7º) with inclinations of 30-50º, with maximum angular deviation of 0.8º-4.6º (Table 5.3). Mean magnetic directions were calculated based on the ChRM calculated from the samples drilled in the same line (growth layer). Site-based mean declinations range between -9.2º and 1.2º, with inclinations varying between 35.3º and 45.7º. The dispersion of magnetic directions is very low, as precision parameter *(k)* values are between ~240 and 2800, and $\alpha 95$ values range between 1.3-4.4º.

Considering that magnetic inclinations vary according to the dip of the calcite laminaes (*Ponte et al.,* 2017), inclination data were corrected by extrapolating to a theoretical horizontal surface using the mean variation rate estimated for the whole data set (decrease of ~ 1º in magnetic inclination for a 10º increase in calcite laminae dip) [see *Ponte et al.*, 2017 for more details]. Corrected inclination values vary between 40.7 and 52.5º (Table 5.1). Obviously, precision parameter *k* increases (~440 to 8700) and $\alpha 95$ values decreases (0.6-2.9º) in the case of corrected data because magnetic inclination values along a growth line, originally biased by the variation of the calcite laminae dip, become less dispersed after extrapolated to a horizontal layer angle.

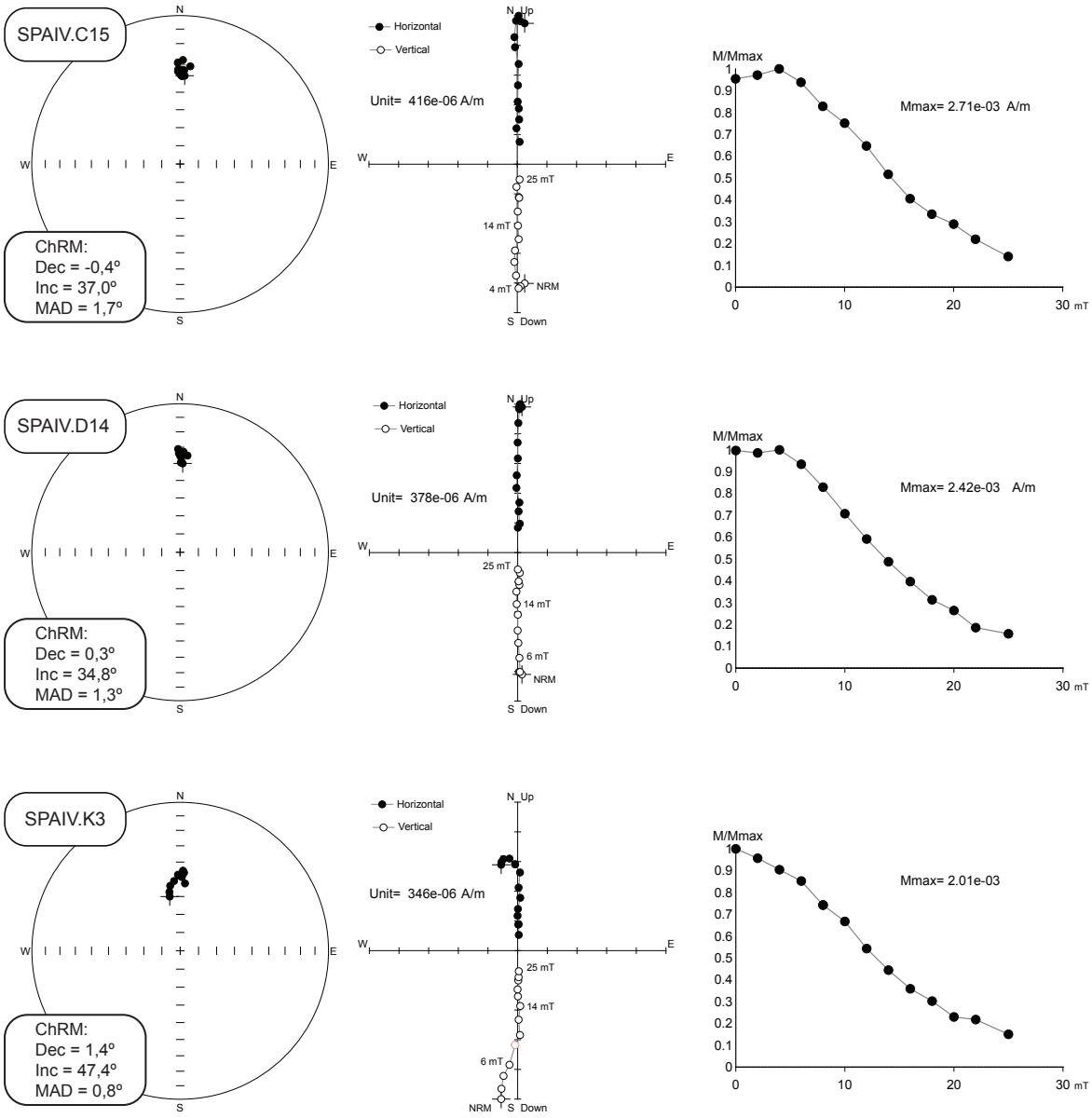

Figure 5.3 Stereographic and orthogonal projections and remanence intensities during alternating field (AF) cleaning of samples SPAIV.C15, SPAIV.D14 and SPAIV.K3. After removing a viscous remanent magnetization below 6-8 mT, the orthogonal projections show a unidirectional magnetic vector pointing to the origin.

Table 5.1 Summary of SPAIV dating and paleomagnetic results for each line: age estimation by StalAge algorithm and its 95% confidence interval (*Age interval*); N is the number of selected samples for mean direction and statistics; *Dec.* and *Inc.* represents magnetic declination ad inclination respectively; *k* corresponds to the precision parameter and *α95* to confidence limit; In the *uncorrected* section the obtained mean magnetic directions for each line are based on the original paleomagnetic data set, while in *corrected* section the calculation is performed with magnetic inclination values corrected for the calcite layer dip effect.

					Uncorrected			*Corrected*		
Line	**Age (BC)**	**Age interval**	**N**	**Dec (º)**	**Inc (º)**	**k**	**α95 (º)**	**Inc (º)**	**k**	**α95 (º)**
1	3341	[3155 ; 3511]	7	-9,1	36,6	243,07	3,9	43,5	440,75	2,9
2	3385	[3201 ; 3563]	3	-5,1	38,5	803,44	4,4	44	2310,91	2,6
3	3429	[3248 ; 3616]	8	-0,2	45,7	925,72	1,8	52,5	3110,84	1
4	3507	[3322 ; 3711]	6	-0,4	45,5	739,68	2,5	51,5	1616,93	1,7
5	3570	[3378 ; 3773]	8	1,2	43,9	512,59	2,4	50,4	980,24	1,8
6	3621	[3409 ; 3811]	4	-1,4	45,2	2785,06	1,7	50,5	8665,92	1
7	3672	[3423 ; 3855]	8	1,2	45,3	1727,27	1,3	51,8	7943,76	0,6
8	3715	[3438 ; 3896]	8	-3,7	41,1	583,33	2,3	47,4	738,32	2
9	3759	[3476 ; 3938]	8	-2	40	869,52	1,9	46,4	2153,45	1,2
10	3810	[3552 ; 3982]	4	-3	38,2	1252,78	2,6	45,3	2132,34	2
11	3864	[3641 ; 4025]	8	-0,5	39	289,3	3,3	44,9	604,67	2,3
12	3924	[3724 ; 4069]	7	-2,1	38	696,3	2,3	44,6	1156,52	1,8
13	3971	[3783 ; 4104]	8	-2,3	38,7	356,54	2,9	45	522,96	2,4
14	4021	[3850 ; 4143]	8	-1,4	35,3	706,11	2,1	41,2	1962,09	1,4
15	4072	[3924 ; 4185]	7	-4,2	35,8	545,47	2,6	40,7	495,08	2,7

5.4.2 Relative Paleointensity (RPI)

Relative paleointensities (RPI) are illustrated in Figure 5.4. The IRM-ARM normalization method was applied to all samples individually, and the mean RPI value for each line (age) is represented in Figure 5.4a, with the respective uncertainty. Normalization of NRM using either ARM or IRM shows very similar results, which is often believed to express RPI reliability [*Kruiver et al.* 1999]. RPI values are nearly constant from 3800 to 3300 yrs BC (fluctuations between 0-20% around the mean value), with the exception of lines 11-12 (3800-3900 yrs BC), where a minimum RPI peak is observed (40% lower than mean value).

The Pseudo-Thellier method has been tested in columns G, H, M and N. In order to achieve the highest temporal resolution, consecutive columns were coupled, resulting in two different records of pseudo-Thellier RPI: G+H (Figure 5.4b) and column M+N (Figure 5.4c). The RPI calculated using classic NRM/ARM and NRM/IRM normalization for the same columns was also plotted for comparison: both methods generally show very similar curves. The record provided by columns G-H and M-N is slightly different: G-H shows small fluctuation around the mean value (0-20%) between 3750 and 3300 yrs BC, while the RPI record of samples

from columns M-N slowly increases during this period. Columns M-N also show a maximum peak near 4000 yrs BC, which is not present in columns G-H. However, the minimum RPI peak near 3900 yrs BC, also observed in Figure 5.4a with classic methods, is clearly present in both G-H and M-N curves.

5.5 Discussion

The main focus of this study is to discuss the reliability of the magnetic records of speleothems, both in direction and relative intensity of the geomagnetic field. The speleothem under study has been shown to carry a primary detrital remanent magnetization (DRM), carried by detrital and low coercive minerals (magnetite and/or maghemite) inherited from the terra rossa soils capping the cave [*Font et al.,* 2014]. The magnetization includes a weak viscous magnetic component cleaned below 8 mT and a high intensity (~10^{-3} A/m) characteristic remanent magnetization (ChRM), several orders higher than the majority of speleothems described in the literature. The complete paleomagnetic dataset used in this study exhibits the same characteristics as previously published, with well-defined magnetic vectors and low maximum angular deviations (MAD). These aspects make the speleothem under study a good candidate for testing the reliability of speleothem as suitable recorders of paleomagnetic and paleointensity data. Beforehand, *Ponte et al.* (2017) showed that the shape of the speleothem, more exactly the dip of the calcite laminae, may bias the values of the recorded magnetic inclination, through a process of particle rolling along the speleothem surface. This can be resolved or at least minimized by considering samples located in the horizontal surface, where particle rolling is minimum [*Billardelo*, 2013] or by applying a correction as calculated in *Ponte et al.* (2017). *Ponte et al.* (2017) analyzed several samples per site (a site corresponding to a time interval of ~1.1cm thick calcite laminae) and for which the dip of the calcite laminae varies from sub-horizontal to vertical. Results showed that the relationship between the surface slope and the recorded magnetic inclination is linear and allows extrapolation of the recorded magnetic inclinations to a theoretical horizontal surface. The shortcoming of this method is that it is more time consuming, because it requires the analysis of a larger set of samples, but it is statistically more precise because it provides site-based mean directions instead of a sample-based mean direction of a sample located at the horizontal surface. Since the speleothem under study does not have horizontal calcite laminae, we applied this empirical correction to the more complete paleomagnetic dataset of the SPAIV speleothem presented here and compare this dataset with other paleomagnetic and paleointensity records from neighboring regions.

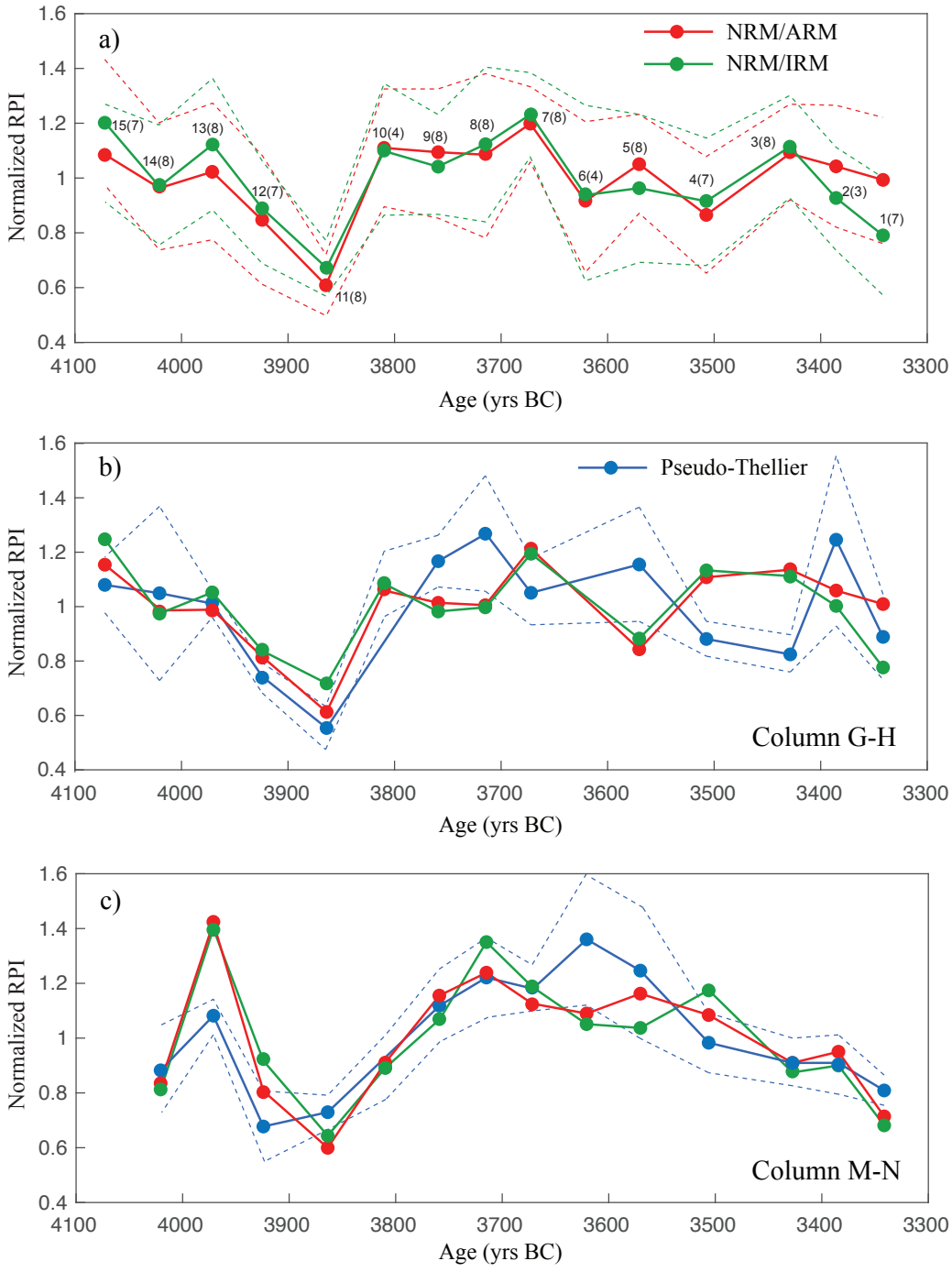

Figure 5.4 Relative paleointensity (RPI) curves from SPAIV. The values are normalized by their mean value. (a) Standard normalization: mean value for NRM/ARM and NRM/IRM in each line (age). The uncertainty of the mean (Δx_{avg}), represented by the dashed lines, is calculated by the following expression: $\Delta x_{avg} = \Delta x/\sqrt{N}$, where N is the number of samples used in the mean and $\Delta x = (x_{max} - x_{min})/2$. The corresponding line number (Figure 5.1) and the number of samples used in the mean (N) are indicated below each point. Standard normalization and pseudo-Thellier method results for the columns G and H (b), and for columns M and N (c). Uncertainty of pseudo-Thellier method is represented by a 95% confidence interval (dashed lines).

Paleomagnetic data contemporaneous with the age of the SPAIV speleothem are very scarce or come from areas located far from Portugal. According to *Noel and Batt* [1990], geographically separated magnetic directions in a decadal timescale can only be accurately compared (with mean angular errors of approximately 2º) when the areas under study are within a maximum of 1200 km. The only paleomagnetic data for which the distance from Algarve is less than 1200 km are archaeomagnetic data collected in northern Spain [*Carrancho et al*., 2013] and paleomagnetic data from the volcanic Canary Islands [*Kissel et al.,* 2015], which are used for comparison. Recently, paleomagnetic data obtained from a speleothem (flowstone) located in the western Alps (Italy), 1500 km from Algarve, were provided by *Zanella et al.* [2018]. The distance from Algarve is slightly above the 1200 km limit, but this case study is important to consider for comparison since it is the only paleomagnetic data from a speleothem located relatively nearby. Also note that paleomagnetic data from RDM1 and RDM8 from the Alps correspond to sample-based (individual) directions, while the SPAIV data are site-based mean directions based on a number of samples per line (age). Beforehand, we apply the correction via pole method proposed by *Noel and Batt* [1990], which is based on the conversion of paleomagnetic directions to a referenced site using a virtual geomagnetic pole [*Irving*, 1964]. In addition, we also compare our data with magnetic declination and inclination curves from available global PSV models: *SHA.DIF.14k* [*Pavón-Carrasco et al.,* 2014], *CALS10K.1b* [*Korte et al.,* 2011] and *pfm9k.1a* [*Nilsson et al.,* 2014]. These models are based on compilations of paleomagnetic data collected worldwide and use an expansion on a spherical harmonic basis in space and cubic B-splines in time. The main differences between the three models is the sources of the paleomagnetic data: *CALS10k.1b* includes records from sediments, volcanic rocks and archaeomagnetic objects; *SHA.DIF.14k* only includes data from volcanic rocks and archaeomagnetic objects; *pfm9k.1a* incorporates the three kind of data sources, but redistributes the weight given to each kind of source, averaging out the contribution of data from sediments. Despite the importance of sediments for the study of the past geomagnetic field, the corresponding remanent acquisition mechanisms (depositional or post-depositional) are exposed to several factors that may influence the paleomagnetic record, such as flattening and bioturbation, among others. As a consequence, the geomagnetic reconstruction using this paleomagnetic data source suffers from significant smoothing effects [*Roberts and Winklhofer*, 2004; *Panovska et al.,* 2012; *Panovska et al.,* 2015; *Nilsson et al.,* 2014].

The magnetic declination and inclination curves obtained from SPAIV data and the three PSV models mentioned above are represented in Figure 5.5, together with paleomagnetic data from

northern Spain, Canary Islands and Italy (two cores), corrected via pole method. Magnetic declination recorded by SPAIV shows small variations (<5º) from ~ 4100 yrs BC to 3400 yrs BC, but show a significant and consistent decrease of -9º between 3400 and 3300 yrs BC (Figure 5.5). From 4100 to 3300 yrs BP, SPAIV declinations are significantly different from northern Spain and the Canary Islands. Declination data from northern Spain are relatively scattered and present a large uncertainty, making any comparison with our data or with PSV models difficult. Data from the Canary Islands (two data points) exhibit lower uncertainties, which are included in the 95% confidence envelope of the CALS10.1a and SHA.DIF.1K models, but are generally 5º lower when compared to the SPAIV declinations. Magnetic declination values obtained from the alpine flowstone show different behavior between its two cores. The RDM1 core values are strongly scattered, and systematically lower than our data and models. RDM8 core exhibits a more consistent trend, which is strongly similar to the SPAIV data and PSV models between 4000 and 3400 yrs BC (Figure 5.5). However, RDM8 data are generally higher than the declination values predicted by the PSV models before 4000 yrs BC. Concerning the comparison of our data with PSV models, SPAIV declinations generally lie within the range predicted by the *SHA.DIF.14k* model, except for the time interval between 4000 and 3800 yrs BC, where SPAIV magnetic declination is higher. SPAIV declination data also well fit the *CALS10K.1b* model, except for the time interval around ~3500 yrs BC, where the typical decrease in magnetic declinations observed in our data and in the SHA.DIF.14K model is not expressed in the CALS10K.1b model (Figure 5.5). Model *pfm9k.1a* also shows a nearly constant magnetic declination curve during the studied time period, although slightly lower when compared to SPAIV data and model *CALS10K.1b*.

Magnetic inclination recorded by SPAIV generally increases from ~ 4100 yrs BC until approximately 3400 yrs BC, and then abruptly decreases in the last 100 yrs (Figure 5.5). This pattern is very similar to the PSV curve of *SHA.DIF.14k,* and to both RDM1 and RDM8 flowstone cores from the Alps. However, SPAIV magnetic inclination values (red curve in Figure 5.5) are significantly lower when compared to all PSV models and to paleomagnetic data from northern Spain, Canary Islands and western Alps. However, once corrected for the effect of the slope as mentioned above, magnetic inclination values overlap the 95% confidence interval of the *SHA.DIF.14k* model, even though slightly underestimated compared to the mean. A possible explanation is that inclination shallowing may also occur in horizontal layers, even after correcting data by the slope effect [*Billardelo et al.*, 2013].

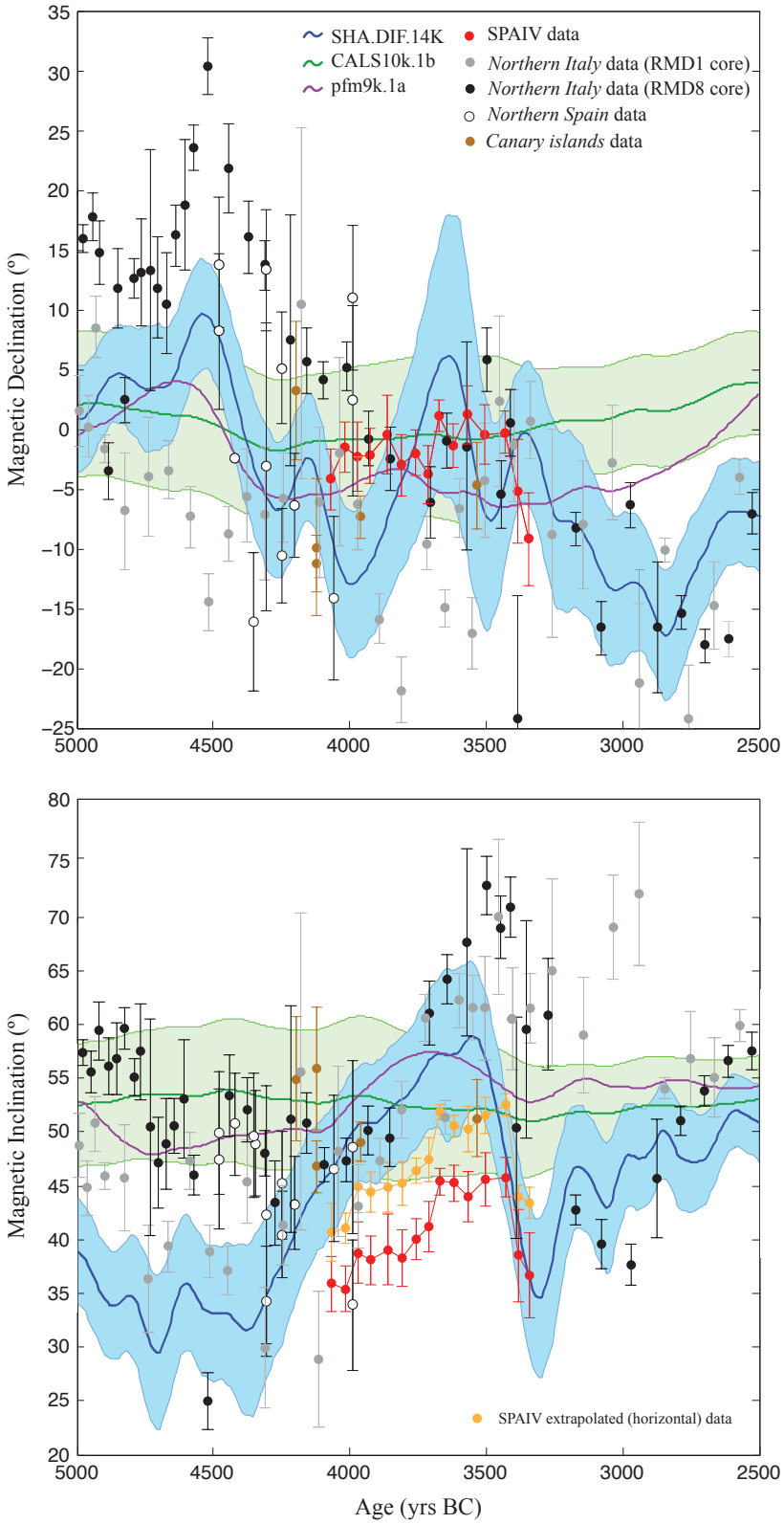

Figure 5.5 Magnetic declination and inclination curves of SPAIV (red lines correspond to the original site-based mean magnetic declination and inclination per line; orange line corresponds the same data corrected by the effect of the slope, see *Ponte et al.* [2017] for more details) compared to PSV models (SHA.DIF.14K, CALS10K.1b and pfm9k.1a) and discrete data from archaeomagnetic objects (northern Spain), volcanic material (Canary Islands) and two flowstone cores (Italian Alps).

Dating errors are also a possible factor, since the age uncertainty of the SPAIV speleothem ranges from 150 to 300 yrs. For example, considering ages 50 to 100 yrs older would shift most of the SPAIV magnetic inclinations within the confidence interval envelope of the *SHA.DIF.14k* model. Errors intrinsic to the models themselves are also not excluded. The smoothing effect due to inclusion of sediment data in models *CALS10K.1b* and *pfm9k.1a* [*Panovska et al.,* 2012; *Nilsson et al.,* 2014] does not allow these models to identify abrupt variations in magnetic inclination, such as those recorded by SPAIV and by the cores from the Alpine flowstone around ~3500 yrs BC (Figure 5.5). The scarcity of paleomagnetic data during some time intervals and the heterogeneous spatial distribution of the studied area around the globe is also an obstacle For example, the data incorporated in *SHA.DIF.14k* for ages younger than 1000 yrs BC represents 83% of the total amount of data, while only 17% are used to constrain the model between 1000 and 12 000 yrs BC. In particular, the time interval of 4100-3500 yrs BC spanning the formation of the SPAIV speleothem is one of the intervals where the number of data is lower.

Relative paleointensity (RPI) from speleothems has been poorly explored. The first investigation of RPI records in speleothems comes from *Osete et al.* [2012], who identified the Blake geomagnetic excursion in a radioisotopically well-dated speleothem from northern Spain. The authors identified a RPI relative maximum within the interval of low RPI characteristic of the Blake geomagnetic excursion, just when the first reversal is completed, which has also been previously reported in other paleomagnetic studies [e.g. *Thouveny et al.,* 2004]. More recently, *Lascu et al.* (2016) dated with accuracy the age of the Laschamp geomagnetic excursion, in a speleothem from North America, by using a combination of high-precision ^{230}Th dates and annual layer counting using confocal microscopy. The authors provided a detailed record of the field directional swing and intensity low (calculated based in the ration of NRM to ARM) that define the Laschamp excursion. Apart from these studies, the paucity of RPI records in general is intimately linked to the fact that RPI estimation in sediments is not straightforward, because it depends not only on the geomagnetic field intensity, but also on the mineralogy, concentration and size of the magnetic carriers [*Tauxe,* 1993]. RPI studies should ideally be performed in sediments where only one magnetic carrier is present (normally magnetite) and with minimal grain size variations. In the case of the speleothem under study, based on Curie temperatures and microscopic observations, *Font et al.* [2014] showed that the mineralogy is dominantly composed by low coercive magnetic minerals, namely detrital (pedogenic) magnetite and maghemite, with a minor contribution of hematite and goethite. Hysteresis and first-order reversal curve diagram indicated a mixture of

single domain and multidomain particles. Dispersion parameters estimated by the unmixing of isothermal remanent magnetization curves pointed to small grain size variations of the magnetite component. These results make the speleothem under study a good candidate for testing the reliability of RPI record.

The average of conventional NRM normalization by both factors (ARM and IRM) for each "line" (age) show a very good agreement (Figure 5.4a), which is usually interpreted as a good indicator of data reliability. However, *Tauxe et al.* [1995] states that similarity between NRM/ARM and NRM/IRM does not constitute a sufficiently rigorous test for reliability, as they do not account for VRM contributions to the NRM. On the contrary, the pseudo-Thellier method allows the selection of a coercivity window where VRM contributions to the NRM are minimal or non-existent. As stated in the results section, figures 5.4b and 5.4c show a good agreement between the RPI calculated using the classic and pseudo-Thellier methods, suggesting that both approaches are reliable in our case. Independently of the method used, RPI values show a significant minimum at 3900-3850 yrs BC, which is systematically observed in all samples pertaining to the same line (line 11-12), independently of their position along the slope (top or base of the speleothem). Comparison with other paleointensity records is difficult, because there is no high-resolution RPI data from sites located nearby Algarve. The only contemporaneous study in a geographically close area is from marine sediments of the portuguese margin (*Thouveny et al.* [2004]), which does not have the required temporal resolution to allow comparison with SPAIV record. *Korte and Constable* (2006) calibrated RPI data from several locations distributed around the globe to allow comparison with paleointensity curves obtained from model CALS7k.2. If long-term trends (several hundreds to thousands of years) well fit the model in some cases, shorter time scales (decades to few hundred years) show much more discrepancies. Since the age of the speleothem under study only encompasses ~800 yr, comparison with model predictions is useless. Despite the absence of comparison with other data and models, similarity between the different methods used and the repeatability of the data among samples from the same line (i.e. calcite laminae) strongly suggest that this speleothem is a good recorder of the Earth's magnetic paleointensity.

5.6 Conclusions

The present paleomagnetic investigation leads to the following major conclusions:

- Remanent magnetization in the stalagmite is primary and paleomagnetic directions are stable with low MAD values;

- Magnetic declination and inclination values are within the range predicted by PSV models and other paleomagnetic data from nearby areas. In particular, magnetic direction of SPAIV mimics the shape of the SHA.DIF.14K model;

- Assuming that SPAIV represents a pristine record of the PSV from 4100 to 3300 yrs BC, its comparison with the different models considered here suggest that the SHA.DIF.14k is the most reliable PSV model;

- When possible, future paleomagnetic research in speleothems should compare magnetic directions in different slopes to test inclination bias and correct it if needed. Otherwise, sampling where calcite laminaes are more inclined should be avoided.

- RPI record is similar using both ARM or IRM as normalizers of NRM, and using the pseudo-Thellier method, which suggest that RPI record in this speleothem is primary and reliable;

These results reinforce the idea that speleothems are good recorders of Earth's magnetic field, in term of direction and intensity, with the advantage of providing both continuous and high resolution recording, and the absence of post-depositional effects.

5.7 Appendix I - Virtual Geomagnetic Poles

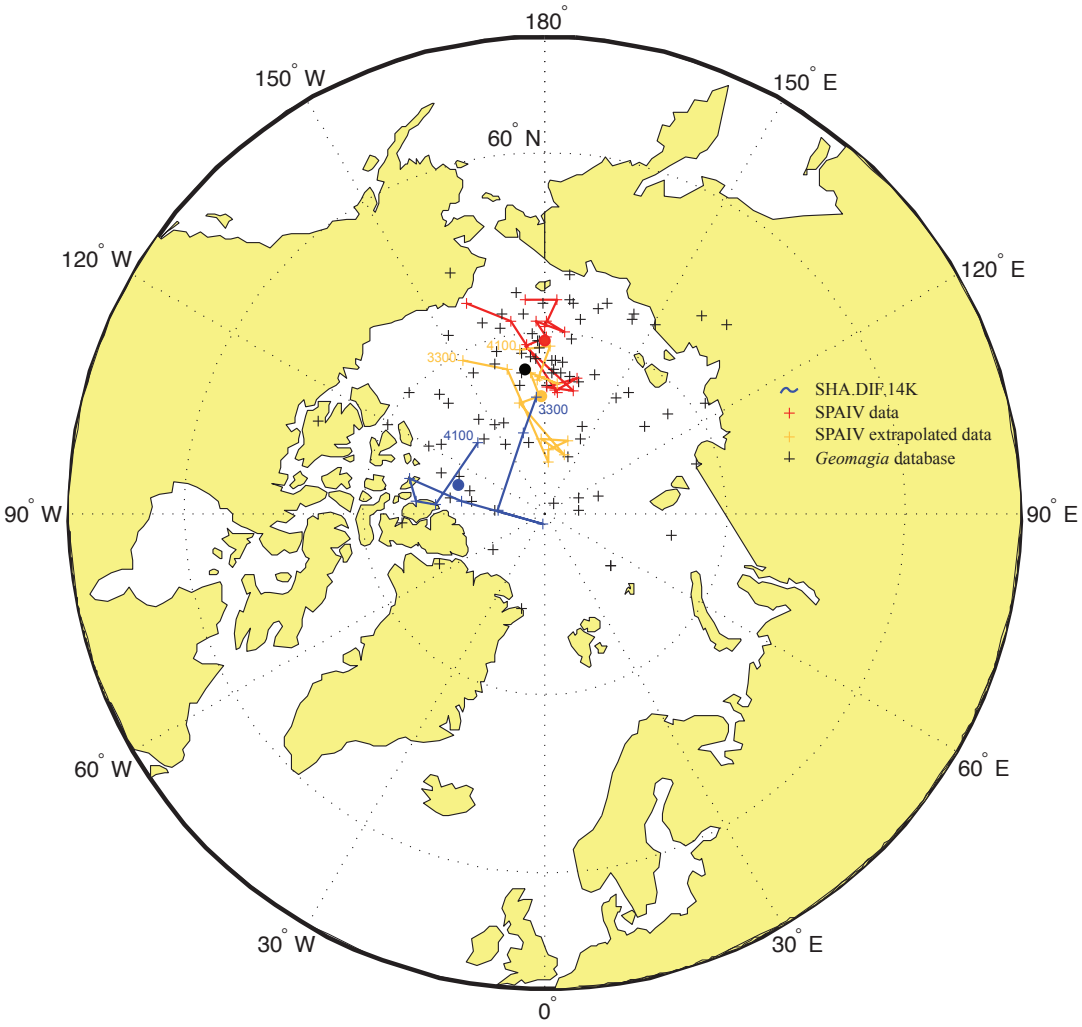

Figure 5.6 Polar wander path estimation by SPAIV data (mean values and extrapolated data) and predicted by model SHA.DIF.14K. Virtual Geomagnetic Poles (VGP) calculated by worldwide paleomagnetic dataset between 3000-4500 yrs BC (*Geomagia* database) is also plotted. Filled points correspond to the mean VGP positions based on SPAIV (red), SPAIV extrapolated (orange), SHA.DIF.14K (blue) and *Geomagia* (black).

The comparison of SPAIV magnetic declination and inclination record can be done with nearby data (<1200 km) or PSV models, as already discussed before. However, available data around the globe may be compared with SPAIV data by comparing their VGP. In theory, assuming the earth as a dipole (Geocentrical axial dipole or GAD theory), the pole position calculated based on all paleomagnetic data should be located at the same coordinates. This does not happen, because the earth is not a perfect dipole, and paleomagnetic data has its own uncertainty. To overcome the presence of the non-dipolar component, usually in paleomagnetism it is considered the averaged VGP for about 10^4 yrs [e.g. *Merrill and*

McFadden, 2003]. For this amount of time, the earth's magnetic field behaves as a dynamo. However, *Pavón-Carrasco et al.* [2014] averaged the position of north magnetic dip poles (calculated using non-dipolar components) in a progressively increased time window by 100 yrs steps from 12000 BC to 1900 AD and concluded that GAD hypothesis is valid, with an error of less than 5º, for averaged magnetic poles during just 2000 yrs. In Figure 5.6, the VGP calculated based on 96 paleomagnetic directions aged between 4500 and 3000 yrs BC (*Geomagia* database) are plotted in the map, together with its averaged position.

VGP have been calculated using mean SPAIV magnetic declination and inclination data on the dipole formula [e.g. *Irving*, 1964]. Considering the influence of the slope in the recorded magnetic inclination [*Ponte et al*, 2017], VGP were also calculated using the extrapolated magnetic inclination values for a hypothesized horizontal surface. The VGP path recorded by SPAIV between 4100 and 3300 yrs BC is represented in an azimuthal projection for latitudes higher than 60º (Figure 5.6). VGP path calculation by the PSV model SHA.DIF.14K and estimations based on other contemporaneous paleomagnetic data collected around the globe (*Geomagia:* http://geomagia.ucsd.edu) are also drawn.

Generally, the pole obtained by SPAIV at 4100 yrs BC starts travelling north (N) for the next few hundred years before turning southeast (SE) after 3400 yrs BC. The extrapolated data shows a similar path but with latitudes ~ 5º higher. VGP path calculated by *SHA.DIF.14K* differs from SPAIV record mainly in longitude. Despite an early small southerly travel, between 3800 and 3600 yrs BC the *SHA.DIF.14K* pole quickly turns north before returning south till 3300 yrs BC. VGP calculated by paleomagnetic data from *Geomagia* database (94 points) between 4500 and 3000 yrs BC are also plotted. The mean VGP coordinates (represented by dots in Figure 5.6) based on SPAIV original data (75.8ºN; 0.3ºE), extrapolated (80.4ºN; 2.1ºW) and *Geomagia* (78.1ºN; 7.5ºW) are located in very near positions. The mean pole position using *Geomagia* data is very similar to the average position of VGP calculated by SPAIV data. Geomagnetic poles and VGP path estimated by *SHA.DIF.14k* are also drawn in the map. The modeled geomagnetic pole is considerably east of that indicated by both *Geomagia* and SPAIV data, despite the variations in latitude following the same tendency of SPAIV. Considering that SPAIV data only encompasses 800 yrs, it is not recommended to give much importance to the similarity of the averaged VGP based on *Geomagia* and SPAIV. However, this results are still good indicators of SPAIV data reliability.

Table 5.2 VGP coordinates calculated for all the studied lines, using the line-based mean uncorrected magnetic inclinations and the mean corrected magnetic inclinations.

				Uncorrected		***Corrected***	
Line	**Age (BC)**	**Age interval**	**N**	**Pole lat**	**Pole lon**	**Pole lat**	**Pole lon**
1	3341	[3155 ; 3511]	7	71,5	-159,7	76	-151,7
2	3385	[3201 ; 3563]	3	73,9	-170,2	77,9	-165
3	3429	[3248 ; 3616]	8	80,1	173,5	86	175
4	3507	[3322 ; 3711]	6	79,9	174,7	85	176,6
5	3570	[3378 ; 3773]	8	78,5	166,7	84	162
6	3621	[3409 ; 3811]	4	79,5	179	84	-176,2
7	3672	[3423 ; 3855]	8	79,7	166,5	85,2	160,4
8	3715	[3438 ; 3896]	8	76,1	-173,6	80,9	-166,6
9	3759	[3476 ; 3938]	8	75,6	179,7	80,5	-176,8
10	3810	[3552 ; 3982]	4	74,2	-177,6	79,4	-173,2
11	3864	[3641 ; 4025]	8	74,9	174	79,4	174,6
12	3924	[3724 ; 4069]	7	74,2	179,6	79	-177,6
13	3971	[3783 ; 4104]	8	74,6	-179,6	79,3	-176,7
14	4021	[3850 ; 4143]	8	72,4	176,8	76,6	175,9
15	4072	[3924 ; 4185]	7	72,3	-174,7	75,7	-172,1

5.8 Appendix II – Table S1

Table 5.3 Paleomagnetic, ARM and IRM for each measured samples: *NRM* is the natural remanent magnetization intensity; *AF steps* represent the number of demagnetization steps and the selected coercivity interval used for PCA analysis; *Dec.* and *Inc.* correspond to magnetic declination and inclination; *Inc C.* is the corrected magnetic inclination; *MAD* is the maximum angular deviation; *Calcite layer dip (CLP)* is the estimated angle of the calcite layers with respect to horizontal plane; *ARM* and *IRM* are anhysteretic remanent magnetization and isothermal remanent magnetization acquired after applying a magnetic field (AF=100 mT and DC=50μT for ARM; 100 mT for IRM).

Sample	NRM (A/m)	AF steps	Dec (deg)	Inc (deg)	Inc C. (deg)	MAD	CLP (deg)	ARM (A/m)	IRM (A/m)
SPAIV_B1	1.00E-03	6 ; [6, 16]	-17.9	35	44.7	4.6	97	0.00301	0.0729
SPAIV_D1	8.96E-04	5 ; [8, 16]	-6.9	35.9	44.1	2.2	82	0.00170	0.0295
SPAIV_G1	1.05E-03	5 ; [6, 14]	-12	31.9	42.0	2.9	100.5	0.00238	0.0386
SPAIV_I1	9.92E-04	5 ; [8, 16]	-7.7	35.7	42.7	2.4	70	0.00229	0.0306
SPAIV_K1	8.57E-04	5 ; [6, 14]	-3.2	37.2	43.1	2.6	58.5	0.00200	0.0333
SPAIV_L1	9.55E-04	5 ; [6, 14]	-5.9	36.6	41.3	3.7	46.5	0.00209	0.0323
SPAIV_N1	1.02E-03	5 ; [6, 14]	-10.5	43.3	46.1	3.2	27.5	0.00372	0.0492
SPAIV_H2	8.04E-04	6 ; [6, 16]	-4.4	37.3	43.1	4.1	57.5	0.00170	0.0224
SPAIV_J2	7.77E-04	5 ; [6, 14]	-4.4	36.6	43.4	4.3	68	0.00157	0.0270
SPAIV_M2	1.13E-03	6 ; [8,18]	-6.8	41.5	45.6	2.1	40.5	0.00337	0.0448
SPAIV_A3	2.76E-03	7 ; [8, 20]	-4	43.7	52.7	1.8	90	0.00550	0.0651
SPAIV_C3	2.33E-03	7 ; [8, 20]	-2.4	43.7	52.6	1.7	88.5	0.00535	0.0619
SPAIV_E3	2.04E-03	7 ; [6, 18]	2	43.7	51.7	2.5	79.5	0.00440	0.0550
SPAIV_G3	2.49E-03	6 ; [8, 18]	0.6	44.6	52.3	1.8	77	0.00500	0.0639
SPAIV_I3	1.60E-03	8 ; [6, 20]	0.9	45.9	52.5	1.3	66	0.00299	0.0445
SPAIV_K3	2.01E-03	7 ; [10, 22]	1.4	47.4	53.0	0.8	56	0.00455	0.0557
SPAIV_L3	1.76E-03	8 ; [8, 22]	1.8	47.7	52.6	1.4	48.5	0.00395	0.0504
SPAIV_N3	1.66E-03	8 ; [4, 18]	-2.3	49.1	52.7	2	35.5	0.00503	0.0657
SPAIV_F4	2.30E-03	7 ; [8, 20]	-4.8	42.3	50.5	2.5	81.5	0.00867	0.1081
SPAIV_H4	1.84E-03	7 ; [8, 20]	1	44	50.7	2	67	0.00380	0.0463
SPAIV_J4	1.98E-03	9 ; [6, 22]	-0.7	45.5	52.3	2.1	67.5	0.00466	0.0596
SPAIV_M4	2.02E-03	8 ; [6, 20]	1.2	47.9	52.1	1.9	42	0.00514	0.0599
SPAIV_O4	1.91E-03	8 ; [6, 20]	3.3	47.8	52.3	1.9	45	0.00660	0.0744
SPAIV_P4	7.01E-04	6 ; [8,18]	-2.5	45.6	50.7	3.7	50.5	0.00226	0.0294
SPAIV_B5	1.11E-03	5 ; [4, 12]	-2.8	40.3	48.0	3.7	77	0.00242	0.0670
SPAIV_D5	1.27E-03	6 ; [6, 16]	3.7	41.2	49.4	2	81.5	0.00251	0.0310
SPAIV_E5	1.33E-03	7 ; [6, 18]	-0.3	42.3	49.6	1.5	72.5	0.00254	0.0321
SPAIV_G5	9.90E-04	5 ; [8, 16]	1.1	42.1	49.6	2	75	0.00235	0.0280
SPAIV_I5	1.19E-03	7 ; [8, 20]	-0.1	44.1	50.7	2.2	65.5	0.00382	0.0507
SPAIV_K5	9.69E-04	6 ; [6, 16]	0.4	48.4	53.7	2.1	52.5	0.00229	0.0353
SPAIV_L5	9.49E-04	6 ; [6, 16]	0.8	46.2	51.6	2.3	53.5	0.00216	0.0276
SPAIV_N5	8.81E-04	5 ; [8, 16]	7.3	46.1	50.4	1.7	43	0.00210	0.0297
SPAIV_J6	1.10E-03	6 ; [6, 16]	-0.9	44.3	50.6	3.3	63	0.00213	0.0288
SPAIV_M6	1.03E-03	6 ; [6, 16]	-1.2	45.7	50.6	4.1	48.5	0.00240	0.0314
SPAIV_O6	1.08E-03	5 ; [6, 14]	-0.3	44	50.0	3	59.5	0.00284	0.0373
SPAIV_Q6	1.53E-03	6 ; [6, 16]	-3.2	46.7	50.8	1.7	40.5	0.00614	0.0747
SPAIV_A7	2.08E-03	8 ; [6, 20]	1.7	44	52.7	2.5	87	0.00370	0.0465
SPAIV_C7	1.82E-03	8 ; [6, 20]	0.3	43.6	52.1	2.4	85	0.00340	0.0414
SPAIV_E7	1.91E-03	8 ; [6, 20]	0	44.4	51.5	1	70.5	0.00363	0.0479
SPAIV_G7	1.88E-03	8 ; [6, 20]	0	44.2	51.3	1.9	71	0.00341	0.0432
SPAIV_I7	1.88E-03	8 ; [6, 20]	3.5	45.1	51.4	1.8	62.5	0.00359	0.0428
SPAIV_K7	1.87E-03	8 ; [4, 18]	0.9	46.5	51.4	1.7	49	0.00396	0.0506

SPAIV_N7	2.00E-03	8 ; [6, 20]	0.7	46.4	51.5	1.9	51	0.00483	0.0576
SPAIV_P7	2.03E-03	8 ; [6, 20]	2.4	48.7	52.1	1.6	34	0.00507	0.0667
SPAIV_B8	2.17E-03	9 ; [6, 22]	2.5	43	51.4	2.9	83.5	0.00330	0.0419
SPAIV_D8	1.66E-03	6 ; [6, 16]	-6.3	38	45.8	2.2	77.5	0.00365	0.0462
SPAIV_F8	1.62E-03	6 ; [6, 16]	-3.2	38.6	45.6	2.7	70	0.00342	0.0422
SPAIV_H8	1.60E-03	6 ; [6, 16]	-5.4	39	45.6	3.3	66	0.00346	0.0435
SPAIV_J8	1.88E-03	7 ; [6, 18]	-5.7	40.7	46.6	2.3	58.5	0.00418	0.0529
SPAIV_M8	2.00E-03	7 ; [6, 18]	-2.5	43.2	49.3	1.7	60.5	0.00463	0.0536
SPAIV_O8	1.30E-03	7 ; [6, 18]	-1.5	41.3	46.4	2.4	50.5	0.00350	0.0454
SPAIV_Q8	1.70E-03	6 ; [6, 16]	-7.2	44.4	48.3	1.9	39	0.00558	0.0653
SPAIV_A9	1.30E-03	7 ; [6, 18]	-3.5	37.1	45.9	2.4	88	0.00267	0.0384
SPAIV_C9	1.28E-03	7 ; [6, 18]	0.3	38.9	47.5	1.9	86	0.00250	0.0331
SPAIV_E9	1.19E-03	7 ; [6, 18]	-1.6	38.3	44.8	2.1	65	0.00255	0.0354
SPAIV_G9	1.18E-03	7 ; [6, 18]	-3	39	46.0	1.8	70	0.00264	0.0340
SPAIV_I9	1.32E-03	7 ; [6, 18]	-2.1	40.4	46.6	1.7	61.5	0.00228	0.0331
SPAIV_K9	1.60E-03	7 ; [6, 18]	-4.6	40	45.1	2.2	51	0.00350	0.0438
SPAIV_N9	1.16E-03	6 ; [6, 16]	0.8	41.8	47.3	2.2	54.5	0.00289	0.0394
SPAIV_P9	9.99E-04	6 ; [6, 16]	-2.5	44.7	48.2	2.4	35	0.00325	0.0439
SPAIV_B10	1.06E-03	6 ; [6, 16]	-0.9	38.1	47.1	2.6	90	0.00204	0.0298
SPAIV_D10	1.34E-03	6 ; [6, 16]	-4.9	35.8	44.0	2.8	82	0.00260	0.0320
SPAIV_H10	1.06E-03	6 ; [6, 16]	-3	38.5	44.7	1.7	61.5	0.00222	0.0271
SPAIV_M10	8.47E-04	6 ; [6, 16]	-3	40.4	45.4	2.2	50	0.00249	0.0321
SPAIV_A11	1.05E-03	8 ; [6, 20]	-2.5	31.4	39.8	2.9	84	0.00491	0.0548
SPAIV_C11	1.65E-03	7 ; [8, 20]	-4.3	38	45.7	2.7	76.5	0.00478	0.0648
SPAIV_E11	1.45E-03	7 ; [6, 18]	0.1	39.8	46.7	1.4	68.5	0.00553	0.0635
SPAIV_G11	1.66E-03	7 ; [4, 16]	3.6	34	41.1	3.2	70.5	0.00585	0.0623
SPAIV_I11	1.60E-03	7 ; [6, 18]	-1.6	40.8	46.8	1.6	60	0.00681	0.0717
SPAIV_K11	1.51E-03	6 ; [8, 18]	1.7	40.8	45.9	3.5	51	0.00666	0.0750
SPAIV_N11	1.80E-03	7 ; [6, 18]	-0.4	41.9	47.0	2	50.5	0.00769	0.0904
SPAIV_P11	2.28E-03	6 ; [6, 16]	-0.7	42.6	46.0	2.9	33.5	0.00995	0.1321
SPAIV_B12	3.01E-03	8 ; [10, 25]	-4	37	46.0	3.8	90	0.00555	0.0765
SPAIV_D12	1.76E-03	7 ; [6, 18]	-5.8	34.6	42.2	3.8	75.5	0.00596	0.0660
SPAIV_F12	1.79E-03	6 ; [6, 16]	-3.3	35.7	42.7	2.3	70	0.00608	0.0686
SPAIV_H12	1.94E-03	8 ; [6, 20]	0.1	38.1	44.4	2.3	63	0.00539	0.0649
SPAIV_J12	1.73E-03	8 ; [6, 20]	0.9	40.1	45.9	1.9	57.75	0.00486	0.0590
SPAIV_M12	2.20E-03	7 ; [6, 18]	0.2	40.5	45.9	1.1	54	0.00752	0.0825
SPAIV_O12	2.12E-03	6 ; [6, 16]	-3	40.1	44.7	1.9	46	0.00692	0.0941
SPAIV_A13	1.71E-03	5 ; [12, 20]	-11.8	38.3	47.1	3.2	87.75	0.00678	0.0755
SPAIV_C13	2.64E-03	7 ; [8, 20]	-5.1	36.7	44.4	1.2	76.5	0.00670	0.0752
SPAIV_E13	2.87E-03	8 ; [6, 20]	0.7	36.1	43.3	2.1	72	0.00638	0.0730
SPAIV_G13	2.89E-03	8 ; [6, 20]	2.6	37.6	44.6	1.5	69.5	0.00640	0.0748
SPAIV_I13	2.37E-03	8 ; [6, 20]	2.5	38.5	44.7	2.3	62	0.00566	0.0632
SPAIV_K13	2.19E-03	8 ; [6, 20]	-2.6	39.4	44.1	2.2	47	0.00556	0.0660
SPAIV_N13	2.98E-03	8 ; [6, 20]	-1.5	41.3	45.4	1.6	41	0.00583	0.0751
SPAIV_O13	2.31E-03	6 ; [6, 16]	-4.4	42.2	45.9	2.1	37	0.00423	0.0516
SPAIV_B14	1.96E-03	6 ; [10, 20]	-5.2	30.5	39.5	2.9	90	0.00350	0.0459
SPAIV_D14	2.42E-03	10 ; [6, 25]	0.3	34.8	41.8	1.3	70	0.00520	0.0614
SPAIV_F14	1.64E-03	7 ; [6, 18]	-2.8	34.3	41.1	2.9	67.5	0.00478	0.0569
SPAIV_H14	1.51E-03	6 ; [6, 16]	-1.9	35.3	42.0	1.6	66.5	0.00350	0.0440
SPAIV_J14	1.32E-03	8 ; [6, 20]	2.8	37.3	42.5	2.3	51.5	0.00295	0.0410
SPAIV_M14	1.05E-03	6 ; [6, 16]	-0.2	37.2	41.3	3.5	41	0.00360	0.0467

SPAIV_N14	1.80E-03	6 ; [6, 16]	-2	37.8	41.5	1.7	37	0.00515	0.0680
SPAIV_O14	1.51E-03	6 ; [6, 16]	-2.5	35.4	39.2	3.8	38	0.00454	0.0570
SPAIV_A15	2.11E-03	9 ; [8, 25]	-9.2	32.1	41.4	1.1	93	0.00485	0.0550
SPAIV_C15	2.71E-03	9 ; [6, 22]	-0.4	37	44.9	1.7	78.5	0.00518	0.0582
SPAIV_E15	2.45E-03	9 ; [6, 22]	-1.3	35.6	43.0	1.7	73.5	0.00491	0.0574
SPAIV_G15	2.28E-03	7 ; [6, 18]	-2.4	36.3	42.9	2.2	66	0.00442	0.0510
SPAIV_I15	2.15E-03	9 ; [6, 22]	-1.8	37.5	42.4	2.4	49	0.00448	0.0519
SPAIV_M15	1.83E-03	7 ; [6, 18]	-6.7	34.4	37.7	4.6	33	0.00559	0.0680
SPAIV_N15	2.15E-03	5 ; [6, 14]	-8.2	37.3	40.3	3.3	30	0.00533	0.0674

5.9 Appendix III – Table S2: Pseudo-Thellier results

Table 5.4 Results of Pseudo-Thellier method. *RPI* is the relative paleointensity estimate, which corresponds to the best-fit slope. *Min* and *max* correspond to the lower and upper limit of the 95% confidence interval, respectively. *Standard error* is the standard error of the slope and *N* is the number of points used for the determination of the slope, within the selected coercivity window (mT).

Sample	*RPI (slope)*	*max*	*min*	*Standard Error*	*N*
SPAIV_G1	0.581	0.681	0.480	0.039	7 [4,16]
SPAIV_G3	0.539	0.584	0.495	0.017	7 [10,22]
SPAIV_G5	0.755	0.892	0.618	0.050	6 [6,16]
SPAIV_G7	0.687	0.765	0.610	0.034	10 [4,22]
SPAIV_G9	0.763	0.824	0.701	0.022	6 [10,20]
SPAIV_G11	0.362	0.414	0.310	0.021	7 [6,18]
SPAIV_G13	0.663	0.695	0.631	0.013	8 [6,20]
SPAIV_G15	0.706	0.772	0.639	0.028	9 [4,20]
SPAIV_H2	0.814	1.018	0.609	0.0797	7 [4,16]
SPAIV_H4	0.576	0.618	0.534	0.0181	10 [4,22]
SPAIV_H8	0.829	0.969	0.690	0.0544	7 [4,16]
SPAIV_H10	0.709	0.788	0.631	0.0305	7 [6,18]
SPAIV_H12	0.483	0.522	0.445	0.0164	9 [4,20]
SPAIV_H14	0.686	0.897	0.474	0.0763	6 [6,16]
SPAIV_M2	0.467	0.524	0.411	0.0232	8 [4,18]
SPAIV_M4	0.508	0.566	0.449	0.0254	10 [4,22]
SPAIV_M6	0.703	0.827	0.579	0.0505	8 [4,18]
SPAIV_M8	0.631	0.706	0.556	0.0292	7 [4,16]
SPAIV_M10	0.461	0.522	-0.400	0.0248	8 [4,18]
SPAIV_M12	0.350	0.417	0.283	0.0272	8 [6,20]
SPAIV_M14	0.456	0.541	0.371	0.0331	7 [4,16]
SPAIV_N1	0.418	0.447	0.390	0.0111	7 [4,16]
SPAIV_N3	0.470	0.516	0.425	0.0186	8 [4,18]
SPAIV_N5	0.644	0.773	0.516	0.0464	6 [6,16]
SPAIV_N7	0.612	0.655	0.569	0.0168	7 [6,18]
SPAIV_N9	0.578	0.647	0.510	0.0266	8 [4,18]
SPAIV_N11	0.377	0.409	0.344	0.0134	8 [4,18]
SPAIV_N13	0.559	0.590	0.523	0.0129	9 [4,20]

6.Magnetism and Climate

Summary

Recent studies in speleothems show a striking link between rock magnetic properties of speleothem and past climate, by comparing oxygen and carbon isotope values with the concentration of ferromagnetic minerals. However, the use of magnetic properties as speleothem's climate proxies is still an early stage, and more studies from different geological context and climate region are urgently needed to better understand these mechanisms. Here, I conducted carbon and oxygen isotope analyses coupled to rock magnetic properties of the same specimens used in the previous chapter in order to study the relationship between climate and speleothem magnetism.

6.1 Introduction

Speleothems have been used for some decades as climate archives of the Earth. Oxygen and carbon isotopes, trace elements, growth rate and other proxies are obtained and studied to reconstruct the past climate in well dated speleothems. Very recently, a new speleothem climate proxy has been introduced: ferromagnetic mineral concentration. *Font et al.* (2014), *Bourne et al.* (2015) and *Jaqueto et al.* (2016) were the first authors to explore the link between iron oxide concentration and other climate proxies. If *Font et al.* (2014) was not able to find a correlation between magnetic parameters and stable isotopes in a speleothem, *Bourne et al.* (2015) and *Jaqueto et al.* (2016) reported a relationship between the magnetic input and stable isotope data. However, the interpretation of the results were distinct: *Bourne et al.* (2015) suggested that increased amount of precipitation during summer in Virginia (enriched by $\delta^{18}O$, according to the authors) favours pedogenic magnetite production in soils and its transport to the cave, resulting in higher (less negative) $\delta^{18}O$ values coincident with also higher magnetite concentration; on contrary, *Jaqueto et al.* (2016) states that higher $\delta^{18}O$ and $\delta^{13}C$ in a Brazilian speleothem correspond to drier periods, which results in less vegetation cover, higher soil erosion and therefore more detrital material (and magnetite) transported to the cave. Different isotope results interpretation are common, since the isotopic composition may be affected and controlled by several factors, which vary from place to place. Further investigation is needed to better understand the factors controlling both oxygen and carbon isotope values and magnetic mineral quantities in speleothems. Here $\delta^{18}O$ and $\delta^{13}C$ profiles were obtained from SPAIV and compared to magnetic minerals concentration, in order to verify if there is a relationship between climate and magnetic parameters.

6.2 Sampling and Methods

For this study, 16 cylindrical samples were drilled along two consecutive perpendicular lines to calcite growth laminae and cut in half, in order to get the highest temporal resolution possible (Figure 6.1). This sampling resulted in 32 samples, over a time span of approximately 800 yr (i.e., with a temporal resolution of ~25 yr). Before being sent for isotopic analysis, IRM acquisition curves were obtained for each sample, which were latter decomposed in CLG functions to identify and characterize their magnetic components (concentration, coercivity and dispersion). After obtaining IRM data, the samples were crushed in an automatic agate mortar in Universidade do Algarve (Gambelas) and the resulting powder was used for isotopic analysis performed at the Laboratory of stable light isotopes of Geotop-UQAM (Canada). δ All ^{13}C- and ^{18}O-content measurements were made on

100 μg powdered sample aliquots following routine protocols at Geotop (e.g., *Helie and Hillaire-Marcel*, 2016). Raw data are corrected using a calibration curve based on two internal reference materials ($\delta^{13}C$=+2.25‰ & -5.01‰; $\delta^{18}O$=-1.40‰ & -23.01‰). These internal reference materials are normalized on the NBS19-LSVEC scale for $\delta^{13}C$ and on the VSMOW-SLAP scale for $\delta^{18}O$ [see *Coplen,* 2006; *Coplen et al.,* 2015]. The quoted $\delta^{13}C$- and $\delta^{18}O$-values (Table 6.1) are expressed in ‰ against VPDB ($\pm 2\sigma < 0.05$‰, for both), based on replicates of reference carbonate materials analyzed simultaneously).

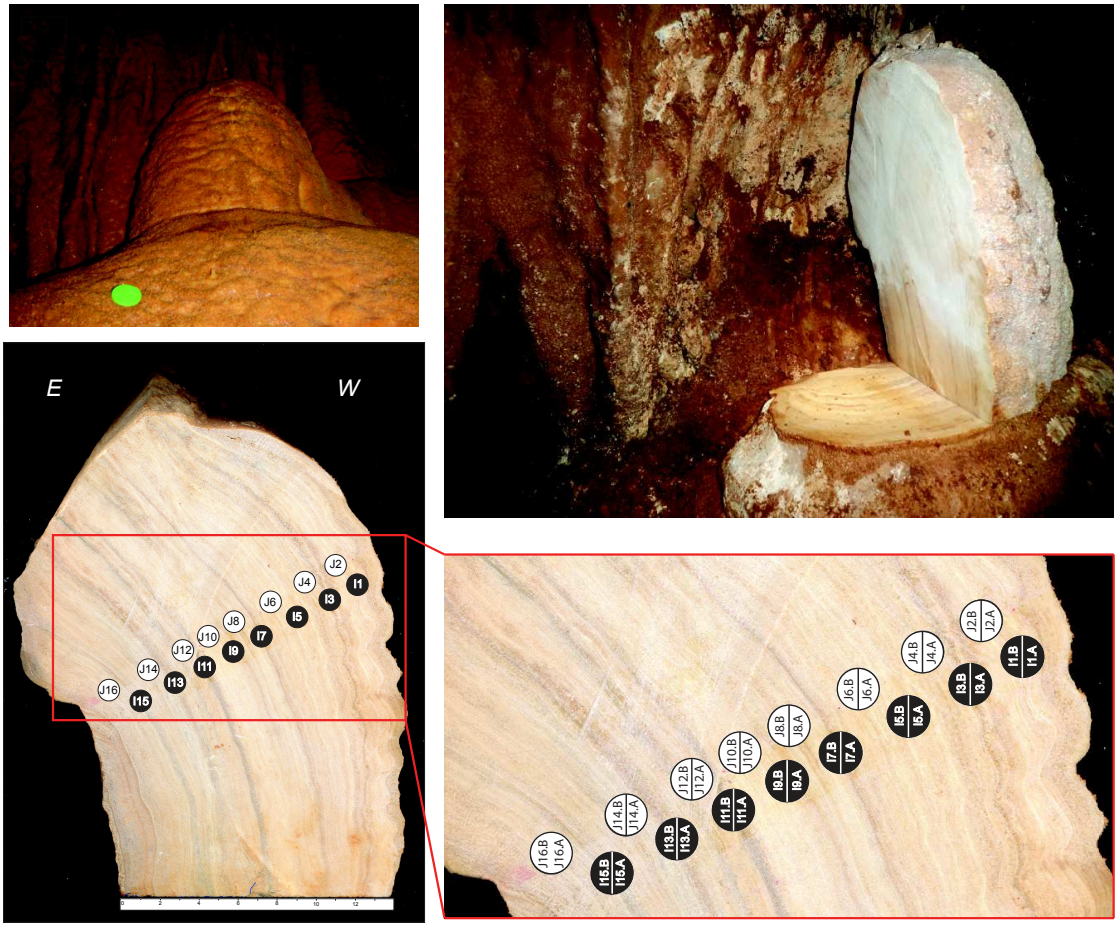

Figure 6.1 Selected samples from SPAIV for isotopic and IRM analysis. Two consecutive columns (I and J) were chosen and the cylindric samples were cut in half. The names of the samples were maintained, adding only the letters A and B to the youngest and oldest half, respectively.

6.3 Results

Magnetic results are resumed in Table 6.1 and Figures 6.2 and 6.3. The saturated isothermal remanent magnetization (SIRM), indicative of the ferromagnetic mineral content, varies from 0.76×10^{-5} to 3.89×10^{-5} A.m^2/kg. The analysis of IRM curves show that the magnetic signal is dominated in by a low-coercive phase, with contributions between ~70% to 90%. Its

coercivity ($B_{1/2}$) and dispersion parameter (DP) is almost constant along the profile, ranging between ~20 and 24 mT and 0.24-0.29, respectively, which are typical values of detrital and pedogenic magnetite. CLG curves also show the presence of two more components. The second is a medium to hard coercivity phase, with $B_{1/2}$ values between 60-100 mT (mean of 81 mT) and DP showing few variation (0.21-0.31), with a mean of 0.26. The third component corresponds to a very hard magnetic phase, where $B_{1/2}$ lies between ~400 to 1000 mT (mean of 682 mT) with DP values varying between 0.32 and 0.46 (mean of 0.40). The second and third components probably correspond to hematite and goethite respectively. The S-ratio is very similar for all the record, ranging between 0.90 and 0.96, which is compatible with the strong dominance of a low-coercive phase.

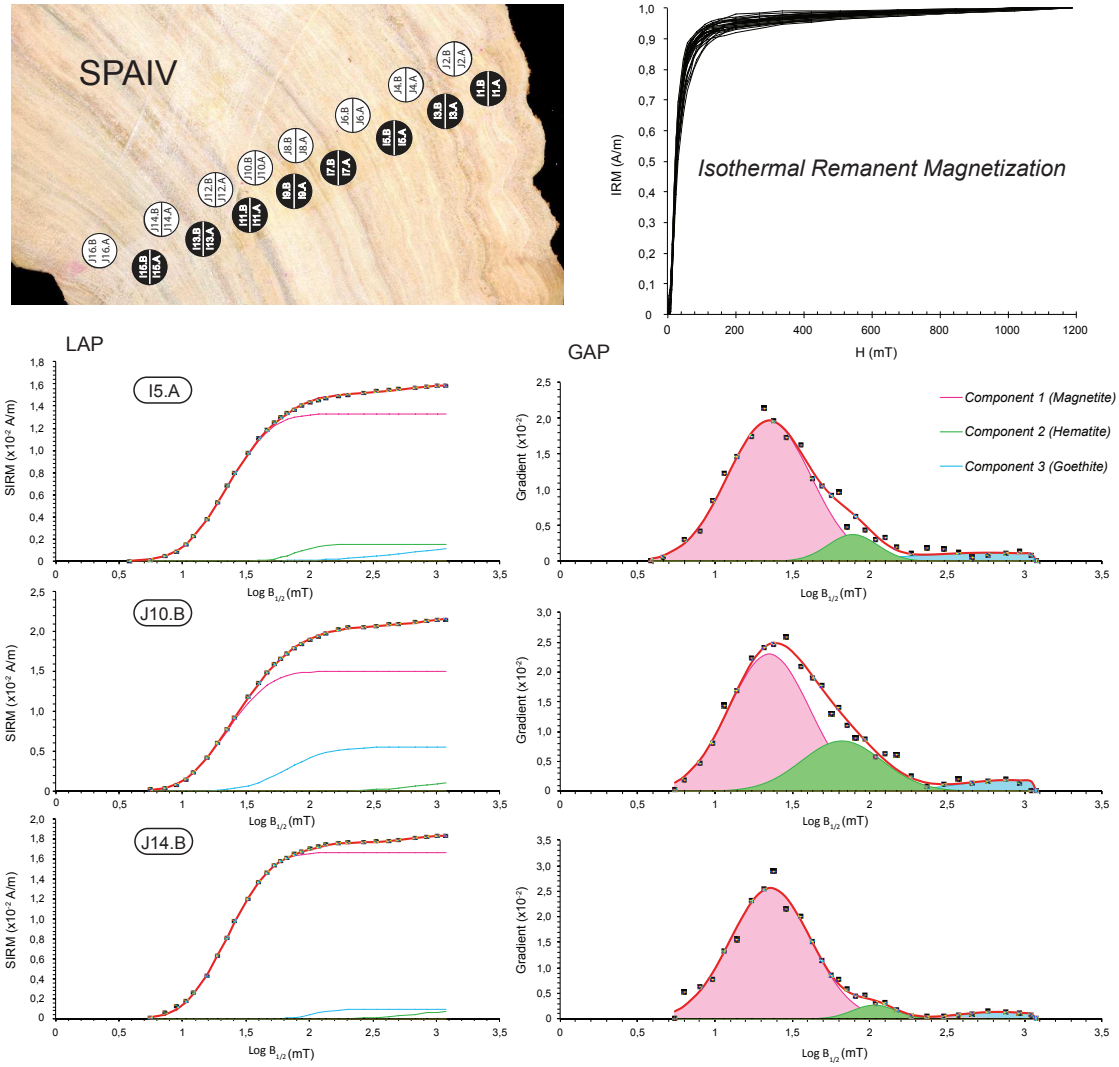

Figure 6.2 Isothermal Remanent Magnetization curves from the measured 32 samples and three examples of CLG treatment from samples I5.A, J10.B and J14.B.

Isotopic results are shown in Figure 6.3 and Table 6.1. $\delta^{18}O$ values vary from -4.74 ‰ to -3.96 ‰ (mean of -4.36 ‰) and $\delta^{13}C$ from -9.39 ‰ and -7.48 ‰ (mean of -8.39 ‰). $\delta^{18}O$ and $\delta^{13}C$ are weakly correlated (R^2=0.38), thus pointing to possible kinetic effects during carbonate precipitation [e.g., *Mickler et al.,* 2006]. Hendy tests [e.g., *Hendy*, 1971] do not necessarily provide conclusive evidence of such effects [e.g., *Dorale and Liu,* 2009]. Thus, assuming that high δ-values would be indicative of drier conditions (and possible kinetic effects), whereas, more negative values would relate to humid conditions with increased precipitations (lower $\delta^{18}O$-values of karst water), thus an enhanced vegetation cover with subsequent soil enrichment in decaying organic matter (leading to lower $\delta^{13}C$-values of dissolved inorganic carbon in karst water), then, one would expect the minimum δ-values to correlate with magnetic parameters indicative of enhanced heavy mineral fluxes. However, if there is no correlation between stable isotopes and the ferromagnetic content (expressed by the SIRM of the component 1, magnetite) in the stalagmite, peaks of high SIRM values generally correspond to minimum in both $\delta^{18}O$- and $\delta^{13}C$-values, as highlighted in Figure 6.3 (with the exception of sample I3.B).

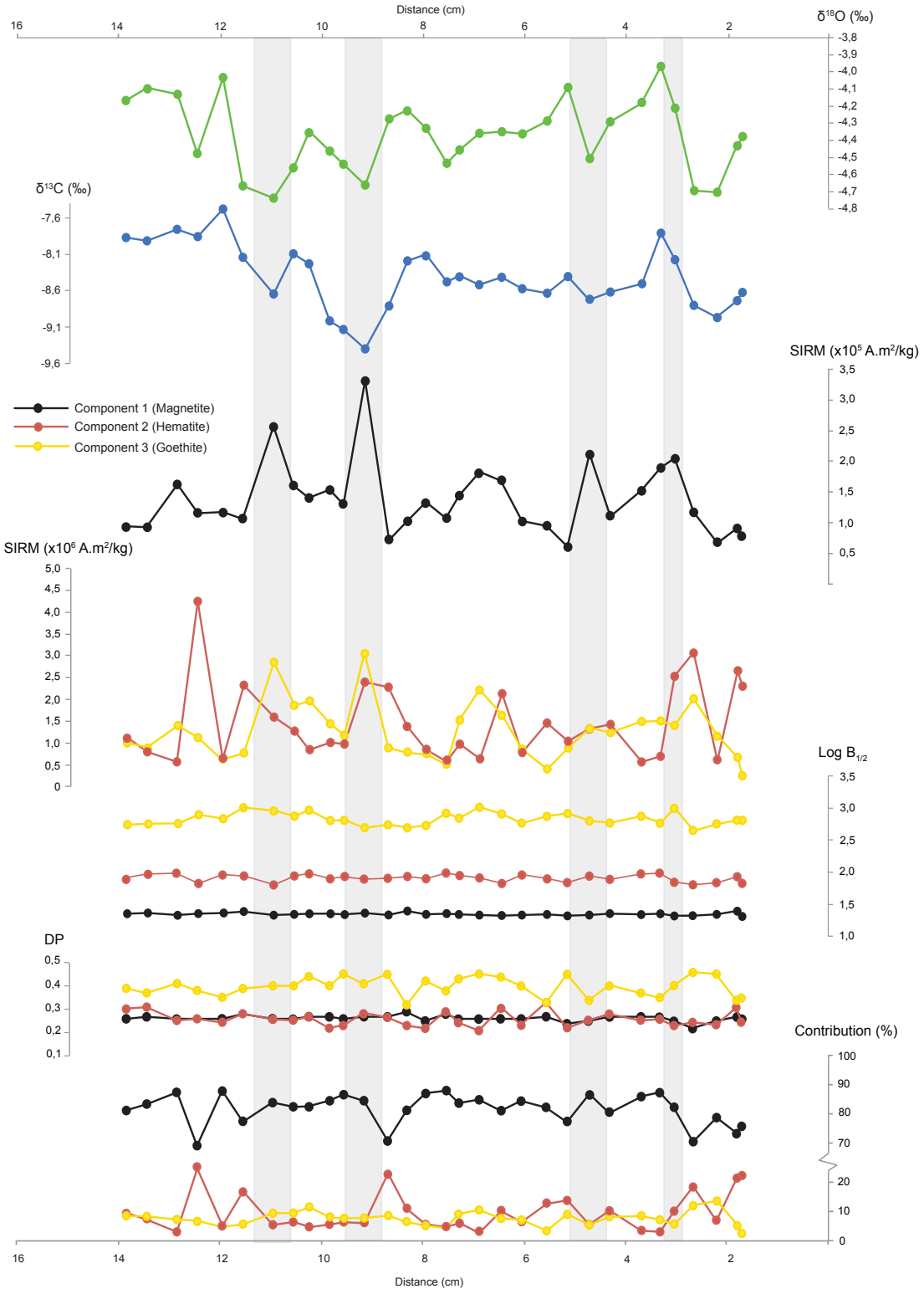

Figure 6.3 Comparison of stable isotope profiles (oxygen and carbon) and several magnetic parameters: SIRM, Coercivity (Log $B_{1/2}$), dispersion parameter (DP) and contribution (%) of the three identified magnetic components (magnetite, hematite and goethite). Gray bands indicate the most important peaks in magnetic mineral content.

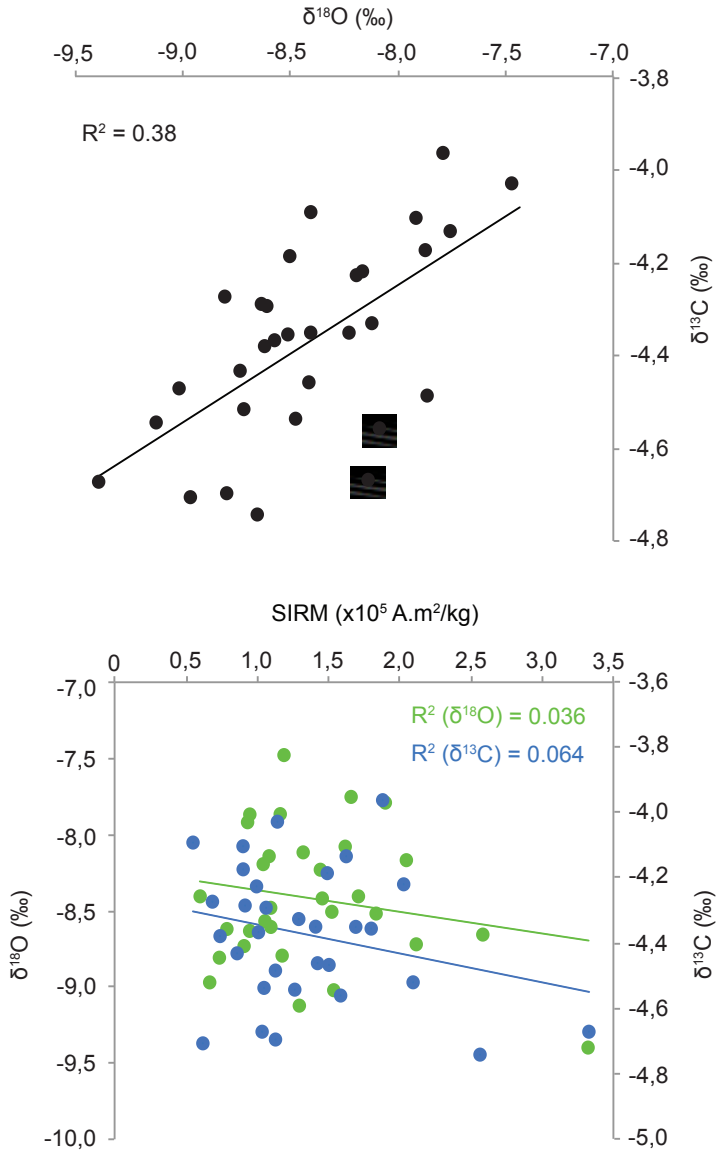

Figure 6.4 Correlation between $\delta^{18}O$ and $\delta^{13}C$ (R^2 = 0.44) and between both isotopes and SIRM of the soft magnetic component (magnetite).

Table 6.1 Resume of magnetic and isotope data. S-ratio and parameters that characterize the three magnetic componentes identified after unmixing of IRM acquisition curves: SIRM, Log $B_{1/2}$, DP a contribution (%). Isotope data ($\delta^{13}C$ and $\delta^{18}O$) are displayed in the last two columns.

			Component 1				Component 2				Component 3					
Sample	**Dist (cm)**	**S-ratio**	**SIRM (Am^2/kg)**	**Log $B_{1/2}$**	**DP**	**%**	**SIRM (Am^2/kg)**	**Log $B_{1/2}$**	**DP**	**%**	**SIRM (Am^2/kg)**	**Log $B_{1/2}$**	**DP**	**%**	**$\delta^{13}C$**	**$\delta^{18}O$**
I1.B	1.7	0.96	7.92E-06	1.31	0.26	75.63	2.29E-06	1.82	0.24	21.85	2.64E-07	2.80	0.35	2.52	-8.62	-4.38
J2.A	1.8	0.92	9.11E-06	1.39	0.27	73.23	2.64E-06	1.93	0.30	21.26	6.86E-07	2.81	0.34	5.51	-8.73	-4.43
J2.B	2.2	0.92	6.70E-06	1.34	0.25	78.65	6.22E-07	1.83	0.23	7.34	1.15E-06	2.75	0.45	13.56	-8.97	-4.71
I3.A	2.65	0.90	1.17E-05	1.32	0.22	70.31	3.05E-06	1.80	0.25	18.13	2.00E-06	2.64	0.46	11.92	-8.80	-4.70
I3.B	3.05	0.96	2.05E-05	1.32	0.25	83.85	2.54E-06	1.84	0.23	10.38	1.41E-06	3.00	0.40	5.77	-8.17	-4.22
J4.A	3.3	0.90	1.90E-05	1.35	0.27	89.72	6.71E-07	1.98	0.25	3.16	1.51E-06	2.77	0.35	7.11	-7.79	-3.96
J4.B	3.7	0.91	1.52E-05	1.34	0.27	88.04	5.80E-07	1.97	0.25	3.35	1.49E-06	2.87	0.37	8.61	-8.51	-4.18
I5.A	4.3	0.92	1.10E-05	1.35	0.27	81.60	1.40E-06	1.89	0.28	10.43	1.07E-06	2.77	0.40	7.98	-8.61	-4.29
I5.B	4.7	0.93	2.12E-05	1.33	0.25	88.81	1.34E-06	1.94	0.25	5.60	1.34E-06	2.80	0.34	5.60	-8.72	-4.52
J6.A	5.15	0.93	5.99E-06	1.32	0.24	78.38	1.03E-06	1.83	0.22	13.39	6.88E-07	2.90	0.45	8.93	-8.40	-4.09
J6.B	5.55	0.95	9.55E-06	1.34	0.27	83.69	1.46E-06	1.90	0.33	12.77	4.05E-07	2.87	0.32	3.55	-8.63	-4.29
I7.A	6.05	0.94	1.05E-05	1.33	0.26	86.33	7.89E-07	1.95	0.23	6.47	8.77E-07	2.77	0.40	7.19	-8.57	-4.37
I7.B	6.45	0.93	1.72E-05	1.32	0.26	82.03	2.13E-06	1.82	0.30	10.16	1.64E-06	2.90	0.44	7.81	-8.41	-4.35
J8.A	6.9	0.93	1.83E-05	1.33	0.26	86.79	6.38E-07	1.91	0.21	3.01	2.23E-06	3.00	0.45	10.53	-8.52	-4.36
J8.B	7.3	0.91	1.46E-05	1.34	0.26	84.53	9.53E-07	1.95	0.24	5.59	1.53E-06	2.84	0.43	8.94	-8.41	-4.46
I9.A	7.55	0.95	1.09E-05	1.35	0.28	90.21	5.94E-07	1.99	0.29	4.91	5.52E-07	2.90	0.38	4.56	-8.48	-4.54
I9.B	7.95	0.94	1.32E-05	1.34	0.25	88.52	8.38E-07	1.90	0.22	5.65	7.54E-07	2.72	0.42	5.08	-8.12	-4.33
J10.A	8.3	0.92	1.04E-05	1.39	0.29	82.58	1.40E-06	1.93	0.23	11.08	8.01E-07	2.69	0.32	6.34	-8.19	-4.23
J10.B	8.7	0.93	7.33E-06	1.33	0.27	70.51	2.27E-06	1.90	0.26	22.22	8.67E-07	2.72	0.45	8.50	-8.81	-4.27
I11.A	9.15	0.92	3.33E-05	1.36	0.27	85.66	2.38E-06	1.90	0.28	6.14	3.06E-06	2.68	0.41	7.89	-9.39	-4.67
I11.B	9.55	0.92	1.30E-05	1.34	0.26	86.39	9.80E-07	1.93	0.23	6.51	1.07E-06	2.80	0.45	7.10	-9.12	-4.54
J12.A	9.85	0.91	1.54E-05	1.35	0.27	84.38	1.00E-06	1.90	0.22	5.60	1.43E-06	2.80	0.40	8.00	-9.02	-4.47
J12.B	10.25	0.91	1.45E-05	1.35	0.27	82.73	8.43E-07	1.97	0.27	4.88	1.97E-06	2.96	0.44	11.38	-8.23	-4.35
I13.A	10.55	0.92	1.62E-05	1.34	0.26	83.48	1.27E-06	1.94	0.25	6.55	1.86E-06	2.87	0.40	9.61	-8.08	-4.56
I13.B	10.95	0.92	2.58E-05	1.33	0.26	85.16	1.58E-06	1.80	0.26	5.23	2.83E-06	2.95	0.40	9.37	-8.65	-4.74
J14.A	11.55	0.94	1.08E-05	1.38	0.28	76.09	2.31E-06	1.94	0.28	16.67	7.72E-07	3.00	0.39	5.56	-8.14	-4.67
J14.B	11.95	0.94	1.19E-05	1.36	0.26	90.03	6.74E-07	1.95	0.24	5.12	6.39E-07	2.83	0.35	4.85	-7.48	-4.03
I15.A	12.45	0.92	1.17E-05	1.35	0.26	68.18	4.29E-06	1.82	0.26	25.00	1.17E-06	2.89	0.38	6.82	-7.86	-4.49
I15.B	12.85	0.93	1.66E-05	1.33	0.26	88.22	5.69E-07	1.98	0.25	3.07	1.39E-06	2.75	0.41	7.51	-7.76	-4.13
J16.A	13.45	0.91	9.42E-06	1.36	0.27	83.26	7.98E-07	1.97	0.31	7.17	8.97E-07	2.73	0.37	8.07	-7.92	-4.10
J16.B	13.85	0.91	9.45E-06	1.35	0.26	81.05	1.10E-06	1.89	0.30	9.57	9.82E-07	2.74	0.39	8.51	-7.87	-4.17

6.4 Discussion

The obtained magnetic mineral concentration profile, expressed as the SIRM soft component (magnetite), presents four main peaks, measured in samples containing well identified dark layers. This is not surprising, since *Font et al.* (2014) noted that the color of the growth layers are indicative of magnetic mineral concentration, with the brownish layers presenting higher values due to higher content in detrital sediments like clays (rich in iron oxides) transported from the overlying soil by dripwater. The expectation is that the transport of detrital material to the cave, and therefore the magnetic particles quantity present in the growth layers are controlled by climatic factors, like precipitation amount, also partly regulating $\delta^{18}O$-values in drip water and calcite. In parallel, one would expect an enhanced vegetation cover leading to lower $\delta^{13}C$ values in dissolved inorganic carbon, and subsequently in calcite. In figure 6.3, it is observed that 3 of the 4 SIRM maximum coincide with relative minimums of $\delta^{18}O$ and $\delta^{13}C$. Particularly, sample I11.A, drilled in the darker layer of the speleothem, stands out for an absolute maximum in SIRM together with the lowest value of $\delta^{13}C$ by far and with a relative minimum of $\delta^{18}O$. A relationship between SIRM and isotopic composition seems thus likely. *Bourne et al.* (2015) interpreted their results in a similar way, but due to the higher $\delta^{18}O$ values of enhanced summer precipitation in Virginia, their $\delta^{18}O$-SIRM relationship is reverse. A distinct pattern is proposed by *Jaqueto et al*. (2016). The isotopic compositions they measured were positively correlated with SIRM. They interpreted this feature as a result of changes in soil erosion/vegetation cover, impacting the carbon isotopic signal. Let us conclude here that different results and interpretations are expected, since the magnetism of speleothems and its relationship with climate is almost unexplored, whereas interpretations of oxygen and carbon isotopes in speleothems can be sometimes very tricky, due to the high number of factors controlling their behaviour in speleothems.

Despite the encouraging evidence that extreme values of SIRM generally match low $\delta^{18}O$- and $\delta^{13}C$-values, the overall low correlation between SIRM and isotopic data discards any unequivocal interpretation. Constraining and interpreting isotopic data in speleothems requires a continuous monitoring of cave conditions over a considerable amount of time (a few years, at least; e.g., *Verheyden et al.,* 2008). Annual variations of temperature inside and outside the cave and amount of precipitation, pCO_2, regular measurement of isotopic composition of the dripwaters, are just some of the parameters that would help understand the karst system and how it answers to climate variations. Another possible cause for the inconclusive results is the reduced time interval recorded in the speleothem (approximately

800 yrs), which is very short compared to other speleothem studies (in the order of tens of thousands of years). Significant climate changes may not have occurred during the period measured in SPAIV, resulting in reduced variations in $\delta^{18}O$- and $\delta^{13}C$-values. The resolution of the sampling is also far from ideal. With the samples cut in half, it was possible to reduce the time span of a sample from approximately 50 yrs to 25 yrs, but may not be sufficient to identify, for example, interannual variability in drier/wetter periods. Precipitation in Algarve is extremely irregular, with very dry years alternating with more humid seasons, from year to year. The North Atlantic Oscillation (NAO) index has a high correlation with precipitation in the south of Portugal, with negative index being favourable for high rainfall amount due to a shift of the storm tracks to lower latitudes. Although with irregularities, *Zhang et al.* (2011) estimated a high-frequency periodicity of the NAO cycles of 2-3 years and also quasi-cycles of 8-9 years. If similar conditions prevailed during the interval recorded by the stalagmite, the time resolution of 25 yrs would have smooth out precipitation variability.

Despite introduced some decades ago, the use of speleothems for past climate reconstruction has still a large margin to grow and develop. As examples, isotopic data has been acquired recently in fluid inclusions trapped inside the calcite matrix of the speleothem (*Affolter et al.,* 2014) and the use of magnetism as a climate proxy in speleothems is in early stages.

6.5 Conclusions

Two consecutive columns of SPAIV have been submitted to IRM and isotopic analysis. The main objective was to verify a possible relationship between SIRM of magnetite (indicative of magnetite concentration) with $\delta^{18}O$- and $\delta^{13}C$-values in calcite, a relationship reported in recent studies. Our results remain equivocal. For samples including brownish calcite layers, with high magnetization values, there seems to some linkage with low $\delta^{18}O$- and $\delta^{13}C$-values. However, for the majority of samples the relationship of magnetic mineral content and isotopic composition presents very low correlation coefficient. These results complicate any attempt to establish a relationship between magnetic mineral input in the cave and climate. There are several possibilities that explains the inconclusive results. One of the most relevant is the ignorance about the processes that dominate isotopic composition of the speleothems in that specific location and the associated dynamics of the cave. Cave monitoring and more climate proxy data should be performed before risking an interpretation of the data reported in this chapter. Additionally, the time resolution of the sampling (25 yrs) was not be adequate to capture the short-term variations in precipitation amount (2-3 years) that characterize Algarve,

whereas the short time span of the speleothem (~800 yrs) did not permit to capture larger amplitude, long-term climate changes.

7. Final Conclusions

In my PhD, paleomagnetic and climate data has been acquired from a portuguese speleothem. Magnetism in speleothems and its relationship with climate are in early stages of development, and these results bring some new and important information. Here is a list of some conclusions about this work:

1. The magnetic mineralogy of the speleothem is dominated by a low coercivity-phase, interpreted to be magnetite.

2. Paleomagnetic directions obtained from cubic (2x2x2cm) and cylindric (1.1 cm in diameter) samples collected along subhorizontal togradually subvertical calcite growth layers of a transversal cross section of the SPA speleothem show very stable and high intensity ($\sim 10^{-3}$ A/m) magnetic directions, with weak viscous remanent magnetization and low errors.

3. A systematic decrease in magnetic inclination values measured in samples with steeper calcite layers, in all analysed lines, suggests that remanent magnetization is influenced by calcite layer dip.

4. Anisotropy of Magnetic Susceptibility (ASM), mostly controlled by calcite as indicated by negative values of the magnetic susceptibility, indicates that the magnetic fabric is oblate, where k_3 represents the crystallographic direction of the calcite growths and thus mimics the shape of the speleothem.

5. The orientation of the Anisotropy of Anhysteretic Remanent Magnetization (AARM) ellipsoid, controlled by the orientation of the ferromagnetic particles, varies according to the slope of the layers; i.e., the steeper the slope, the shallower and more disperse the k_{1ARM} directions.

6. We suggest that increased misalignment of the ferromagnetic particles results in a net distribution of directions that is shallower than that of the ambient geomagnetic field and PSV models. This inclination error may result from the influence of physical mechanism, such as particle rolling and slipping during transport along the slope.

7. Avoiding sampling in lateral sides of speleothems is recommended, unless a correction is applied. In this work, a correction factor is calculated based on the extrapolation of the magnetic inclinations to hypothetical horizontal layers.

8. Despite the handicap of the surface slope influence on magnetic inclination, the Earth's magnetic field has been reconstructed between 4100 and 3300 yrs BC. Results show that the

magnetic declination and inclination lie in the range of the compared data and models. The best correlation is achieved with the SHA.DIF.14K model, suggesting that the latter is the most reliable PSV model for this time period.

9. The results suggest that magnetic remanence in the studied speleothem is controlled mainly by the ambient magnetic field, as comproved by general agreement with compared data and models, but affected by particle rolling of manetic particles along speleothem sides.

10. Relative paleointensity data estimated using two different methods (normalization of NRM with ARM and IRM and pseudo-Thellier method) display consistent results. These results reinforce the idea that speleothems are good recorders of Earth's magnetic field, in terms of direction and intensity, with the advantage of providing both continuous and high-resolution recording.

11. In this work I provide detailed concentration-and coercivity-dependent magnetic proxy obtained through the analysis of isothermal remanent magnetization (IRM) curves and compared them with carbon and oxygen isotope composition measured in selected samples of the SPA stalagmite. Results show a low statistical correlation between magnetic and isotopic composition. However, higher content of pedogenic magnetite, evaluated here by higher saturation values of the IRM, often correlated with lower $\delta^{18}O$- and $\delta^{13}C$-values compositions, suggesting a casual-to-effect link between climate and magnetic mineralogy.

In a near future, it is crutial to study more speleothems. Obtaining more paleomagnetic records (both directional and intensity) and compare them with contemporaneous data and models is a necessary way to establish speleothems definitely as reliable recorders of the Earth's magnetic field in the scientific community. At the same time, if possible, investigate the mechanisms by which speleothems acquire a remanent magnetization would allow to better understand possible factors affecting it, such as the surface slope influence reported in this study. The use of magnetic mineral concentration as speleothem's climate proxies should also be deepened. In this work, only carbon and oxygen isotopes were measured and the results were inconclusive, but a more multi-disciplinary approach, with the use of several other proxies combined, could have lead to a more conclusive interpretation. Speleothems are rock formations with very distinct characteristics and with an enormous potential to reveal many aspects about the past of earth's magnetic field and climate. With the appearance of new techniques and sophisticated measurement equipment, advances in the knowledge about speleothems and what they can offer will certainly become reality.

List of Figures

List of Tables

List of Acronyms

AARM – Anisotropy of Anhysteretic Remanent Magnetization

AMS – Anisotropy of Magnetic Susceptibility

ARM – Anisotropy of Remanent Magnetization

ChRM – Characteristic Remanent Magnetization

CLG – Cumulative Log-Gaussian

CRM – Chemical Remanent Magnetization

DP – Dispersion Parameter

DRM – Detrital Remanent Magnetization

ENSO – El Niño Southern Oscillation

GAD – Geocentrical Axial Dipole

GAP – Gradient Acquisition Plot

IRM – Isothermal Remanent Magnetization

LAP – Linear Acquisition plot

MAD – Maximum Angle Deviation

MD – Multi-domain

MDF – Mean Demagnetization Field

NAO – North Atlantic Oscillation

NRM – Natural Remanent Magnetization

PSV – Paleosecular Variation

RPI – Relative Paleointensity

SAA – South Atlantic Anomaly

SAP – Standardized Acquisition plot

SD – Single Domain

SEM – Scanning Electron Miscroscopy

SIRM – Saturated Isothermal Remanent Magnetization

TRM – Thermoremanent Magnetization

VGP – Virtual Geomagnetic Pole

VRM – Viscous Remanent Magnetization

Bibliography

Affolter, S., Fleitmann, D., and M., Leuenberger (2014), New online method for water isotope analysis of speleothem fluid inclusions using laser absortion spectroscopy (WS-CRDS), *Climate of the Past*, 10, 1291-1304.

Atsawawaranunt, K., Comas-Bru, L., Amirnezhad Mozhdehi, S., Deininger, M., Harrison, S. P., Baker, A., Boyd, M., Kaushal, N., Ahmad, S. M., Ait Brahim, Y., Arienzo, M., Bajo, P., Braun, K., Burstyn, Y., Chawchai, S., Duan, W., Hatvani, I. G., Hu, J., Kern, Z., Labuhn, I., Lachniet, M., Lechleitner, F. A., Lorrey, A., Pérez-Mejías, C., Pickering, R., Scroxton, N., and SISAL Working Group Members (2018), The SISAL database: a global resource to document oxygen and carbon isotope records from speleothems, *Earth Syst. Sci. Data*, 10, 1687-1713, https://doi.org/10.5194/essd-10-1687-2018, 2018.

Bilardello, D., J. Jezek and S. A. Gilder (2013), Role of spherical particles on magnetic field recording in sediments: experimental and numerical results, *Phys. Earth Planet. Int*., 214, 1–13.

Bilardello, D. (2013), Understanding DRM acquisition of plates and spheres: a first comparative experimental approach, *Geophys. J. Int*., 195, 148–158.

Bourne, M. D., J. M. Feinberg, B. E. Strauss, B. Hardt, H. Cheng, H. D. Rowe, G. Springer, and R. L. Edwards (2015), Long-term changes in precipitation recorded by magnetic minerals in speleothems, *Geology*, 43, 595-598.

Borradaile, G. J. and M. Jackson (2010), Structural geology, petrofabrics and magnetic fabrics (AMS, AARM, AIRM), *Journal of Structural Geology*, 32, 1519-1551, doi: 10.1016/j.jsg.2009.09.006.

Butler, R. F. (1992), Paleomagnetism: Magnetic Domains to Geologic Terranes, *Blackwell*

Scientic Publications, Boston.

Carrancho, A., J. J. Villalaín, F. J. Pavón-Carrasco, M. L. Osete, L. G. Strauss, J. M. Vergès, J. M. Carretero, D. E. Angelucci, M. R. González Morales, J. L. Arsuaga, J. M. Bermúdez de Castro, and E. Carbonell (2013), First directional European paleosecular variation curve for the Neolithic based on archaeomagnetic data, *Earth Planet, Sci. Lett.*, 380, 124-137.

Coe, R. S., S. Grommé, and E. A. Mankinen (1978), Geomagnetic Paleointensities From Radiocarbon-Dated Lava Flows on Hawaii and the Question of the Pacific Nondipole Low, *J. Geophys. Res.*, vol. 83, B4.

Coplen, T. (2006), New guidelines for reporting stable hydrogen, carbon, and oxygen isotope-ratio data, *Rapid Commun. Mass Spectrom*, 20, 3165–3166.

Coplen, T., Brand, W., Gehre, M., Groning, M., Meijer H. A. J., Toman, B., and R. M. Verkouteren (2015), After two decades a second anchor for the VPDB d13C Scale, Geochimica et Cosmochimica Acta 158, 276–289.

Dasgupta, S., Saar, M., Edwards, R., Shen, C., Cheng, H. and E. Calvin Alexander Jr (2010), Three thousand years of extreme rainfall events recorded in stalagmites from Spring Valley Caverns, Minnesota, *Earth Planet, Sci. Lett.*, 300, 46-54.

Dorale, J. A., and Z. Liu (2009), Limitations of hendy test criteria in judging the paleoclimatic suitability of speleothems and the need for replication, *Journal of Cave and Karst Studies*, v. 71, no. 1, 73–80.

Duan, F., Wang, Y., Shen, C., Wang, Y., Cheng, H., Wu, C., Hu, H., Kong, X., Liu, D. and Zhao, K. (2014), Evidence for solar cycles in a late Holocene speleothem record from Dongge cave, China, *Scientific reports 4*, article number 5159.

Dunlop, D. J., and O. Ozdemir (1997), Rock Magnetism: Fundamentals and Frontiers, Cambridge Studies in Magnetism, Cambridge University Press, Cambridge.

Elwood, B. B., Harrold, F. B., Benoist, S. L., Straus, L. G., Morales, M. G., Petruso, K., Bicho, N. F., Zilhão, J., and N. Soler (2001), Paleoclimate and intersite correlation from late Pleistocene/Holocene cave sites: results from southern Europe, *Geoarcheology: An international journal*, Vol. 16, No 4, 433-463.

Elwood, B. B., Harrold, F. B., Benoist, Thacker, P., Otte, M., Bonjean, D., Long, G. J., Shahin, A. M., Hermann, R. P., and F. Grandjean (2004), Magnetic susceptibility applied as an age-depth-climate relative dating technique using sediments from Scladina cave, a late Pleistocene cave site in Belgium, *Journal of Archeological Science*, 31, 283-293.

Elwood, B. B., and W. A. Gose (2006), Heinrich H1 and 8200 yr B.P. climate events recorded in Hall's cave, Texas, *Geology*, V. 34, no 9, 753-756.

Fairchild, I. J., and A. Baker (2012), Speleothem Science: From Process to Past Environments, 450 pp., Wiley-Blackwell, Chichester, U. K.

Fisher, R. (1953), Dispersion on a sphere, *Proc. R. Soc. A*, 217 (1130), 295‑305.

Font, E., C. Veiga-Pires, M. Pozo, C. Carvallo, A. C. Siqueira Neto, P. Camps, S. Fabre, and J. Mirão (2014), Magnetic fingerprint of southern Portuguese speleothems and implications for paleomagnetism and environmental magnetism, *J. Geophys. Res. Solid Earth*, 119, 7993–8020, doi:10.1002/2014JB011381.

Gázquez, F., Calaforra J., Forti, P., Stoll, H., Ghaleb, B. and Delgado-Huertas, A. (2014), Paleoflood events recorded by speleothems in caves, *Earth Surf. Process. Landforms,* doi: 10.1002/esp.3543.

Ghaleb, B., C. Veiga-Pires, D. Moura, and C. Hillaire-Marcel (2014), Multi-proxy constraints on ages of low U-content, young and "dirty" speleothems: Example from southern Portugal cave deposits, abstract presented at EGU, Wien, Austria.

Gómez-Paccard, M., J. C. Larrasoaña, S. Giralt, and A. P. Roberts (2012), First paleomagnetic results of mid- to late Holocene sediments from Lake Issyk-Kul (Kyrgyzstan): Implications for paleosecular variation in central Asia, Geochem. Geophys. Geosyst., 13, Q03019, doi:10.1029/2011GC004015.

Griffiths, D. H., R. F. King, A. I. Rees, and A. E. Wright (1960), The remanent magnetism of some recent varved sediments, *Proc. R. Soc. Lond. A.,* 256, 359-383.

Helie, J. F. and C. Hillaire-Marcel (2016), Suitability of IAEA-603 as replacement to NBS19 for very small $CaCO_3$- sample analysis, Ref. 5 in *Certified reference material IAEA-603 calcite: Stable Isotope Reference Material for* $\delta^{13}C$ *and* $\delta^{18}O$, Reference sheet RM-603, International Atomic Energy Agency, Vienna.

Hellstrom, J. (2006), U–Th dating of speleothems with high initial ^{230}Th using stratigraphical constraint, *Quat. Geochronol*., 1, 289–295.

Hendy, C. H. (1971), The isotopic geochemistry of speleothems - I. The calculation of the effects of differentmodes of formation on the isotopic composition of speleothems and their a pplicability as palaeoclimatic indicators, *Geochim. Cosmochim*. Acta, 35: 801–824.

Hill, C. and P. Forti (1997) Cave Minerals of the World, *National Speleological Society* (2nd Edition 1997), 463 pp, hardbound, ISBN 1-879961-07-5.

Hirt, A. H. and B. S. G. Almqvist (2012), Unraveling magnetic fabrics, Int. J. Earth Sci. (Geol. Rundsch), 101, 613–624, doi: 10.1007/s00531-011-0664-0.

Hrouda, F. (1986), The effect of quartz on the magnetic anisotropy of quartzite, *Stud. Geophys. Geod.*, 30 (1), 39–45.

Irving, E. (1964), Paleomagnetism and its application to geological and geophysical problems, *John Wiley*, New York.

Jackson, M. J., S. K. Banarjee, J. A. Marvin, R. Lu and W. Gruber (1991), Detrital remanence, inclination errors, and anhysteretic remanence anisotropy: quantitative model and experimental results, Geophys. J. Int., 104, 95-103.

Jaqueto, P., R. Trindade, G. Hartmann, V. Novello, F. Cruz, I. Karmann, B. Strauss and J. Feinberg (2016), Linking speleothems and soil magnetism in the Pau d' Alho cave (Central South America), *Journal of Geophysical Research*, volume 121, issue 10, 7024-7039, doi: 10.1002/2016JB013541.

Jelinek, V. (1981), Characterization of the magnetic fabric of rocks, *Tectonophysics*, 79, 63–67.

Jezek, J., S.A. Gilder and D. Bilardello (2012), Numerical simulation of inclination shallowing by rolling and slipping of spherical particles, *Comput. Geosci.*, 49, 270–277.

King, R. F. (1955), The remanent magnetism of artificially deposited sediments, *Geophysical Journal International*, Vol. 7, 115-134.

Kirschvink, J. L. (1980), The least-squares line and plane and the analysis of palaeomagnetic data, *Geophysical Journal of the Royal Astronomic Society*, volume 62, issue 3, 699-718.

Kissel, C., A. Rodriguez-Gonzalez, C. Laj, F. Perez-Torrado, and J. C. Carracedo (2015), Paleosecular variation of the earth magnetic field at the Canary Islands over the last 15 ka, *Earth Planet, Sci. Lett.*, 412, 52-60.

Knudson, M., Riisager, P., Olsen, J. and Seidenkrantz, M. (2012), Evidence of suess solar cycle bursts in subtropical Holocene speleothem 18O records, *The Holocene*, doi: 10.1177/0959683611427331.

Korte, M. and C. G. Constable (2016), On the use of calibrated relative paleointensity records to improve millennial-scale geomagnetic field models, *Geochemistry, Geophysics, Geosystems,* Volume 7, Nº 9, doi:10.1029/2006GC001368.

Korte, M., C. Constable, F. Donadini, and R. Holme (2011), Reconstructing the Holocene geomagnetic field*, Earth Planet, Sci. Lett.*, 312, 3-4, 497-505.

Kruiver, P. P., Y. S. Kok, M. J. Dekkers, C. G. Langereis, and C. Laj (1999), A pseudo-Thellier relative paleointensity record and rock magnetic and geochemical parameters in relation to climate during the last 276 kyr in the Azores region, *Geophys. J. Int.*, 136, 757-770.

Kruiver, P. P., Dekkers, M. J., and D. Heslop (2001). Quantification of magnetic coercivity components by the analysis of acquisition curves of isothermal remanent magnetisation, *Earth and Planetary Science Letters*, 189 (3-4), 269/276.

Lachniet, M. S. (2009), Climatic and environmental controls on speleothem oxygen-isotope values, *Quaternary Science reviews,* 28, 412-432.

Lascu, I., J. M. Feinberg (2011), Speleothem Magnetism, *Quaternary Science reviews*, 30, 3306-3320, doi: 10.1016/j.quascirev.2011.08.004.

Lascu, I., J. M. Feinberg, Dorale, J. M., Cheng, H., and R. L. Edwards (2016), Age of the Laschamp excursion determined by U-Th dating of a speleothem geomagnetic record from North America, *Geology*, 44, 139-142.

Latham, A. G., H. P. Schwarcz, D. C. Ford, and G. W. Pearce (1979), Paleomagnetism of speleothem deposits, *Nature*, 280, 383-385.

Latham, A. G., H. P. Schwarcz, D. C. Ford, and G. W. Pearce (1982), The paleomagnetism and U-Th dating of three Canadian speleothems: evidence for the westward drift, 5.4-2.1 ka BP, *Canadian Journal of Earth Sciences*, 19, 1985-1995.

Latham, A. G., H. P. Schwarcz, and D. C. Ford (1986), The paleomagnetism and U-Th dating of Mexican speleothem, Earth and Planetary Science Letters, 79, 195-207.

Latham, A.G., D. C. Ford, H. P. Schwarcz, and T. Birchall (1989), Secular variation from Mexican speleothems: their potential and problems, *Physical Earth Planetary Interiors,* 56, 34-48.

Latham, A.G., and D. C. Ford (1993), The paleomagnetism and rock magnetism of cave and karst deposits, *Applications of Paleomagnetism to Sedimentary Geology*, SEPM Special Publication, vol. 49, 149-155.

Lean, C. B., A. G. Latham, and J. Shaw (1995), Palaeosecular variation from a Vancouver Island speleothem and comparison with contemporary North American records, *Journal of Geomagnetism and Geoelectricity*, 47, 71-87.

Lechleitner, F., Amirnezhad-Mozhdehi, S., Columbu, A., Comas-Bru, L., Labuhn, I., Pérez-Mejías, C., and K. Rehfeld (2018), The potential of Speleothems from Western Europe as recorders of regional climate: a critical assessment of the SISAL database, *Quaternary*, 1, 30. doi: 10.3390/quat1030030.

Liu, Q., Roberts, A., Larrasoaña, J., Banarjee, S., Guyodo, Y., Tauxe, L., and F. Oldfield (2012), Environmental magnetismo: principles and applications, *Reviews of geophysics*, 50 (4).

Luetscher, M., Boch, R., Sodemann, H., Spotl, C., Cheng, H., Edwards, R., Frisia, S., Hof, F. and W. Muller (2015), North Atlantic storm track changes during the Last Glacial Maximum recorded by Alpine speleothems, *Nature Communications*, doi: 10.1038/ncomms7344.

Martin, K. (1990), Paleomagnetism of speleothems in Gardner cave, Washington, *National Speleological Society Bulletin*, 52, 87-94.

Maxbauer, D. P., Feinberg, J. M., and D. L. Fox (2016), MAX UnMix: A web application for unmixing magnetic coercivity distributions. *Computers and Geosciences*, *95*, 140-145. https://doi.org/10.1016/j.cageo.2016.07.009.

McCabe, C., M. Jackson, and B. B. Ellwood (1985), Magnetic anisotropy in the Trenton limestone: results of a new technique, anisotropy of anhysteretic susceptibility, *Geophys. Res. Lett.*, 12, 333-336.

McDermott, F. (2004), Palaeo-climate reconstruction from stable isotope variations in speleothems: a review. *Quat. Sci. Rev,* 23, 901-918.

Merrill, R. and P. McFadden (2003), The geomagnetic axial dipole field assumption, *Phys. EarthPlanet. Inter.*, 139, 171-185.

Mickler, P. J., Stern, L., and J. L. Banner (2006), Large kinetic isotope effects in modern speleothems*, Geological Society of America Bulletin*, 118 (1-2), 65-81. doi: 10.1130/B25698.1.

Morinaga, H., H. Inokuchi, and K. Yaskawa (1986), Magnetization of a speleothem in Akiyoshi Plateau as a record of the geomagnetic secular variation in West Japan, *Journal of Geomagnetism and Geoelectricity*, 38, 27-44.

Morinaga, H., H. Inokuchi, and Yaskawa, K. (1989), Palaeomagnetism of speleothems (speleothems) in SW Japan, *Geophysical Journal*, 96, 519-528.

Nilsson, A., R. Holme, M. Korte, N. Suttie, and M. Hill (2014), Reconstructing Holocene geomagnetic field variations: new methods, models and implications*, Geophys. J. Int*., 198, 229–248.

Noel M., and C. M. Batt (1990), A method for correcting geographically separated remanence directions for the purpose of archaeomagnetic dating, *Geophys. J. Int.*, 102, 753–756.

Openshaw, S., A. Latham, and J. Shaw (1997), Speleothem palaeosecular variation records from China; their contribution to the coverage of Holocene palaeosecular variation data in East Asia; Paleosecular variation and intensity, *Journal of Geomagnetism and Geoelectricity*, 49, 485-505.

Osete, M. L., J. Martin-Chivelet, C. Rossi, R. L. Edwards, R. Egli, M. B. Munoz-Garcia, X. F. Wang, F. J. Pavon-Carrasco, and F. Heller (2012), The Blake geomagnetic excursion recorded in a radiometrically dated speleothem, *Earth Planet. Sci. Lett.,* 353, 173–181.

Panovska, S., C. C. Finlay, F. Donadini, and A. M. Hirt (2012), Spline analysis of Holocene sediment magnetic records: Uncertainty estimates for field modeling*, J. Geophys. Res.*, 117, B02101, doi:10.1029/2011JB008813.

Panovska, S., M. Korte, C. C. Finlay, and C. G. Constable (2015), Limitations in paleomagnetic data and modelling techniques and their impact on Holocene geomagnetic field models*, Geophys. J. Int*, 202, 402-418. doi: 10.1093/gji/ggv137.

Pavón-Carrasco, F. J., M. L. Osete, J. M. Torta, and A. De Sanctis (2014), A geomagnetic field model for the Holocene based on archaeomagnetic and lava flow data, *Earth and Planetary Science Letters*, 388, 98–109.

Ponte, J. M., E. Font, C. Veiga-Pires, C. Hillaire-Marcel, and B. Ghaleb (2017), The effect of speleothem surface slope on the remanent magnetic inclination, *J. Geophys. Res. Solid Earth*, 122, doi:10.1002/2016JB013789.

Roberts, A. P., and M. Winklhofer (2004), Why are geomagnetic excursions not always recorded in sediments? Constraints from post-depositional remanent magnetization lock-in modeling, *Earth Planet, Sci. Lett.*, 227, 345–359.

Rochette, P. (1988), Inverse magnetic fabric in carbonate-bearing rocks, *Earth and Planetary Science Letters*, 90, 229-237, doi: 10.1016/0012-821X(88)90103-3.

Rossi, C., Mertz-Kraus R. and M. Osete (2014), Paleoclimatic variability during the Blake geomagnetic excursion (MIS5d) deduced from a speleothem record, *Quat. Sci. Rev.,* 102, 168-180.

Sagnotti, L., P. Macrì, R. Lucchi, M. Rebesco, and A. Camerlenghi (2011), A Holocene paleosecular variation record from the northwestern Barents Sea continental margin, Geochem. Geophys. Geosyst., 12, Q11Z33, doi:10.1029/2011GC003810.

Scholz, D., and D. L. Hoffmann (2011), An algorithm designed for construction of speleothem age models, *Quaternary geochronology*, 6, 369-382.

Schmidt, V., D. Gunther, and A. M. Hirt (2006), Magnetic anisotropy of calcite at room-temperature, *Tectonophysics*, 418, 63–73.

Strauss, B. E., J. H. Strehlau, I. Lascu, J. A. Dorale, R. L. Penn, and J. M. Feinberg (2013), The origin of magnetic remanence in speleothems: Observations from electron microscopy and rock magnetism*, Geochemistry Geophysics Geosystems*, 14, 5006-5025.

Strikis, N., Cruz, F., Cheng, H. and I. Karmann (2011), Abrupt variations in South Americam monsoon rainfall during the Holocene based on a speleothem record from central-eastern Brazil, *Geology,* vol 39, no 11, 1075-1078, doi:10.1130/G32098.

Tarling, D. H., and F. Hrouda (1993), The Magnetic Anisotropy of Rocks, Chapman and Hall, London.

Tauxe, L. (1993), Sedimentary records of relative paleointensity of the geomagnetic field: theory and practice, *Rev. Geophys*., 31, 319-354.

Tauxe, L., T. Pick, and Y. S. Kok (1995), Relative paleointensity in sediments: a pseudo-Thellier approach, *Geophysical Research Letters*, Vol. 22, NO. 21, 2885-2888.

Tauxe, L., and D. V. Kent (2004), A simplified statistical model for the geomagnetic field and the detection of shallow bias in paleomagnetic inclinations: Was the ancient magnetic field dipolar?, in Timescales of the Paleomagnetic Field, edited by J. E. T. Channell et al., 101–115, AGU, Washington, D. C., doi:10.1029/145GM08.

Tauxe, L., K. P. Kodama, and D. V. Kent (2008), Testing corrections for paleomagnetic inclination error in sedimentary rocks: a comparative approach, *Phys. Earth Planet. Inter.*, 169, 152–165.

Terrinha, P., R. Rocha, J. Rey, M. Cachão, D. Moura, C. Roque, L. Martins, V. Valadares, J. Cabral, A.C. Azeredo, L. Barbero, E. Clavijo, R. P. Dias, J. Gafeira, H. Matias, J. Madeira, C. Marques da Silva, J. Munhá, L. Rebelo, C. Ribeiro, J. Vicente, J. Noiva, N. Youbi, and M. K. Bensalah (2013), A Bacia do Algarve: estratigrafia, paleogeografia e tectónica. In: Geologia de Portugal, Vol. II: Geologia Meso-cenozóica de Portugal. Eds. Rui Dias, Alexandre Araújo, Pedro Terrinha, José Carlos Kullberg. Lisboa : Livraria Escolar Editora, 2013, Cap. III.1., p. 29-166.

Thellier, E., and O. Thellier (1959), Sur l'intensité du champ magnétique terrestre dans le passé historique et géologique, *Ann. Geophys.*, 15, 285-378.

Thouveny, N., J. Carcaillet, E. Moreno, G. Leduc, and D. Nérini (2004), Geomagnetic moment variation and paleomagnetic excursionssince 400 kyr BP: a stacked record from sedimentary sequences of the Portuguese margin, *Earth Planet, Sci. Lett.*, 219, 377-396.

Trindade, R., Jaqueto, P., Terra-Nova, F., Brandt, D., Hartmann, G., Feinberg, J., Strauss, B., Novello, V., Cruz, F., Karmann, I., Cheng, H., and R. Lawrence Edwards (2018), Speleothem record of Geomagnetic South Atlantic anomaly recurrence, *Proceedings of the National Academy of Sciences*, 115 (52) 13198-13203; doi: 10.1073/pnas.1809197115.

Veiga-Pires, C., B. Ghaleb, J. Hélie, D. Moura, J. Luis, and C. Hillaire-Marcel (2011), A first Last Glacial Maximum to Younger Dryas stalagmite record from southern Portugal, *Geophysical Research Abstracts*, EGU 2011, 13.

Verheyden S., Genty D., Deflandre G., Quinif Y., and E. Keppens (2008), Monitoring climatological, hydrological and geochemical parameters in the Père Noël cave

(Belgium): implication for the interpretation of speleothem isotopic and geochemical time-series, *International Journal of Speleology*, 37 (3), 221-234.

Verosub, K. L. (1977), Depositional and postdepositional processes in the magnetization of sediments, *Rev. geophys. Space Phys.,* 15(2), 129–143.

Wong, C. I. and D. O.Breecker (2015), Advancements in the use of speleothems as climate archives, *Quaternary Science Reviews*, 127, 1-18.

Zanella, E., Tema, E., Lanci, E., Regattieri, E., Isola, I., Hellstrom, J., Costa, E., Zanchetta, G., Drysdale, R. and F. Magrì (2018), A 10,000 yr record of high-resolution Paleosecular Variation from a flowstone of Rio Martino Cave, Northwestern Alps, Italy, *Earth Planet. Sci. Lett.*, 485, 32-42.

Zhang, X., Jin, L., Chen, C., Guan, D., and M. Li (2011), Interannual and interdecadal variations in the North Atlantic Oscillation spatial shift, *Chinese Science Bulletin*, Vol 56, No 24, 2621-2627.

Zhu, Z. M., S. H. Zhang, C. Y. Tang, H. Y. Li, S. C. Xie, J. L. Ji, and G. Q. Xiao (2012), Magnetic fabric of speleothems and its formation mechanism, *Geochemistry Geophysics Geosystems*, volume 13, number 6, Q06006, doi:10.1029/2011GC003869.

Zhu, Z., Feinberg, J. M., Xie, S., Bourne, M. D., Huang, C., Hu, C., and H. Cheng (2017), Holocene ENSO-related cyclic storms recorded by magnetic minerals in speleothems of central china, *Proceedings of the National Academy of Sciences*, 114(5), 852–857, doi:10.1073/pnas.1610930114.